Stromule-mediated plastid-nucleus interaction

DISSERTATION

zur Erlangung des
Doktorgrades der Naturwissenschaften (Dr. rer. nat.)

vorgelegt der

Naturwissenschaftlichen Fakultät I – Biowissenschaften
der Martin-Luther-Universität Halle – Wittenberg
von Sedef Özyürek

Gutachter: Prof. Dr.Ralf Bernd Klösgen,

Prof. Dr. Bettina Hause,

Prof. Dr. Stefanie Müller-Schüssele

Die vorliegende Dissertation wurde unter Anleitung von Dr. Martin Schattat in der Abteilung für Pflanzenbiochemie (Prof. Dr.Ralf Bernd Klösgen, Martin-Luther-Universität Halle-Wittenberg) angefertigt.

Eingereicht am: 26.09.2023

Tag der Verteidigung: 21.02.2024

Summary

The principal question for plastid-nucleus signalling, which has not been resolved hitherto, is how plastid-created signals are transferred to the nucleus. Recently it has been suggested that proteins and other molecules could be transferred from the plastid to the nucleus via plastid-derived stroma-filled tubules, so-called **stromules**. Based on short time laps and snap shot data it was suggested that plastids form stromules to "reach out" for the nucleus to connect to it and subsequently transfer their signals through those connections. Despite this intriguing idea, the available data leave critical questions about this proposed relationship unanswered, such as: How do plastids find the nucleus during steady-state or stress conditions?

My thesis is dedicated to close some of those gaps in our knowledge. In preliminary work to this thesis time lapse experiments indicated that at least in *A. thaliana*, plastids might not reach out to the nucleus, but instead, nucleus movement pulls out stromules from nucleus associated stationary plastids. Thus, the hypothesis for *A. thaliana* was that nucleus-associated stromules in *A. thaliana* are for plastids, a means of ensuring contact with the nucleus. In order to test this hypothesis, I investigated the nucleus movement in different *A. thaliana* mutants, affecting plastid morphology and number. I found that plastids indeed restrict nucleus movement by being held in place and by being attached to the nucleus, forming stromules with limited length. The collected data clearly shows that the model developed in *N. benthamiana* does not hold true for *A. thaliana* and that here stromules might be rather nucleus tethers then signalling conduits. By inducing plastid clustering and stromule formation by laser induced stress in N. benthamiana, I collected data, continuous imaging data, revealing the key role of nucleus movement for plastid clustering and stromule-plastid-nucleus contacts. Indicating that the model for N. benthamiana needs to be redrawn. By creating a triple marker line, I was able to visualize the actin surrounding the nucleus as well as plastids stromules and the nucleus itself. By time lapse imaging and inhibitor treatment I was able to collect evidence that stromule tips in A. thaliana are most likely bound to the nucleus associated actin. This suggests that the anchor, responsible for stromule formation has to mediate between the plastid envelope and actin. Identification of the plastid membrane anchor would allow the creation of specific stromule mutants, which are a vital tool for future characterization of the role of these stromule-mediated interactions. Taken together in my thesis I collected data, which show that the current model for stromule nucleus interactions has to be redrawn and the suggested role of microtubules revaluated.

Zusammenfassung

Bis her ist noch ungeklärt wie genau beim der Signalübertragung aus den Plastiden auf den Zellkern die Signalmoleküle zum Zellkern gelangen. Vor einigen Jahren wurde die Hypothese aufgestellt, dass Proteine und andere Moleküle über von Plastiden gebildete, mit Stroma gefüllte Röhrchen, sogenannte Stromuli, von den Plastiden zum Zellkern transportiert werden könnten. Basierend auf kurzen Zeitreiheexperimenten und Schnappschussdaten wurde spekuliert, dass Plastiden Stromuli bilden, um nach dem Kern zu „greifen“, sich mit ihm zu verbinden und anschließend ihre Signale über diese Verbindungen zu übertragen. Trotz dieser faszinierenden Idee lassen die verfügbaren Daten kritische Fragen zu diesem vorgeschlagenen Vorgang unbeantwortet, wie zum Beispiel: Wie finden Plastiden den Kern unter stationären oder Stressbedingungen?

Meine Dissertation möchte einige dieser Wissenslücken schließen. In der Vorarbeit zu dieser Dissertation deuteten Zeitrafferexperimente aus der AG Schattat darauf hin, dass zumindest bei *A. thaliana* die Plastiden keine Stromuli aussenden um den Kern zu erreichen, sondern dass die Bewegung des Kerns selbst Stromuli aus den mit dem Kern verbundenen stationären Plastiden herauszieht. Daher lautete die Arbeitshypothese für meine Arbeit, dass in *A. thaliana* kernassoziierte Stromuli ein Mittel für Plastiden sind, um den kontinuierlichen Kontakt mit dem Kern sicherzustellen.

Um diese Hypothese zu testen, untersuchte ich die Kernbewegung in verschiedenen *A. thaliana* Mutanten, die sich auf die Morphologie und Anzahl der Plastiden auswirkt. Ich fand heraus, dass Plastiden tatsächlich die Bewegung des Zellkerns einschränken, indem sie selbst an Ort und Stelle gehalten und gleichzeitig am Zellkern befestigt sind. Die begrenzte Länge von Stromuli sorgt dann dafür, dass der Zellkern sich nur eingeschränkt von den Plastiden wegbewegen kann. Die gesammelten Daten zeigen deutlich, dass das in *N. benthamiana* entwickelte Modell nicht auf *A. thaliana* zutrifft und dass Stromuli hier eher der Kernbindungen als für die Signalleitung dienen.

Durch die Induktion von Plastiden-Clusterbildung und Stromulibildung durch laserinduzierten Stress in *N. benthamiana* sammelte ich kontinuierliche Bildgebungsdaten, die die Schlüsselrolle der Kernbewegung für Plastiden-Clusterbildung und Stromulen-Plastiden-

Kernkontakte aufdecken. Dies weist darauf hin, dass das Modell für *N. benthamiana* ebenfalls überarbeitet werden muss und das in dem neuen Modell die Bewegung des Zellkerns mit einbezogen werden muss.

Durch die Erstellung einer dreifachen Orgenellenmarkerlinie war ich in der Lage, das den Kern umgebende Aktin sowie die Stromuli und den Kern selbst sichtbar zu machen. Durch Zeitrafferaufnahmen und Inhibitorbehandlung konnte ich Beweise dafür sammeln, dass Stromulispitzen in *A. thaliana* höchstwahrscheinlich an das kernassoziierte Aktin gebunden sind. Dies legt nahe, dass der Anker, der für die Stromulenbildung verantwortlich ist, zwischen der Plastidenhülle und Aktin vermitteln muss. Die Identifizierung des Plastidenmembranankers würde die Schaffung spezifischer Stromuli-Mutanten ermöglichen, die ein wichtiges Instrument für die zukünftige Charakterisierung der Rolle dieser Stromuli-vermittelten Interaktionen darstellen.

Zusammenfassend gesagt habe ich in meiner Dissertation Daten gesammelt, die zeigen, dass das aktuelle Modell für Stromule-Kern-Wechselwirkungen neu gezeichnet und die vorgeschlagene Rolle von Mikrotubuli neu bewertet werden muss.

Table of Contents

List of Figures

List of Tables

Abbreviations

ACC	1-Aminocyclopropane-1-carboxylic acid
ABA	Abscisic acid
ABD2	actin-binding domain 2 from FIMBRIN 1
AIM	acetosyringone infiltration medium
ARC	ACCUMULATION AND REPLICA- TION OF CHLOROPLAST
ATG	AUTOPHAGY GENE
A. thaliana	*Arabidopsis thaliana*
A. tumefaciens	*Agrobacterium tumefaciens*
AvrBs3	avirulence protein bacterial spot 3
AvrRps4	
bidest.	distillation water x2 times
bp	base pair
CaMV	Cauliflower Mosaic Virus
Carb	Carbenicillin
CHUP1	CHLOROPLAST UNUSUAL POSITIONING 1
CTD	cytochalasin D
CLSM	confocal laser scanning microscopy
DMSO	dimethyl sulfoxide
DNA	Deoxyribonucleic acid
dNTP	Deoxynucleoside triphosphate
dpi	days post-infiltration
DsRed	drFP583 (ref) fluorescent protein
E.coli	*Escherichia coli*
eGFP	enhanced green fluorescent protein
ER	endoplasmic reticulum
ETI	effector-triggered immunity
FNRtp	FERREDOXIN-NADP(H) OXIDOREDUCTASE transit peptide
Gent	Gentamycin
GFP	Green fluorescent protein
GV	GV3101
GUS	β -Glucuronidase
H2B	HISTONE 2B
H_2O_2	hydrogen peroxide (ROS molecule)
hpi	hours post-infiltration
HR	hypersensitive response
h	hours
JA	Jasmonic acid
IPTG	Isopropyl-β-D-thiogalactopyranosid
LACS	Long-chain acyl-CoA synthetase
Lat B	latrunculin B

LB-Medium	Luria Bertani – Medium
LBA	LBA 4404
LRR	leucine-rich repeat
LSM	laser scanning microscope
mOrange2	monomeric orange fluorescent protein 2
MAP4	MICROTUBULE ASSOCIATED PROTEIN 4 (from mouse)
MCS	membrane contact sites
min	minutes
MSL	plastid-localized homologs of the bacteria mechanosensitive channel MscS
NADPH	nicotinamide adenine dinucleotide phosphate hydrogen
NLS	nucleus localization signal
N. benthamiana	*Nicotiana benthamiana*
N. tabacum	*Nicotiana tabacum* (tobacco)
NRIP	N RECEPTOR-INTERACTING PROTEIN
R-gene	resistance gene
ROS	reactive oxygen species
OD_{600}	optical density
OEP	outer envelope membrane
pARC	PARALOG OF ARC6
PCR	Polymerase-chain-reaction
pETC	photo-synthetic electron transport chain
PGM	phosphoglucomutase
PHD	plant homeodomain
PI	propidium iodine
pn marker	plastid (*FNRtp:eGFP*) – nucleus marker (*H2B:mCherry*)
P. syringe	*Pseudomonas syringe*
SA	salicylic acid
sec	seconds
SP	SignalPeptid
TMV	Tobacco Mosaic Virus
tp	transit peptide
UBQ10	Ubiquitin -10
wt	wild type
Xop	Xanthomonas outer protein

Introduction and Goals

I. Introduction

1.1 Plastids are of endosymbiotic origin

Plastids are vital organelles found in plant cells and some parasites (Gray et al., 2001; Inaba et al., 2011). Plastids are believed to be of endosymbiotic origin and originate from free-living photosynthetic cyanobacteria. This endosymbiosis is supposed to have been established approximately 1.2 to 1.5 billion years ago (Dyall et al., 2004; Inaba et al., 2011; Nott et al., 2006). The ancestral prokaryotic genome most likely contained all the information needed to support a self-sustaining photoautotrophic lifestyle. However, since the endosymbiotic relationship has been established, the plastid genome has experienced a progressive and consequential reduction in coding capacity. While several genes which are not required for endosymbiotic survival may have vanished altogether, the vast majority of genes (>3,000 polypeptides) have been transferred to the host's nuclear genome, and only a few (less than 100) remain in the endosymbiont's genome (Daniell et al., 2016; Inaba et al., 2011; Martin et al., 2002; McFadden, 2001; Yang et al., 2021). As a consequence of gene transfer in the domestication process, the resulting endosymbiotic plastids are no longer self-sufficient and rely on the delivery of nucleus-encoded and cytoplasm-translated proteins (Inaba, 2010; Nott et al., 2006). In today's green plants, the nucleus controls not only chloroplast development but also its physiological functions and has to ensure the supply of needed plastid proteins (Daniell et al., 2016; Erickson et al., 2017; McFadden, 2001; Nott et al., 2006; Yang et al., 2021).

1.2 Plastids send signals back to the nucleus

This arrangement necessitates that the plastid communicates its physiological state to the nucleus to direct the expression of nuclear-encoded chloroplast genes, a process referred to as "retrograde signaling" (Chan et al., 2016; Inaba et al., 2011; Mielecki et al., 2020). Retrograde signaling (plastid to the nucleus) is essential for two reasons. First, functional multiprotein complexes in plastids, such as photosystems, are composed of subunits encoded by the nuclear and plastid genomes, which have to be co-ordinately expressed for proper assembly. Second, external environmental factors such as light, temperature, or effector proteins, injected into the plant cell by plant pathogens, affect plastid metabolism and function. The plastid must regulate

nuclear gene expression and protein flow to adapt to these changing conditions and stresses (Inaba et al., 2011).

Consequently, it has been proposed in the past that when plastids are dysfunctional, they send signals to the nucleus, affecting the expression of nuclear-encoded and plastid-targeted genes. Various treatments (e.g., herbicides and antibiotics) and/or mutant screens have been used to identify components important for plastid-to-nucleus retrograde signaling. This led to the identification of several candidate retrograde signals (Chan et al., 2016), such as tetrapyrroles (Strand et al., 2003; Woodson et al., 2011), phosphoradenosines (Estavillo et al., 2011), carotenoid oxidation products (Avendaño-Vázquez et al., 2014; Ramel et al., 2012; Van Norman et al., 2014), isoprenoid precursors MEcPP (Xiao et al., 2012), carbohydrate metabolites and hydrogen peroxide (H_2O_2) (Mullineaux et al., 2020). Besides metabolites also, proteins have been suggested to act as retrograde signals, including chloroplast and nuclear proteins, as well as cytosolic and mobile proteins (Bobik & Burch-Smith, 2015).

1.3 The nature of retrograde signals

Retrograde signals are divided into two different categories. First, those believed to be slower-acting (e.g., plastid metabolites) due to their slow accumulation and inability to directly modulate gene expression (Krause et al., 2012). This subclass of signals is almost certainly involved in coordinating nuclear and chloroplast gene expression during plastid development. Moreover, the second group of signals is thought to be involved in the rapid response to environmental changes. Although the release mechanism is unknown, protein signals are reported to be effectively "released", being able to directly influence gene expression when a cell requires a rapid nucleocytoplasmic response (e.g., attack by a pathogen, (Krause & Krupinska, 2009). Because of this and their potential to be visualized by fluorescence protein fusions make proteinogenic retrograde signals interesting for microscopy-based inquiries. Therefore, the known examples are introduced in more detail.

WHIRLY1: Only a few examples that experimentally support the idea of protein export from the plastid to the nucleus exist in the literature. The first instance of a protein repositioning from the plastid to the nucleus has been empirically shown for WHIRLY1 from *Arabidopsis thaliana*. This was done by creating transplastomic tobacco plants expressing HA-tagged AtWHIRLY1 (Isemer et al., 2012). Although the protein in those plants is exclusively synthesized in plastids, the authors found it also in the nucleus, suggesting a movement of the protein from the plastids to the nucleus. Interestingly, these transplastomic lines exhibited increased expression of the

nuclear trans-acting factor of pathogen response-related genes (*PR*; *PR1* and *PR2*) (Isemer et al., 2012).

PTM: PTM is another protein that is a chloroplast envelope-bound plant homeodomain (PHD) transcription factor (Sun et al., 2011). However, in contrast to WHIRLY1, PTM is attached to the plastid envelopes from the cytosolic side, which is why it does not have to cross the envelope membranes to reach the nucleus, where it accumulates after it is proteolytic released from the plastid surface. In the nucleus, it activates the transcription factor ABA-INSENSITIVE 4 (ABI4), which allows the status of the plastid to be sent to the nucleus (Krause et al., 2012).

NRIP1: The other instance where an experiment supported the migration of a plastid stroma localized protein to the nucleus is localization studies of the plant protein N RECEPTOR-INTERACTING PROTEIN 1 (NRIP1). In stable uninfected transgenic plants of *Nicotiana benthamiana* (N-containing, NRIP1-Cerulean expressing plants), this protein is predominantly found in the chloroplast (Caplan et al., 2008, 2015). When challenged with the Tobacco Mosaic Virus effector (TMV) p50, NRIP1 localization changes, and it can be observed not only in the plastid but also cytoplasm and the nucleus. Moreover, the localization change is enhanced when N is present, the p50 immune receptor from *Nicotiana tabacum*. Interestingly, in the context of this transport plastids showed changes in position and structure. In order to understand this observation better, the plant immune system will be explained briefly in more detail.

1.4 Retrograde signaling during the plant immune response

Plants operate innate immune responses via membrane-associated and intracellular receptors, which recognise the presence of a pathogen infection. Upon pathogen infection, plants activate innate immune responses through membrane-associated and intracellular receptors, making it arduous to determine the contribution of each component individually. (Man Ngou et al., 2020). Most plasma membrane-localized receptors distinguish conserved pathogen-associated molecular patterns (PAMPs) or host-cell-derived damage-associated molecular patterns (DAMPs) and prompt PAMP - or DAMP-triggered immunity (PTI-DTI), respectively (Jones & Dangl, 2006; Man Ngou et al., 2020; Sohn et al., 2009).

Moreover, plants also initiate a robust defence response by precisely identifying one or more pathogen secreted proteins (when recognized also called avirulence proteins). Phytopathogenic viruses, fungi, bacteria, and oomycetes can transfer such protein molecules, also known as effectors, into the host cytoplasm. They target plant cellular processes often associated with plant immunity, such as PAMP and DAMP pathways, which can enhance pathogen propagation (Jones & Dangl, 2006; Toruño et al., 2016). As a counter measure, plants evolved R genes to

recognize effector proteins and initiate another level of defence response to prevent pathogen spread, resulting in effector-triggered immunity (ETI) (Jones & Dangl, 2006; Khan et al., 2016). Plant intracellular immune receptors are members of a family of proteins identified as nucleotide-binding leucine-rich repeat (NB-LRR) proteins. NLRs recognize and trigger effector-triggered immunity (ETI), which frequently develops in a hypersensitive cell death response (HR). This fast and local cell death prevents phytopathogens from spreading within plant tissue (Klement & Goodman, 1967). As part of the ETI response, plastid-derived signals such as reactive oxygen species (ROS) and salicylic acid (SA) are believed to play critical roles.

1.5 How do retrograde signals travel from the plastid to the nucleus?

Although progress has been made in understanding which molecules might represent plastid-derived retrograde signals, how these molecules cross the plastid envelope membranes, travel through the cytoplasm, and finally reach the nucleus plasma remains open. In *Arabidopsis thaliana* and *Nicotiana benthamiana* plants, plastids have been observed to form during PTI / DTI responses, ETI responses, long tubular out folds of the envelope membranes, so-called stromules (Caplan et al., 2015; Erickson et al., 2014; Krenz et al., 2012). These structures are explicitly triggered during the initial stages of HR-PCD, following a plant receptor's recognition of an effector protein. Experiments by Caplan et al. 2015 suggest that stromules contacting the nucleus are beneficial for the ETI reaction (PCD), indicating a role for stromules in this important responsibility. The discovery of the formation of stromule-nucleus contacts during ETI responses by Caplan and co-workers provided a possible explanation for efficient plastid-to-nucleus signal transfer. This is further supported by observations that pro-defence signals such as hydrogen peroxide (H_2O_2) and salicylic acid are sufficient to trigger stromule-nucleus-contact formation (Caplan et al., 2015). It was proposed in this study that these tubules represent conduits for efficient retrograde signals, allowing the deposit of those molecules in close proximity to nucleus pores. In a follow-up study, this hypothesis was extended, adding the idea that stromules also guide plastid bodies towards the nucleus, allowing them to accumulate in close nucleus proximity and by this shortening the distance retrograde signals have to travel (Hanson & Conklin, 2020; Park et al., 2018).

Although this model of plastids reaching out for the nucleus with stromules is compelling, sufficiently long time-lapse imaging data supporting this hypothesis is missing. Additionally, data from different species and tissues, showing that the observations made in *N. benthamiana* are a general rule or an exception are missing too.

1.6 Therefore, this thesis will focus on …

Stromules and stromule-mediated plastid-nucleus interactions and will evaluate with **A**) time-lapse imaging in *A. thaliana* under ETI-induced and non-induced conditions if the observations from *N. benthamiana* are general rule or species-specific with **B**) time-lapse imaging in *N. benthamiana* if the proposed model for the role of stromules in plastid-nucleus interactions in this species holds true or has to be refined and with **C**) genetic tools to evaluate the direct or indirect involvement of stromules in the effector-triggered immune response.

1.7 What is "stromule"?

Nevertheless, what are stromules, and what is known about them?
Stromules are thin stroma-filled tubules defined by the outer and inner envelope membranes protruding from the plastid's surface into the cytoplasm (Erickson et al., 2017; Gray et al., 2001). These extensions range from a few µm to more than 65 µm. Stromules are about 0.4-0.8 µm in thickness (Gray et al., 2001). The long thin nature of stromules makes them distinct from other shapes the envelope membranes can form. It is assumed for plastids to be able to form stromules to have a relaxed membrane envelope. This wobbly membrane was observed very early in plastid research and the term "mobile jacket" was coined for it (Gray et al., 2001; Gunning, 2005; Hanson & Sattarzadeh, 2008; Holzinger, Buchner, et al., 2007; M. Schattat, Barton, & Mathur, 2011; M. Schattat, Barton, Baudisch, et al., 2011). It was suggested that stromules can shape easily because of this mobile loose membrane, and they are brisk extensions that change shape frequently (Gray et al., 2001; Park et al., 2018). This shape-changing manifests branching, extending, kinking, or retracting movements and takes place within seconds to minutes (Erickson et al., 2018; Gunning, 2005; Park et al., 2018; M. Schattat, Barton, & Mathur, 2011); we can observe these extensions form chloroplast. However, not only the chloroplast but also amyloplasts, etioplasts, and chromoplasts show stromule formation (Caplan et al., 2015; Erickson et al., 2017, 2018; Gray et al., 2001; Köhler et al., 1997; Natesan et al., 2005; M. H. Schattat, Klösgen, et al., 2012).

1.8 Stromules have been known for more than a century

The probably first depiction of a stromule-like structure was by the Australian botanist Haberlandt in 1888. He illustrated a chloroplast chain linked by thin strands of up to 30µm in length in *Selaginella martensii* and *S.kraussiana* with the help of light microscopy (Gray et al.,

2001). Even though he assumed that this chain-like structure could be the term interconnected plastids, it is thought that the structures described as these chloroplast chains correspond to the forms we call stromule today (M. H. Schattat et al., 2015). With further improvement of microscopes in the early twentieth century, stromule-like structures were reported more frequently. These reports showed that these extensions are present in an array of different plant species and even different types of plastids. However, the term "stromule" (stroma-filled tubule) was coined much later in 2000 by Köhler and Hanson (Köhler & Hanson, 2000), who targeted a few years before green fluorescence protein to the stroma of plastids in *N. tabacum*. These experiments showed that these extensions are indeed filled with stroma and provided a means for easy and straightforward visualization of these delicate structures (Köhler et al., 1997, 2000; Köhler & Hanson, 2000). (**Figure 1.1**)

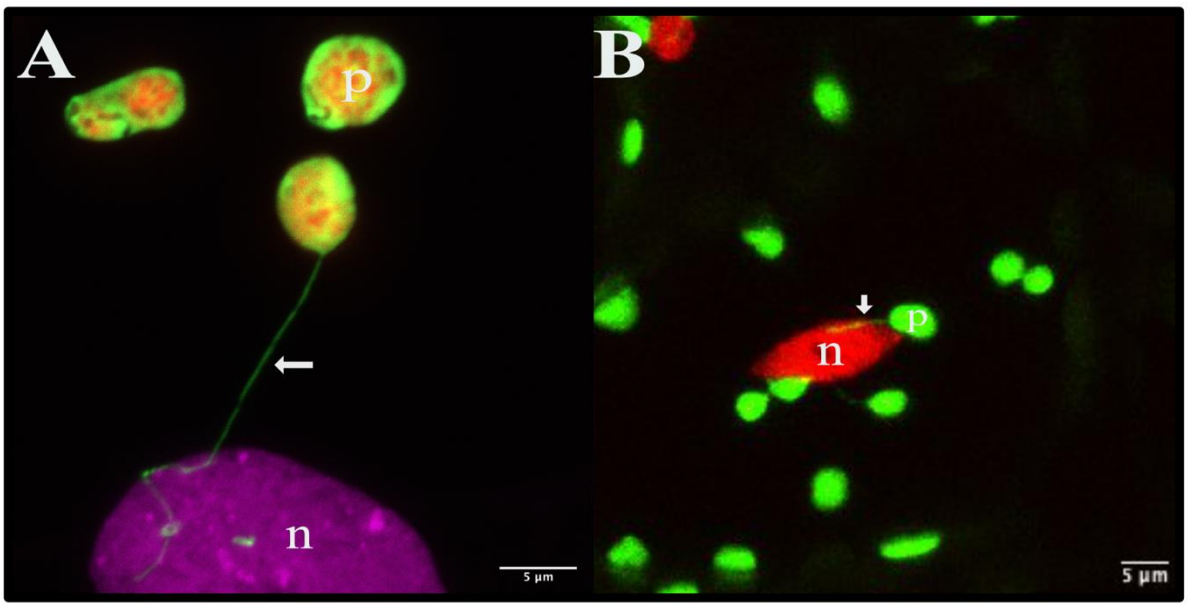

Figure 1.1 Stromule formation A CLSM fluorescence image of **A** *N. benthamiana* lower leaf pavement cell expressing a nucleus marker (*H2B:mCherry* in magenta) as well as a plastid stroma marker (*FNR: EGFP* in green), chlorophyll autofluorescence is depicted in red; p = plastid body, n = nucleus, arrow = stromule; **B** LSM image of an *Arabidopsis thaliana* upper epidermis cell expressing the plastid (green) and nucleus (mcherry) marker pLSU4::P35s:FNRtp:eGFP:T35s:pUBQ10:H2B:mCherry:TNos; scale bar corresponds to 5 µm.

1.9 How are stromules built?

It is suggested that two main requirements are necessary to form the plastid membrane into stromules, excess of plastid envelope membrane and forces, which reshape this membrane.

Membrane surface area: A completely spherical plastid has the minimum surface area to volume ratio and therefore no membrane available to change its shape. The ability to alter shape is facilitated by increasing the amount of membrane that is available. It is known that two plastid

envelope ion channels (plastid-localized homologs of the bacteria mechanosensitive channel MscS), MSCS-LIKE 2 and MSCS-LIKE 3 (MSL2 and MSL3) from *Arabidopsis thaliana*, control the plastid osmatic homeostasis during the development and normal growth and keep the plastid in a "deflated" state, characterised by an excess of envelope membrane. Therefore, in the wild type, *A. thaliana* has ovoid shaped plastids. However, a msl1/msl2 double mutant (*msl2-1/msl3-1*) shows enlarged, sphere-like plastids due to continuous water influx. Interestingly, stromules do not form in this mutant with "overinflated" epidermal plastids (Erickson & Schattat, 2018; Veley et al., 2012). This demonstrates that the plastid osmotic state must be regulated to generate the extra membrane necessary for stromule production.

Forces: If enough membrane is supplied, physical force applied to the envelope membranes can change their shape and can shape it into a tubular structure. Four different mechanisms, which can be responsible for the formation of tubular extensions from lipid vesicles, have been described so far (pulling motors, polymerization of membrane-associated proteins, pushing from an internal cytoskeleton, and induction of spontaneous curvature via protein insertion into the membrane (Roux, 2013). Current data shows that the movement of "pulling motors" along a cytosolic cytoskeleton to create force explains most stromule activity (Erickson & Schattat, 2018).

Cytoskeleton elements: It is suggested that cytoskeleton elements (actin and microtubule) support stromule extension of non-green plastids in the hypocotyl epidermis of *Nicotiana tabacum* (Kwok & Hanson, 2003). The authors found by inhibiting the cytoskeletal element's function (actin using cytochalasin D (CTD) and latrunculin B (Lat B); microtubules using oryzalin and aminoprophosmethyl (APM)) that stromule number and length decreased and plastid morphology was distinctively changed (Kwok & Hanson, 2003).

Anti-actin drug treatment produced stromule-filled loops, which are presumably stromules that have shrunken back into the plastid body. On the other hand, anti-microtubule drugs caused shorter and thicker stromules. Moreover, a combined treatment of actin and microtubule inhibitors, significantly reduced stromule frequency and had cumulative effects on stromule length reduction and plastid morphology. This early research revealed that cytoskeleton elements are required for stromule formation and that actin and microtubules contribute differently to maintaining stromule shape and quantity. A later study in *Nicotiana tabacum* leaf epidermis (Natesan et al., 2009) and *Oxyria digyna* mesophyll (Holzinger, Wasteneys, et al., 2007) revealed that microtubules had a minor role, with only actin inhibitors having any effect

on stromule frequency. These papers altered the focus away from microtubules and toward actin and the discovery of putative actin-associated motor proteins involved in stromule elongation. Therefore, it was surprising when Erickson et al., 2017 and Park et al., 2018 demonstrated the importance of microtubules (MTs) for stromule extension in *N. benthamiana*, by time lapse imaging and drug treatments. Park et al., 2018 found that stabilization of MTs results in augmented stromule frequency in chloroplasts of green leaf tissue of *N. benthamiana* and suggested that AFs function as an attachment point for stabilizing stromules, not necessarily for stromule extension. Taking together cytosolic cytoskeleton elements are necessary in one form or the other to create the forces needed for stromule formation.

1.10 Functions suggested for stromules

A well-established approach for evaluating the biological function of a process or a structure for plant survival is to isolate plants incapable of performing the process of interest or forming the structure of interest. This is mainly done by mutagenesis screens or approaches based on natural variation. However, so far, no plants displaying a total lack of stromules have been identified, making it necessary to look for alternative ways to determine their function until such mutants are available. An approach to understanding the importance of stromules has been to challenge plants with different stresses, metabolites, or chemicals and use the change in stromules frequency to measure the plant's reaction. In addition to a wide range of stromule-inducing conditions, several mutants with altered stromule frequencies have also been identified (reviewed in (Mathur, 2021)) **(Table 1-2)**. However, based on the obtained results no specific stress or process was identified by this method. Instead stromules seem induced when plants generally are exposed to stress or undergo changing physiological conditions. Still, several stromule functions have been proposed in the past 20 years (Hanson & Conklin, 2020). Here, I want to introduce the primary suggested function, which seems the most likely and has been addressed by more recent studies: *Stromules increase the interactive surface presented by the plastid to optimise molecule exchange between the plastid and its surroundings*. This idea is primarily based on microscopic studies in which stromules have been observed in association with other organelles. This is supported by observations of stromule formation in response to stress and other conditions, which generally require a higher rate of interorganellar exchange of metabolites, proteins, and signaling molecules (**Figure 1.2**) (Hanson & Conklin, 2020).

Gene	Changed expression level due to	Morphology of stromules/chloroplast	Proposed mechanism	Citation
ARC3, ARC6, ARC5	Lower expression in mutants	Considerably boosted stromules from larger chloroplasts	Partial chloroplast division apparatus	(Holzinger et al., 2008; Pyke, 1999)
ATG5	Mutant, Lower expression	Enhanced stromule abundance and length during starvation conditions	Autophagosome pathway interrupted; affects stress/ loss of membrane repossession	(Ishida et al., 2008)
CHUP1	Overexpression	Ectopic protrusions, some of which are stromules	Outer envelope membrane localization. Altered protein: lipid ratio	(Oikawa et al., 2008)
LACS9	Transient overexpression	Ectopic chloroplast extensions	Plastidial acyl-coenzyme A synthetase participating in the administering of fatty acids produced by chloroplasts	(Breuers et al., 2012; Schnurr et al., 2002)
MSL2, MSL3	Double mutant	Blow-up spherical plastids without stromules, but the extensions appear upon plant dehydration.	The osmoregulatory mechanism, including plastid mechanosensitive ion channels	(Veley et al., 2012)
OEP7	Overexpression	Ectopic chloroplast extensions	OEM localized. Altered protein: lipid ratio	(Yong Jik Lee et al., 2001)
PARC6	Mutant	Epidermal plastids abnormally elongated and clustered	Impaired division apparatus	(Ishikawa et al., 2020)
PGM1	Mutant	Elongated chloroplasts with loose grana.	Defective in sugar—starch metabolism. Accumulate sucrose during the diurnal cycle.	(Caspar et al., 1985; M. H. Schattat, Griffiths, et al., 2012)

Table 1.1 Some genes whose expression levels affect chloroplast extensions (stromule) in *Arabidopsis thaliana*. The table is adapted from (Mathur, 2021).

The involvement of chloroplasts, mitochondria, and peroxisomes in the same metabolic pathways has long been known, with photorespiration being a pathway that requires the transport of metabolites between the three compartments (Bobik & Burch-Smith, 2015). Indeed, these three organelles are frequently detected together (Bobik & Burch-Smith, 2015), raising the possibility that stromules increase the surface area accessible for interaction between them (Hanson & Hines, 2018).

During cytoplasmic streaming, mitochondria and peroxisomes, much smaller than the plastid, appear to pile up against extended stromules in some situations (Fester & Hause, 2005; Kwok & Hanson, 2004). Mitochondria often migrate along stromules or form associations. Extending stromule tips, possibly due to movement along the same actin scaffold (Fester & Hause, 2005;

Kwok & Hanson, 2004). The interactions between stromules and peroxisomes or mitochondria have been described as temporary (Barton et al., 2017; Gunning, 2005).

Organism/ Tissue	Condition	Morphology of stromules/chloroplast	Proposed mechanism	Citation
Fresh callus and cell suspensions of Tobacco	Correlated to tissue/organ-specific development/cautious interpretation.	Chloroplast body present. Mainly elongated plastids and stromules	High sucrose and phytohormone media. Possible effect on internal membranes in chloroplasts	(Köhler & Hanson, 2000)
Tomato	(Ripe fruit)	Enhanced stromule abundance	Mostly leucoplasts and chromoplasts. It might fall under tubular organelles	(Waters et al., 2004)
Epidermal leaf tissue of *Arabidopsis thaliana*	Vacuum infiltration of 40 mM sucrose or glucose solution into leaves	Enhanced stromule abundance	The mechanism is not precise. Speculated as an osmotic response	(M. H. Schattat & Klösgen, 2011)
Tobacco	Cells undertaking arbuscule formation during mycorrhizae colonization	Increased localization of chloroplasts to the nucleus and the formation of stromules	Cell invasion triggers ROS accumulation and alters cellular sugar status, and peroxisomes may respond.	(Fester et al., 2001; Fester & Hause, 2005)
Nicotiana benthamiana	Abutilon mosaic virus-infected cells	Enhanced stromule abundance	A combination of ROS-induced reactions that impact chloroplast envelope	(Krenz et al., 2010, 2011, 2012)
Tobacco, wheat	1-Aminocyclopropane-1-carboxylic acid (ACC)	Enhanced stromule abundance	Mimics pathogen attack conditions when the cell produces ethylene (ACC is the first precursor in the committed ethylene synthesis pathway)	(Gray et al., 2012)
Nicotiana benthamiana, Arabidopsis thaliana	Application to photosynthetic electron transport chain (pETC) inhibitors	Enhanced stromule abundance	implicate internal light-sensitive redox signaling pathways	(Brunkard et al., 2015)
Tobacco, wheat	1 µM silver nitrate	Reduces stromule abundance	Prevents ethylene activity. Might be linked to ROS regulation	(Gray et al., 2012)

Table 1.2 Some conditions and treatments affect the stromule extensions in different plant species. The table adapted from Mathur 2021(Mathur, 2021).

One experiment found an equal number of mitochondria and peroxisomes to associate with the plastid body and the stromule (Barton et al., 2017). However, few conclusions can be drawn

because interactions between stromules, peroxisomes, or mitochondria have seldomly been thoroughly explored or quantified.

Stromules may increase exchange by trapping smaller organelles during cytoplasmic streaming, potentially boosting the duration or number of connections with the plastid, despite the transient nature of such interactions. On the other hand, the interaction between the plastid and nucleus is currently gaining more attention(Caplan et al., 2015; Erickson et al., 2017; Sampath Kumar et al., 2018)

1.11 Plastid-nucleus interaction and stromules

The nucleus is a unique organelle to which plastids might seek an optimized way of exchanging molecules. As a result of gene transfer as part of the chloroplast domestication process, the nucleus plays a special role for plastids. As described earlier in the introduction, retrograde plastid-to-nucleus signalling helps to coordinate this special relationship. Retrograde signalling has been identified and studied mainly with the help of genetic tools. However, whether a physical interaction between both organelles is needed for efficient communication is still unclear. Based on observations of stromules that bridge the distance between plastid bodies and the nucleus in response to effector-triggered immunity, it was suggested that plastids at a greater distance from stromules to reach out to the nucleus to directly deliver plastid-derived defence signals (Caplan et al., 2015).

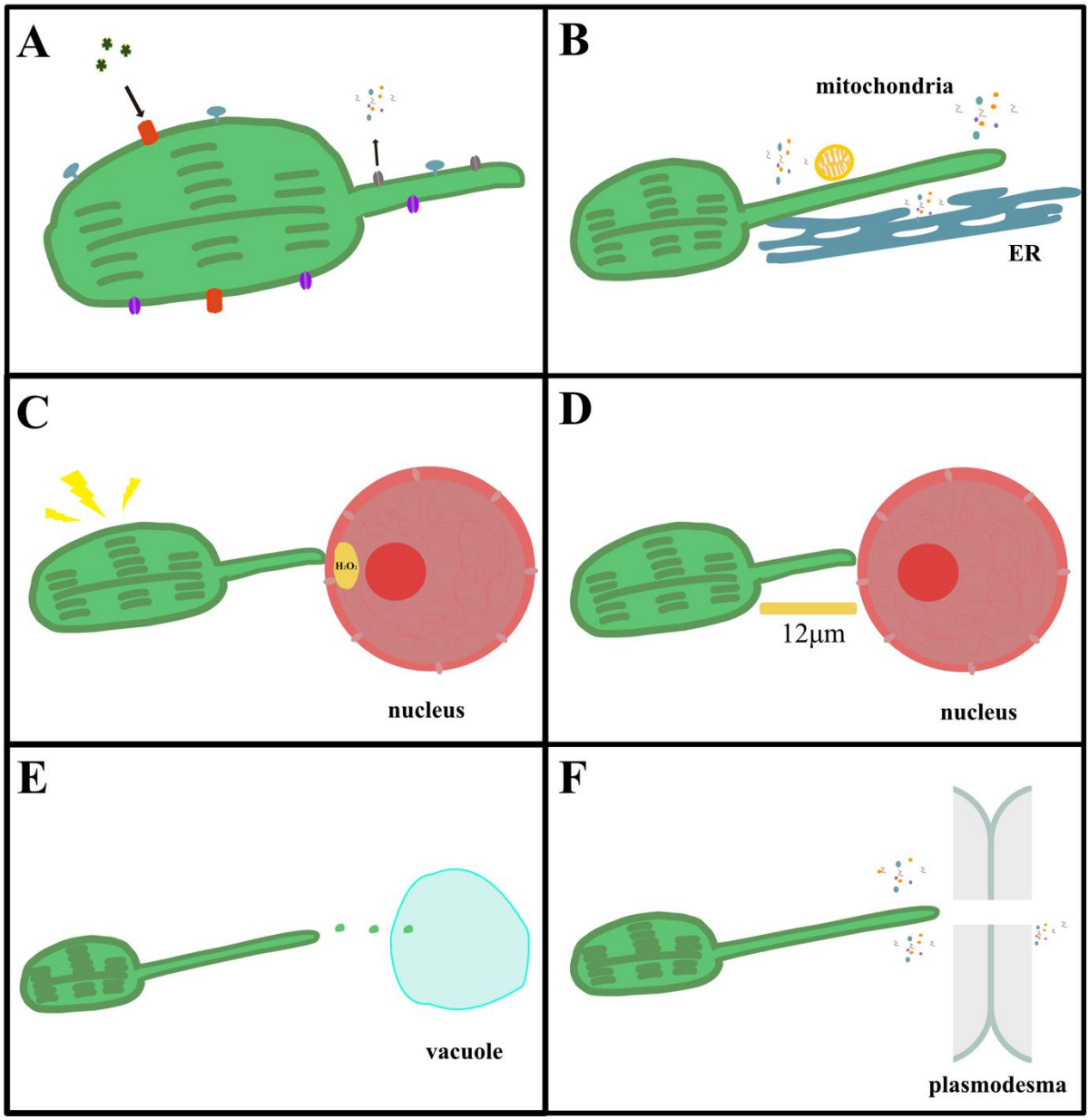

Figure 1.2 Potential role of the stromules. Stromules extend from the envelope membrane to the inner membrane and further expand the compartment within the cytoplasm; they can play a role in import and export. B Chloroplasts can exchange molecules with various compartments; stromules can locate the stromal compartment near a decreased diffusion distance. C When a pathogen attacks plant cells, chloroplasts reveal reactive oxygen species, which stromules may transfer; these ROS-related compounds to the nucleus, resulting in altered gene expression. D Stromules may serve the purpose of gathering chloroplasts at the nucleus by supplying directional information or by pulling them there. E Stromule tips may detach and enter the vacuole for protein recycling or eliminating hazardous compounds. F Near plasmodesmata, stromules may transmit signals to other cells. The figure is adapted from (Hanson & Conklin 2020).

This hypothesis assumes that stromules are directly involved in signal transfer. Later, the role of stromules in this interaction was extended. It was suggested that rather than sending the signals through stromules to the nucleus, stromules are means of finding the nucleus in the

cell's void and guiding the movement of the plastid body toward the nucleus (Kumar et al., 2018) **(Figure 1.3)**.

Although these two listed publications made important initial observations, experimental data is missing to fully support the suggested function of stromules in plastid-nucleus interactions. On the one hand, published data rely on snapshots or short time-lapse experiments, which do not cover the complete process from tissue exposure to the initial trigger (recognition of the ETI-inducing effector) to the fully formed plastid-nucleus complexes. Therefore, the dynamics of those organelles and the stromule's role in this are still unclear. However, the available information on stromules in response to ETI in *A. thaliana* is only available for plastids. It lacks the context of the nucleus, leaving open whether the reported observations made in *N. benthamiana* also apply to *A. thaliana* (Caplan et al., 2015).

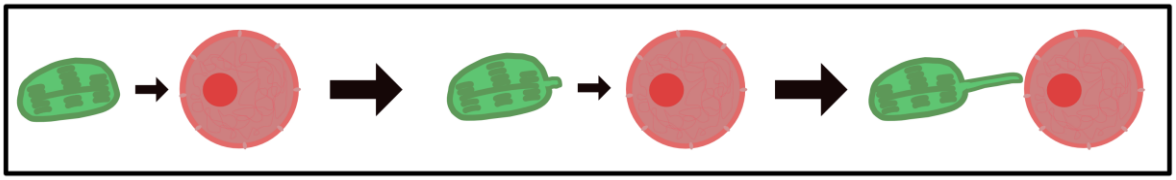

Figure 1.3 Possible representation of plastid nucleus interaction in *N. benthamiana.* Plastids can send the stromule formation to the nucleus and contact the nucleus surface.

II. Goals

To understand the extent to which plastid-nucleus interactions take place and which role stromules play in this process, the main goal of this thesis is to use *Nicotiana benthamiana* lower epidermis and *Arabidopsis thaliana* upper epidermis as model systems and:

A) use long-term time-lapse imaging in *N. benthamiana* with the aim to test if the proposed model for the role of stromules in plastid-nucleus interactions in response to a triggered ETI in this species holds true or has to be refined;

B) use time-lapse imaging in *A. thaliana* under ETI-induced conditions with the aim of understanding if the observations made in *N. benthamiana* are a general rule or species-specific (MultigeneEffectorTriggeredImmunity =METI);

C) use time-lapse imaging in *A. thaliana* under non-induced conditions to understand the nucleus-plastid interactions previously described stromule-promoting zone in upper epidermis cells in this species.

III. Material and Methods

Material

3.1 Equipment and devices

Device – Equipment	Supplier
BioDocAnalyze (2.2)	Biometra, Göttingen, Germany
Biometra thermal cycler	AnalytikJena, Jena, Germany
Biometra thermal cycler trio	AnalytikJena, Jena, Germany
Celldensetymeter RS	Fisher Scientific
E.coli Pulser	BioRad Laboratories GmbH, Munich, Germany
Eppendorf thermo Cycler	Eppendorf AG, Hamburg, Germany
G24 Enviromental Incubator shaker	New Brunswick Scientific, N.J, USA
Inforse HT Ecotron shaker	Infors AG, Bottmingen, Switzerland
Leica LSM Stellaris 8 Confocal Microscope	Leica Microsystems, Wetzlar, Germany
Mini Table Centrifuge	Biozym
Mitsubishi P95 printer	Biometra, Göttingen, Germany
MICRO STAR 17R	VWR, Part of Avantor
Scanner	Canon Electronic
Table weight	Sartorius
TB2 Thermoblock	Biometra, Göttingen, Germany
Trans-Blot Turbo Transfersystem	BioRad Laboratories GmbH, Munich, Germany
ThermoMixer C	Eppendorf AG, Hamburg, Germany
Vortex-Genie 2	Scientific Industries, Bohemia, USA
ZEISS Epifluorescence Microscope	Carl Zeiss, Jena, Germany
ZEISS LSM 780 Laser Scanning Microscope	Carl Zeiss, Jena, Germany

Table 1.3 list of the devices

3.2 Chemicals

Chemical	Supplier
Acetosyringon	Carl Roth, Karlsruhe, Germany
Bacto -Agar	Becton Dickinson
Benzo(a)pyrene	Carl Roth, Karlsruhe, Germany
Biozym LE	Biozym Scientific GmbH, Hessisch Oldendorf, Germany
Biozym LE GP Agarose	Biozym Scientific GmbH, Hessisch Oldendorf, Germany
Calciumnitrat $4H_2O$	Carl Roth, Karlsruhe, Germany
Estradiol (E2)	Carl Roth, Karlsruhe, Germany
Ethanol	Carl Roth, Karlsruhe, Germany
Ethidiumbromid	Carl Roth, Karlsruhe, Germany
Glycerin	Carl Roth, Karlsruhe, Germany
Meat extract	Carl Roth, Karlsruhe, Germany
Mes	Carl Roth, Karlsruhe, Germany
Murashige & Skoog-Medium, incl. modified vitamins	Duchefa, Haarlem, Netherlands
Peptone	Carl Roth, Karlsruhe, Germany
Pyto agar	Duchefa, Haarlem, Netherlands
Silwet L77	Leu + Gygax
Sucrose	Carl Roth, Karlsruhe, Germany
TRIS	National diagnostics
Tween 20	Carl Roth, Karlsruhe, Germany
X-Gal	Duchefa Biochemie
Yeast extract	Carl Roth, Karlsruhe, Germany
1-Naphthaleneacetic acid (NAA) (#N0640)	Carl Roth, Karlsruhe, Germany
Isopropyl β-D-1-thiogalactopyranoside (IPTG), dioxane free	Carl Roth, Karlsruhe, Germany

Table 1.4 Chemicals

3.3 Antibiotics

Antibiotic	Stock concentration	Solvent	Standard working concentration	Supplier
Kanamycin	100 mg/ml	H_2O	50 - 100 µg/ml	Duchefa, Haarlem, Netherlands
Ampicillin	100 mg/ml	H_2O	100 µg/ml	Duchefa, Haarlem, Netherlands
Carbenicillin	100 mg/ml	H_2O	100 µg/ml	Duchefa, Haarlem, Netherlands
Rifampicin	50 mg/ml	DMSO	100 µg/ml	Duchefa, Haarlem, Netherlands
Spectinomycin	100 µg/ml	H_2O	50 - 100 µg/ml	Duchefa, Haarlem, Netherlands
Streptomycin	100 µg/ml	H_2O	50 - 100 µg/ml	Duchefa, Haarlem, Netherlands
Gentamycin	20 mg/ml	H_2O	40 µg/ml	Duchefa, Haarlem, Netherlands
Hygromycin	40 mg/ml	H_2O	40 µg/ml	Duchefa, Haarlem, Netherlands

Table 1.5 antibiotics used

3.4 Consumable and kits

Kits	Supplier
NucleoSpin® Plasmid EasyPure	MACHEREY-NAGEL
NucleoSpin Gel® und PCR Clean-up	MACHEREY-NAGEL

Table 1.6 Kits for molecular biology

3.5 Enzymes

Enzymes	Supplier
BsaI-HF®v2 (Restriction enzymes)	Biolabs
BpiI (Restriction enzymes)	Thermo Fisher Scientific
T4 DNA-Ligase (5U/µl) (DNA-Ligation)	Thermo Fisher Scientific
T4 DNA-Ligase (30U/µl) (DNA-Ligation)	Thermo Fisher Scientific
Phusion HF DNA-Polymerase (DNA-Synthase)	Thermo Fisher Scientific
GoTaq® DNA-Polymerase (thermostable) (DNA-Synthase)	Promega Corporation
dNTP (10 mM) deoxynucleoside triphosphate	Carl Roth, Karlsruhe, Germany

Table 1.7 Enzymes

3.6 Bacterial strains

Microorganism	Strain
Escherichia coli	Top 10
Agrobacterium tumefaciens	GV3101
Agrobacterium tumefaciens	LBA4404

Table 1.8 Bacterial strains

3.7 Plant material

Species	Line	Gene(s)	transgene	Citation
A. thaliana	Col-0	WT		
	Col-0 pn	WT	FNReGFP & H2B:mcherry	(Erickson et al., 2017)
	Col-0 an	WT	eGFP:ABD2:eGFP H2B:mcherry	unpublished
	msl2_msl3	msl2 At5g10490 msl3 At1g58200	*none*	(Veley et al., 2012)
	msl2_msl3 pn	msl2 At5g10490 msl3 At1g58200	FNReGFP & H2B:mcherry	unpublished
	kac1_kac2	kac1 At5g10470 kac2 At5g65460	None	(Suetsugu et al., 2016)
	kac1_kac2 pn	kac1 At5g10470 kac2 At5g65460	FNReGFP & H2B:mcherry	unpublished
	Kac1_kac2_chup1	kac1 At5g10470 kac2 At5g65460 chup1 At3g25690	None	(Suetsugu et al., 2016)
	Kac1_kac2_chup1 pn	kac1 At5g10470 kac2 At5g65460 chup1 At3g25690	FNReGFP & H2B:mcherry	unpublished
N. benthamiana	Wild type	none	none	
	N. benth pn	WT	FNReGFP & H2B:mcherry	(Suetsugu et al., 2016)

Table 1.9 Plant material

3.8 Culture media

Bacterial and plant culture medium was autoclaved for 20 minutes at 121°C before use.

LB-Medium (Luria Bertani- Medium)	**Component, amount (liter)**
For solid medium	peptone or tryptone, 10 g/l yeast extract, 5 g/l NaCl, 10 g/l Bacto agar 1.2%
YEB medium (Yeast Extraction Buffer)	
For solid medium	beaf extract (powder), 5 g/l yeast extract, 1 g/l peptone, 5 g/l sucrose, 5 g/l $MgCl_2$ (optional), 0,5 g/l Bacto agar 1.2%

***Arabidopsis thaliana* minimal medium (AT medium)**	**Component, amount (liter)**
Macronutrients (Macronutrients are prepared as individual stocks)	
	KNO_3 (1M), 5 ml
	KH_2PO_4 (1M), 2,5 ml
	$MgSO_4$ (MgO_4S*7H_2O) (1M), 2 ml
	$Ca(NO_3)_2*4H_2O$(1M), 2 ml
	Fe(EDTA) (1M), 2ml
Micronutrients (Micronutrients are prepared as one solution. Of this solution only 1 ml / l medium is needed)	
	H_3BO_3 (70mM)
	$MnCl_2*4H_2O$ (14mM)
	$CuSO_4*5H_2O$ (0,5mM)
	$ZnSO_4*7H_2O$ (1mM)
	$NaMoO_4*2H_2O$ (0,2mM)
	NaCl (10mM)
	$CoCl_2*6H_2O$ (0,01mM)

Table 1.10 Bacterial and plant culture medium

3.9 Plasmids

Modules used from the MoClo Plant Tool Kit

Name	Descriptions
pAGM1301 (G1)	L0-Acceptor for CT-Module, Spectinomycin- L0-Acceptor for Pro+ 5'-UTR Module, Spectinomycin-Resistance
pICH41295 (G2)	Level zero acceptor for Pro + 5U modules
pICH47742 (C3)	L1-Acceptor (Position 2, Forward orientation), Carbenicillin-Resistance
pICH47751 (D3)	L1-Acceptor (Position 3, Forward orientation), Carbenicillin-Resistance
pAGM4723 (A5)	L2-Acceptor, Kanamycin-Resistance
pICH41766 (D5)	L2-End-Linker (for 3 L1-Module)
pICH51277 (A3)	Promoter (0.4 kb), 35s (CaMV) + 5'UTR, Ω (Tobacco Mosaic Virus)
pICH87633 (D3)	Promoter, nos, (*A. tumefaciens*) + 5'UTR, Ω (Tobacco Mosaic Virus)
pICH88103 (F3)	Promoter + 5'UTR, ocs, (*A. tumefaciens*) + 5'UTR
pICSL50009 (B8)	C terminal HA tag (6x Human influenza hemagglutinin)
pICH41414 (F11)	3'-UTR, Polyadenylation signal + Terminator, 35S (CaMV)
pICH41432 (D12)	3'-UTR, Polyadenylation signal + Terminator, ocs (*A. tumefasciens*)

Other plasmids

Name	Descriptions
pGGA11:mOrange2	See for details: (Prautsch et al., 2022)
pGGA11:XopQ:mOrange2	See for details: (Prautsch et al., 2022)
plsu4 pn	genes on T-DNA: HygR, p35S:tpFNReGFP:t35S, pUBQ10:AtH2B:mcherry:tNOS (Erickson et al., 2017)
L2	Genes on T-DNA: BastaR; p35S:eGFP:ABD2:eGFP:tNOS; pUBQ10:H2B:mcherry:tNOS) (not published)
L2	Genes on T-DNA: BastaR; BastaR; p35S:eGFP:ABD2:eGFP:tNOS; pUBQ10:NLS40:mKOK:GUS:tOCS; pOCS:ssu:E2Crimson:tOCS (not published)

Table 1.11 Plasmids

3.10 Software and online tools

Software	Application	Supplier
Affinity designer	Figure/tables – images editor	Serif (Europe) ltd
Combine ZP	Stack images, digital image processing	Alan Hadley
Fiji v.2.0.0- rc-31	Image processing and analysis	Wayne Rasband National Institutes of Health, USA (http://imagej.nih.gov//ij), (Schindelin et al., 2012)
Geneious prime	DNA sequence analysis	Biomatters, Inc. Boston, MA, USA
Imaris 9.6.1	Microscopy image analysis	Oxford instruments
Inkscape	Vector graphics editor	Inkscape project
Leica Application Suite X (LAS X)	Microscopy	Leica Microsystems, Wetzlar, Germany
Mendeley	Reference management	Elsevier
Microsoft Home and Student 2016, Microsoft Office 365 (PowerPoint, Excel, Word)	writing text, figures/tables, and data analysis	Microsoft Corporation, Redmond, WA, USA
Snapgene 5.2.5	DNA sequence analysis	Gsl Biotech LLC, Boston, MA, USA
SigmaPlot 12.6	Statistical tests, data analysis, and graph plotting	Systat Software Inc. Illinois, Chicago, USA
ZEN 2.3 SP1 FP3 (black-blue version)	Microscopy	Carl Zeiss, Jena, Germany

Online	Application	Supplier
NCBI Gene Database	Gene sequences for cloning	National Center for Biotechnology Information, U.S. National Library of Medicine, Rockville Pike, Bethesda, MD, US

Table 1.12 Software and online tools

Methods

3.11 Imaging stable transgenics and transiently expressing *N. benthamiana*

Plant line selection in *N. benthamiana*: Stable transgenic *N. benthamiana* plants carrying the transgenes *p35S::FNReGFP* (plastid) and *pAtUBQ10::H2Bmcherry* (nucleus) were used to visualize plastids and nuclei. To select homozygous *N. benthamiana* transgenic plants, the seeds were sterilized and grown on ½ MS medium (containing ½ strength MS salts, 0.8% Phyto agar) with appropriate antibiotics including hygromycin **(Supplementary Figure 1, Supplementary Table 1)**. The germination rate and the fluorescence intensities of each T2 line were checked and the Nb-pn line#04-01 was selected for further experiments. The plants were grown in soil in a greenhouse under long-day conditions (16 h light/8 h dark), with a daytime temperature of 23°C, a night-time temperature of 19°C, and humidity around 55%.

Bacterial strains and constructs: For all transient assays, we utilized the *Agrobacterium tumefaciens* strain LBA4404 (Hoekema et al., 1983). Constructs for the expression of XopQ-mOrange2 and LBA4404 mOrange2 were generated in pGGA11, a binary vector based on the backbone of pBGWFS7. pGGA11 providing a 35S promoter and a C-terminal mOrange2 (similar to pGGA1 cloning described in (Schulze et al., 2012). For details see also **Supplementary Table 1**. Stable transgenic plants were generated by the help of GV3101 (pMP90) (Koncz & Schell, 1986).

***A. tumefaciens* mediated transient expression:** For inoculations, plasmids were transformed into *A. tumefaciens* strain LBA4404 via electroporation (Bio-Rad, E.coli Pulser, Munich, Germany). The strains harboring the binary vectors were grown overnight in 5 ml YEB liquid cultures supplemented with the appropriate antibiotics to grow LBA4404 (100 μg mL^{-1} rifampicin and 20 μg mL^{-1} streptomycin) and for selected the plasmid (e.g. pGGA11=100 μg mL^{-1} spectinomycin). The *A. tumefaciens* cultures were subjected to centrifugation and then re-suspended in Agrobacterium infiltration medium (AIM), which comprises 10 mM $MgCl_2$, 5 mM MES at pH 5.3, and 50 μm acetosyringone. The fully developed leaves of 5–7-week-old *N. benthamiana* plants were inoculated with bacteria that harbored the respective plasmid. As control AIM alone was infiltrated. To visualize plastid shape and nucleus position the used *N. benthamiana* stably expressed the following organelle marker genes: *p35S::tpFNReGFP*:*t35S* (plastid) and *pAtUBQ10::H2Bmcherry*:*tNOS* (Nucleus) plants. The OD_{600} was adjusted to 0.2 for each bacterial strain (Erickson et al., 2018).

Effector triggered immunity response quantification of starting point: Before taking a long-term movie, we first analyzed the Effector triggered immunity response starting point in *N. benthamiana*. Leaf discs were collected from fully expanded leaves from infiltration spots (see inoculations). A single leaf disc of each infiltration spot was harvested using a cork borer. Infiltered spots (lower leaf epidermis) were mounted on the microscope slide (3 replicates per treatment). In order to provide optimal conditions for longer time periods leaf discs were mounted on AT medium (contains 1 % agar) agar discs of the size of leaf discs. A drop of tap water was used in the leaf disc to prevent the leaf disc from drying out during imaging **(Supplementary Figure 3A-3B)**. Microscope slides were kept, next to the soil grown plants, in a greenhouse under long-day conditions (16 h light/8 h dark), with a day temperature of 23°C, a night temperature of 19°C, and around 55% humidity **(Supplementary Figure 3C)**. ETI response was examined with the Zeiss microscope with different time points of 16h, 24h, and 48h.

Long-term Movie acquisition *N. benthamiana*: Infiltrated *N. benthamiana* transgenic pn line plants (always refer as #04-01 line number) were used to record long-term movies of plastid and nucleus interaction. A single leaf disc of each infiltration spot was harvested using a cork borer to quantify the ETI effect on plastid nucleus interaction. To observe ETI, mOrange control, and AIM control spots together, 3 spots were mounted next to each other on the same microscope slide **(Supplementary Figure 3D)**. The setup allowed to take up to 5 movies in parallel. Movies were started approx. 24h (1day) post inoculation (dpi) using a confocal microscope (Zeiss LSM 780 microscope on a AxioObserverZ1 inverted stage, Carl Zeiss GmbH, Jena, Germany). Movies were recorded a z-stacks with a Plan-Apochromat 20×/0.8 M27 (Carl Zeiss GmbH, Jena, Germany) lens. Fluorescence was excited by a 488 nm laser line from a multiline argon laser (25 mW) and a 561 nm diode laser. Emission was acquired in individual channels: eGFP (493–556 nm), mCherry (596-623 nm), and chlorophyll (658 758 nm). A separate channel was used to record the transmitted light image. Preliminary work optimized the laser intensity (488 nm 1.8 percent; 561 nm 2%), pixel dwell time (0.79 s), line averaging (2 times) and image size (2,048x2.048). Frames of the time lapse experiment were 12min apart. This was done to minimize the effect of laser light on the cells. The stability of chlorophyll fluorescence was used to estimate the impact of laser light on plant tissue based on its sensitivity to bleaching. The microscope manufacturer's software (ZenBlack), was used to control the microscope setup (Carl Zeiss GmbH, Jena, Germany).

Analyzing long-term movies *N. benthamiana*: For image analysis z-stack time lapse data were projected into 2D by maximum intensity projection using ZenBlack or Fiji (Schindelin et al., 2012) Z-projected time laps data was analyzed as described in the results section for plastid nucleus interactions and construct expression.

3.12 Long-term imaging of *A. thaliana*

Genotyping of chup1-3/kac1-2/kac2-2 (ckk) and kac1-2/kac2-2 (kk): The seeds were provided by Noriyuki Suetsugu (Suetsugu et al., 2010) to ensure that mutants carry said mutation and provide their identity by genotyping. Before experiments the identity of transgenic seeds was confirmed by genotyping the respective genes for the expected mutations. The kac1-2 mutant carries a 54T deletion and thus disrupts the recognition sites CspI (and the isoshizomers) in the kac1-2. chup1-3 mutant carries a C-to-T substitution (Q75STOP, exon3 61 C-to-T) and thus produces the recognition sites Tsp509I (and the isoshizomers) in the chup1-3. In order to distinguish between wild type and kac1-2 or chup1-3 I performed PCR followed by CAPS analysis and sequencing (Kac1-2-for: 5´GCTGCTGCTTCAATTCTTGC3´; Kac1-2-rev: 5`ATCAGTAGCTTCTTGTCTCAACTCC3`; chup1-for 5`TTCACCTTCAAGTTTCACTTC3`, chup1-rev: 5`GACAAAGAACAGTCTGTGG3´). kac2-2 carries a T-DNA insertion in the 22th exon of KAC gene. I used the primers for RT-PCR in (Suetsugu et al., 2010) PNAS to test for T-DNA presence. Based on fluorescence brightness of the organelle markers the selected *ckk* and *kk* lines (used for the time-lapse experiment) were genotyped (line #2, #3, #4 for *ckk* and 4 and 5 for *kk*).
DNA isolation protocol: 2 young leaves were chosen and transferred into a 1.5 ml tube. DNA extraction buffer was added to the leaves (400 µl; containing 200mM Tris / HCl pH 7,5, 250mM NaCl, 25mM EDTA and 0,5% SDS). Leaves were shredded with micro-pestles via twisting and applying pressure (Before application, pestles were washed for 30 sec in EtOH 70%).

Bacterial strains and construct in *A. thaliana*: Stable transgenic lines of *A.thaliana* were mediated by *A.tumefaciens* strain GV3101 (pMP90) (Koncz & Schell, 1986) Bio-Rad, *E. coli* Pulser (Munich, Germany) was used for bacterial transformation, and the floral dip method (Davis et al., 2009) was used to create transgenic to *A. thaliana* seeds.

Plastid nucleus marker information: *Arabidopsis thaliana* col-0 was used as a wild type in this study. The plastid nucleus marker construct is based on the *tpFNReGFP* marker described

in (M. H. Schattat & Klösgen, 2011) which consists of the N-terminal transit peptide of the FNR protein fused to eGFP. The construct us driven by a short p35S promotor. The TMV omega leader sequence acts as a 5´UTR. As terminator a t35S was chosen. The nucleus marker is composed of the histone H2B from *A. thaliana* fused to the N-terminus of mcherry. The construct is driven by the pAtUB10 promotor and is terminated by the NOS terminator. As a T-DNA backbone plsu4 was chosen

Plant growth conditions: Transgenic and wild type *A. thaliana* plants were soil-grown at 100 to 120 $\mu E/m^2 s^1$ in short-day conditions (8 h light/16 h dark) at 60% relative humidity and 21°C.

Preparation of leaf samples for imaging: Leaves were collected from the youngest fully expanded rosette leaves of 10 –12-week-old plants and placed in a 1,5 ml tube containing water a vacuum was applied to this tube using a 10 ml syringe placed on top when the plunger of the tube is pulled; upon release water is forced into the intracellular space resulting in low light scattering making microscopy pictures more clear.

Acquisition of individual z-stacks for still images and time series: Movies were recorded with a Zeiss LSM 780 microscope on a AxioObserverZ1 inverted stage (Carl Zeiss GmbH, Jena, Germany). C-Apochromat 63×/1.20 W Korr M27 (Carl Zeiss GmbH, Jena, Germany) lens. Fluorescence was excited by a 488 nm laser line from a multiline argon laser (25 mW) and a 561 nm diode laser. Emission was acquired in individual channels: eGFP (493–556 nm), mCherry (596-623 nm), and chlorophyll (658 758 nm). The microscope manufacturer's software (ZenBlack), was used to control the microscope setup (Carl Zeiss GmbH, Jena, Germany).

Data analysis of still images: Measurements of still images were performed via standard analysis tools of Fiji.v.2.0.0-rc-43; for data handling, Microsoft Excel (version 14.4.4); for statistical work Sigmaplot 13.

Measurements of the cell and nucleus size: Still images were imported into LSM Image Browser Version 3.5 to trace the cell contours to show the correlation between cell and nucleus size. Only contours/shapes were imported to Fiji to measure the size of the epidermal cells. Analysis was done with the help of contrast and threshold settings to identify epidermal cells.

With the "analyze particles" tool cell numbers size was measured. Cell outlines and fluorescence images of nuclei were merged to measure nucleus size and to assign this measurement to the respective cell size measurement. In case detection of nuclei failed the size was measured manually.

Time-lapse movie acquisition: A chamber was created to prevent leaves from drying out during movies by applying a c-shaped string of silicon grease to a glass slide. The leaf section was placed with a drop of tap water in the middle of the silicon "c" and covered with a glass coverslip (high precision No. 1.5%H 170 +/- 5 um). Excess water was removed from under the coverslip using a paper towel, thus allowing for gas exchange.
Imaging was done using a Zeiss LSM 780 microscope (Carl Zeiss GmbH, Jena, Germany) based on an inverse AxioObserver and equipped with a 63x lens (C-Apochromat 63x/1.20 W Korr M27, Carl Zeiss GmbH, Jena, Germany). Fluorescence was induced via a 488 nm laser line of a multiline argon laser (25 mW) and a 561 nm laser. Fluorescence was recorded in single-track mode. Individual channels for eGFP (493-556 nm), for mCherry (596-623 nm), and chlorophyll (653-758 nm) were defined. The transmitted light image was recorded in a separate channel. In preparatory work, laser intensity (488 nm 1.2%, 561 nm 0.5%), pixel dwell time (1.58 us), line averaging (2 times), pixel number (1,024 x 1,024) as well, and the frame rate (3 min) was optimized to minimize the impact of laser light on the cells. Based on its sensitivity to bleaching, the stability of the chlorophyll fluorescence was used to estimate the effect of the laser light on the plant tissue.

Time-lapse movie processing: At least ten movies for WT, *msl2-1_msl3-1*, *kk* and *ckk* were acquired. Because it was known from previous work in upper epidermis of WT *A. thaliana* that cell size has an impact on nucleus size and nucleus movement as well as stromule behavior (Erickson et al., 2017), for all aspects cells of different size categories were analyzed separately. Because epidermis cells are rather flat cells and almost all plastids reside at the “bottom” of the cell, an epidermis represents a quasi 2D space. In order to simplify analysis stacks were projected into 2D by a maximum intensity projection.

Time-lapse analysis: The maximum intensity projections of time-lapse movies were imported into Imaris, which was used for nuclei tracking and speed measurements; the program detected the nuclei of the upper epidermis with the help of the round shape, approximate size, and the

estimate of the maximum distance in the mCherry channel (DsRed) stomata nuclei were excluded during these measurements. Nuclei were taken into consideration for speed measurements when Imaris was capable of locating and tracking a nucleus for at 9 frames, which corresponds to approximately 30 minutes. The first frame of the maximum projections was utilized for measurements of the nucleus size in the movies to get a single image, and the maximum intensity projection was imported into Fiji 2.0.0, duplicating the first frame from the mCherry channel; this image was used to measure the different sizes via threshold. Statistical tests were performed with SigmaPlot12. Graphs were plotted using Excel or SigmaPlot12.

Plastid nucleus marker lines: For recording time-lapse z-stacks of plastids and nuclei, fully expanded leaves of primary selected 4-week-old pLSU4::P35S:FNRtp:eGFP:T35S: PUBQ10:H2B:mCherry:tNos (hereafter called pLSU4::pn) transgenic plants were utilized. The T0 seeds were germinated and incubated for 4 days on AT media (Ruegger et al., 1997) plates containing 40 µg mL−1 hygromycin and 250µg mL−1 cefotaxime. Resistant plants were screened for fluorescence and transferred to soil. After 4 weeks of cultivation on the soil at 21◦C under short-day conditions (8 h light/16 h dark) with a light intensity of 120µE m−2 s −1, mature rosette leaves were harvested and prepared for imaging.

IV. Results

4 A Plastid-nucleus interaction during Effector triggered immunity

Transient expression mediated by *Agrobacterium tumefaciens* in *N. benthamiana* is an often-used strategy to study ETI responses (Erickson et al., 2018). The possibility of introducing multiple constructs needed for a complex experiment by mixing different strains of *A. tumefaciens* is one of the benefits of this method, allowing comparatively fast testing of a given hypothesis. It is known that during the ETI response, *N. benthamiana* demonstrates a strong stromule and plastid accumulation response (Caplan et al., 2015). To test which role stromules play during ETI-induced plastid accumulation, I aimed to record time-lapse data covering the plastid accumulation process from an early stage (normal plastid distribution) to late stages (finished plastid-nucleus accumulation) **(example in Figure 4.1)**.

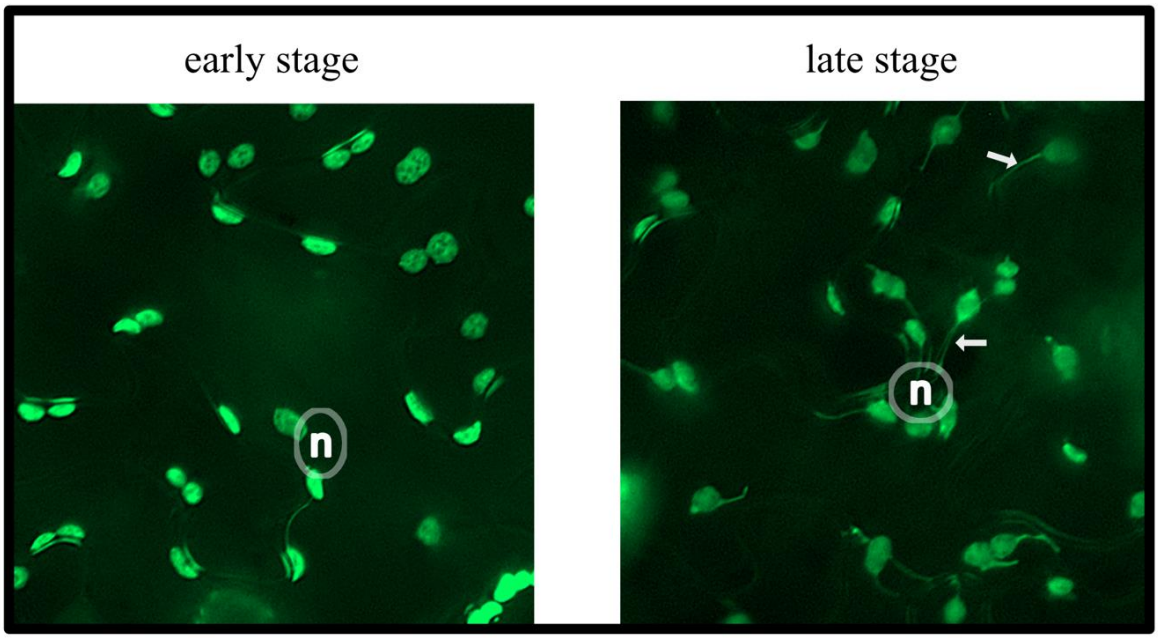

Figure 4.1 Example of normal distribution of plastid around the nucleus and finished plastid-nucleus accumulation during ETI. The confocal snap-shot images of *N. benthamiana* FNReGFP line in abaxial cells treatment with XopQ effector protein from *Xanthomonas.* The image shows the early stage of plastid/stromule -nucleus localization and late-stage localization of these organelles. Enhanced Green Fluorescence Protein (eGFP) was used to observe the plastid. The white circle represents nucleus localization and the arrow = stromule.

As a trigger for ETI, the effector XopQ (XANTHOMONAS OUTER PROTEIN Q) from *Xanthomonas campestris pv. euvesicatoria* (formerly known as *Xanthomonas campestric pv.*

vesicatoria) was used. XopQ is recognized by *N. benthamiana* plants by ROQ1 (RECOGNITION OF XopQ 1), and ETI reactions, such as hyper-sensitive programmed cell death (HR PCD), are initiated (Erickson et al., 2018; Prautsch et al., 2022; Schultink et al., 2017). Transient expression of XopQ in *N. benthamiana* was identified as a potent trigger of stromule formation in an effector-based expression screen by Christina Lampe (Erickson et al., 2018).

4.1 Evaluation of XopQ-induced expression time point in *N. benthamiana* in a transient assay

To understand which role stromules play during ETI-induced plastid accumulation, I planned to record a time-lapse movie. In order to consolidate imaging time, it was necessary to evaluate at which point, following *A. tumefaciens* inoculation, cell compartments start to react to the expressed XopQ. To follow plastid-nucleus-stromule interactions, *N. benthamiana* plants carrying the transgenes p35S::FNReGFP (plastid) and pAtUBQ10::H2Bmcherry (nucleus) ,from here on called "pn", were used to visualize plastids and nuclei. XopQ was expressed with the help of the *A. tumefaciens* lab strain LBA4404, which is known to only weakly impact stromule frequency and plastid relocation (Erickson et al., 2014).

In order to evaluate the time span in which transient expression of XopQ triggers plastid relocation, pn transgenic *N. benthamiana* plants were inoculated with LBA4404:XopQ:mOrange2, LBA4404:mOrange2, and AIM (Agrobacterium Infiltrations Medium). XopQ was C-terminally fused to mOrange2 for visualization of the protein. Untagged mOrange2 was used as bacterial, and the AIM infiltration as buffer control.

Spots of infiltrated leaves were harvested subsequently after 16 hours, 24 hours, and 48 hours. All the observations in this work were made in lower epidermis cells of *N. benthamiana* plants using maximum intensity projections of z-stacks obtained by confocal microscopy **(Figure 4.2)**. The images show that after 16 hours, no fluorescence was visible in the XopQ:mOrange2 infiltration spots; the same was true for the two controls. However, images taken 24 hours after infiltration show that the Agrobacterium strain LBA4404:mOrange2 inoculation resulted in protein accumulation and clear fluorescence signals **(Figure 4.2)**. In LBA4404:XopQ-mOrange2 infiltration spots accumulation started to be visible in a few cells. In the following 24h, protein accumulation further increased, resulting at 48h in clearly visible fluorescence signals for LBA4404:XopQmOrange2 and LBA4404:mOrange2 infiltrated spots. As expected, no fluorescence was visible in the AIM-infiltrated spots (control) **(Figure 4.2)**.

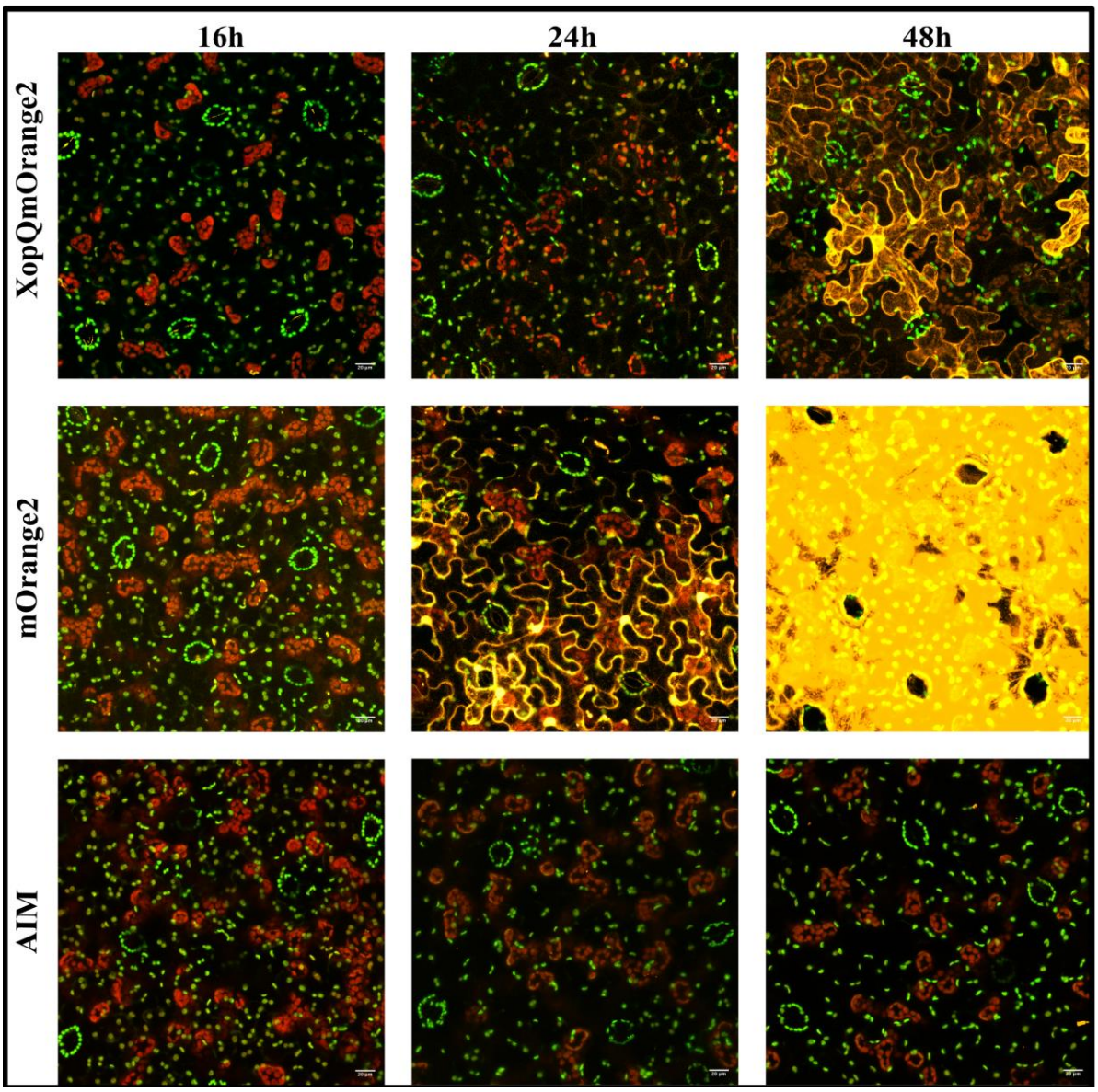

Figure 4.2 XopQ treatment on *N. benthamiana* lower epidermis. The confocal images of *N. benthamiana* pn line in abaxial cells treatment with XopQ effector protein from *Xanthomonas* (XopQmorange2); as a bacterial control agrobacterium LBA (mOrange2) and second control Agrobacterium Infiltration Medium (AIM); confocal images were taken 16h, 24h, and 48h after infiltration (OD=0.2). Plastid localized fluorescence initiates from Green Fluorescence Protein (eGFP) f, red for the chlorophyll, and orange for Effector XopQ or only for control. White bars represent a length of 20 µm.

Taken together, XopQ:mOrange2 accumulates between 16h-24h post inoculation and increases rapidly within the following 24h. Thus, the optimal time point for the planned time-lapse experiments is between 24h-48h post-inoculation, and based on this finding the time plan shown in **Figure 4.3** for the experiment was designed. An imaging chamber was constructed out of silicon spacers on a glass slide to keep the tissue hydrated and fixed in place for the planned imaging experiment. After positioning the sample leaf discs on an agarose cushion, the chamber was covered with a cover slip **(see Supplementary Figure 3 A-B-C)**. In this chamber

expression continued, cells stayed viable during the experiment and prepared specimens were kept in the green house to supply the normal growth conditions.

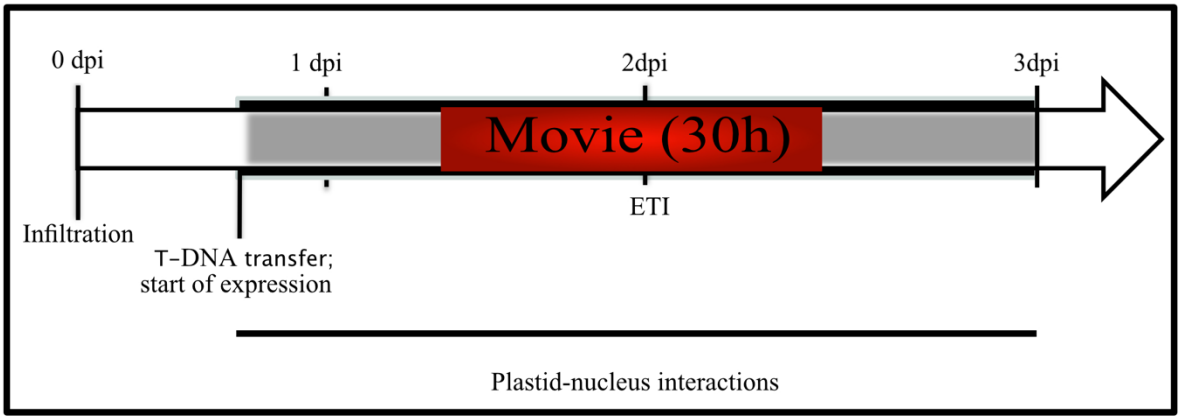

Figure 4.3 Schematic timeline of long-term imaging. Expected timeline for expression of XopQ and captured plastid-nucleus interaction via long-term imaging

4.2 Long-term observation during ETI in *N. Benthamiana*

Based on the short-time (snapshots) experiment **(Figure 4.2)**, we expected to see the accumulation of the effector protein and the plant's response during long-term imaging between 24h-48h **(Figure 4.3)**. Thus, the first long-term movie was started 20h post infiltration of XopQ. The experiment was expected to cover early stromule formation and aggregation events. In order to capture the reaction of the tissue to XopQ as well as the control treatments in one imaging session, besides the XopQ:mOrange2 infiltrated leaf disc, a leaf disc with the bacterial control as well as a leaf disc with the buffer infiltration control was placed in the chamber **(Supplementary Figure 3 D)**.

Although visible XopQ:mOrange2 expression was expected to be noticeable between 24h and 48h, no expression was visible in the recorded time frame. After reviewing the imaging data, the accumulation of XopQ:mOrange2 was delayed compared to the mOrange2 control and was only visible at the very end of the imaging time. Despite the expression of XopQ:mOrange2, no typical XopQ-induced stromule response was visible. This imaging experiment was repeated twice, spanning around 20h-30h per movie. However, the effector protein XopQ:mOrange2 appeared at different time points each time. Furthermore, strong stromule formation was never observed as it was in the initial snapshot experiment **(Figure 4.4)**.

In order to re-examine the time point of the tissues' response to XopQ:mOrange2 expression, additional snapshots were taken at later time points between 40h-46h post infiltration. As seen before 3 out of 4 experiments showed a strong XopQ:mOrange2 expression and stromule

reaction **(summary in Figure 4.4)**. This led to the conclusion that the continuous imaging procedure is most likely delaying XopQ:mOrange2 expression and suppresses the reaction of the infiltrated tissue.

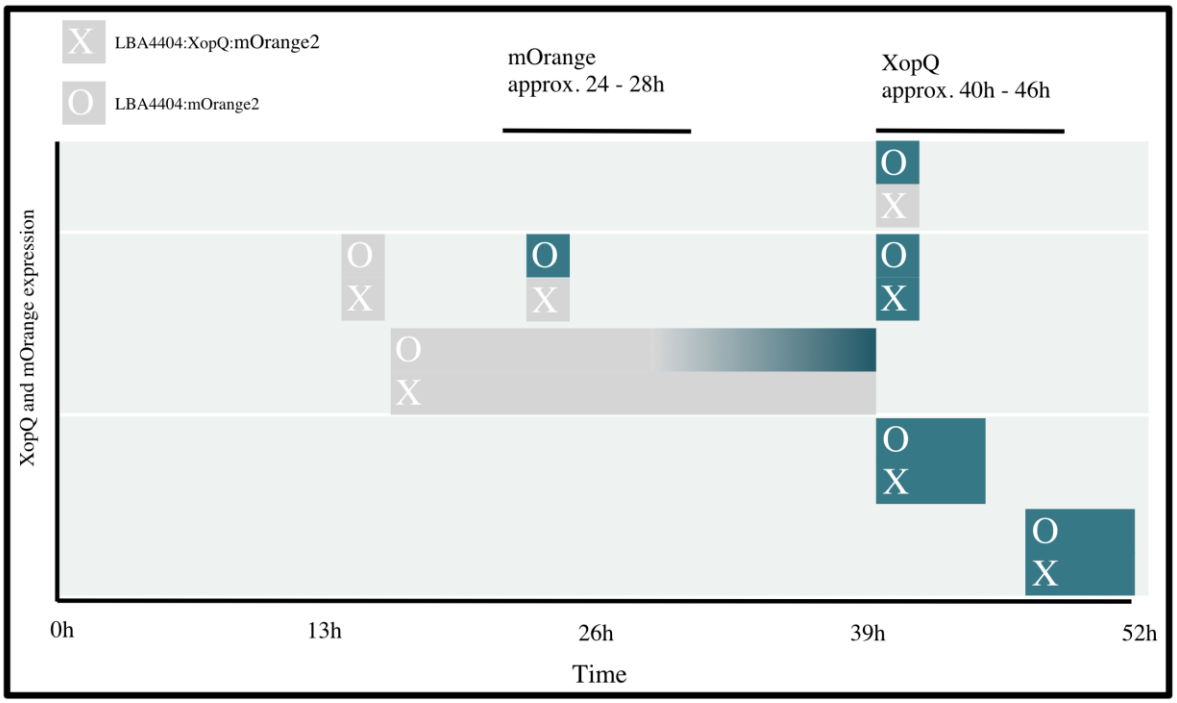

Figure 4.4 Expression time points with long-term and snapshot images. The timetable shows the expression time points for XopQ (X) and mOrange2 (O) between 0-52h post infiltration. Blue color presents the expression start point, and gray shows no expression. The long-term movie demonstrates a long bar, and snapshots show a square bar.

Additionally, there seems to be high inconsistency in the time point of visible expression, which makes it difficult to predict the optimal time frame for long-term recording. Taking this together, I decided not to pursue this experimental approach further.

4.3 Long-term observation during long term imaging induced stress in *N. Benthamiana*

Surprisingly, in the AIM control experiment (buffer infiltration), relocation of plastids to the nucleus and formation of stromules was observed **(Figure 4.5)** without any effector being present. Reviewing the imaging data revealed a surprisingly mobile nucleus traveling throughout the cell in an oscillating motion. Plastids moved at the beginning of the movie to the anticlinal cell walls, where they formed small clusters and stayed until the end of the recording. This change in plastid position and behaviour is most likely due to the exposure of the tissue to the laser's excitation light. Although this reaction's cause is speculative, it provided an unexpected opportunity to study plastid-nucleus interactions during plastid clustering and

which role stromules might play during this time. Therefore, more such time-lapse experiments were recorded. In total, 15 movies were taken of non-infiltrated tissue to understand the dynamic of plastid-nucleus interaction during imaging **(Supplementary table 2)**.

Each movie's duration was between 18h and 25h, adding to a total record time of 289h. We examined 75 nuclei **(Supplementary table 2)**, which were visible at all time points of imaging. Nuclei that moved out of the area of the point of view due to tissue drift or nucleus movement were ignored. In order to get a first quantitative impression of how the number of the plastids around the nucleus changes throughout the long-term movies, the number of plastids around the nucleus at the beginning and end of the movies was counted **(Figure 4.5- Figure 4.6)**.

The images in figure 4.5 show to which extent imaging induces plastid clustering around the nucleus. At the movie's start, an average of 2 plastids are in contact with the nucleus. At the end of the imaging procedure, this increased to almost 4 plastids **(Figure 4.6 - Supplementary table 2)**. This clearly indicates that, to a certain extent, more plastids gain direct contact with the nucleus. In order to clarify if stromules are used as a guide for plastid movement in this context, I examined stromules in the context of plastid and nuclei interactions.

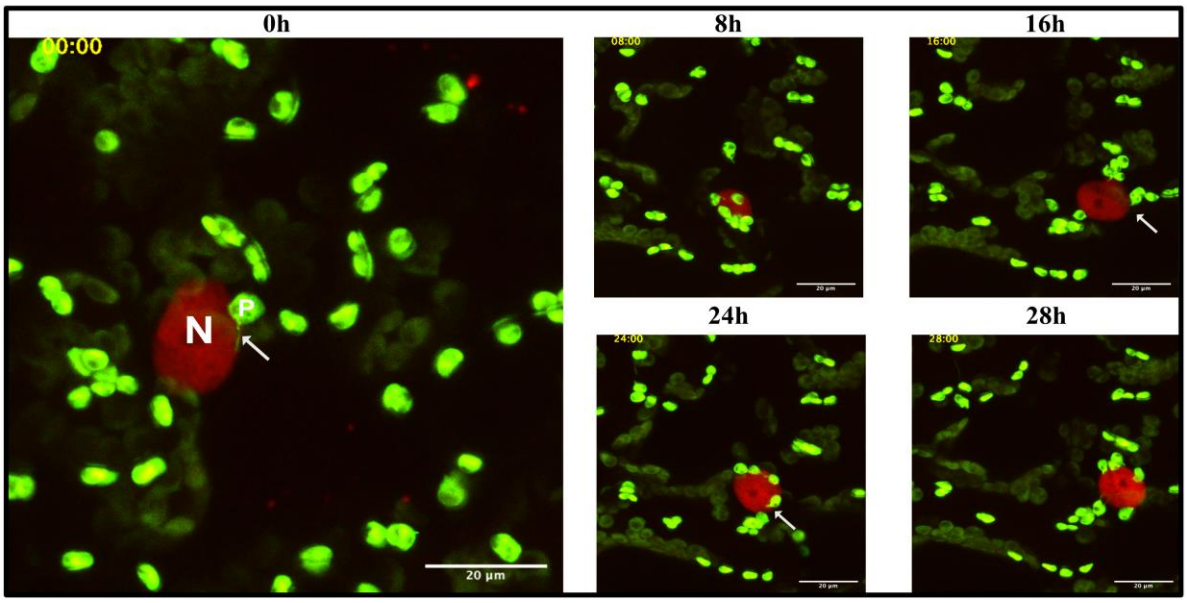

Figure 4.5 Example of plastid clustering during long-term imaging. Long-term movies of the *N. benthamiana* pn line in treatment AIM in abaxial cells. Nucleus-plastid interaction changes during long-term imaging. The enhance Green Fluorescence Protein (eGFP) for the plastid and red for the nucleus was used at different time points. Yellow bars show hours (top left), 0,8h,16h,24h,28h, Nuclei = "n" and plastid = "p"; arrow = stromule, and white bars represent a length of 20 µm.

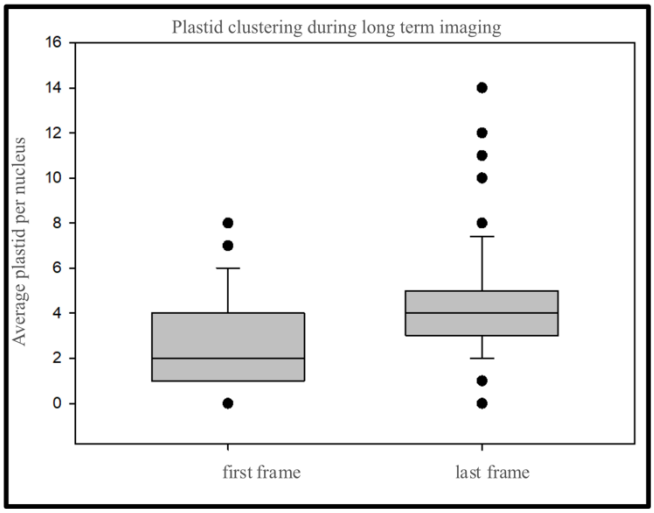

Figure 4.6 Plastid clustering during long-term imaging. The bar graph of the average plastid around the nucleus in the first and last frames during long-term imaging in the *N. benthamiana* lower epidermis in 15 movies (75 nuclei tracked). Mann-Whitney U Statistic (P = <0.001) (**Supplementary table 2 - 7**)

4.4 Nucleus movement is important for plastid clustering

Intending to estimate the importance of stromules for plastids getting in close proximity to nuclei, I created a classification system containing categories describing different possibilities of how a plastid could get in direct contact with the nucleus. The classes are based on the movement direction of the organelles and if a stromule is involved or not. The first categorization was considered based on the organellar movement when the plastid-nucleus was getting close association, which organelle did the first movement for this association. To understand the role of the stromule in the proximity of the plastid and the nucleus, the classes were divided into 3 categories, depending on whether they had stromule formation or not and whether they were matched with the direction of movement of the stromule. This resulted in 6 categories when the plastid and nucleus got close association; this counted for us as a movement, and we checked how this movement occurred. In category one, the plastid and nucleus showed close association; however, the first movement was by the plastid. The plastid moved to the nucleus direction and showed the contact side. **(Figure 4.7 A 1)**. If the stromule made this interaction, the plastid had a stromule, and the stromule touched the nucleus surface and seem to pull the plastid in the direction of the nucleus surface; we put them in category 3 **(Figure 4.7 A 3)**.

In some cases, the plastid had a stromule; however, the plastid's movement and stromule direction were opposite; this movement was in category number 5 **(Figure 4.7 A 5)**. Moreover, plastid-nucleus contact could be via nucleus movement; this means the nucleus could be the first organelle to move and get close to the plastid surface or shows a close association;

therefore, category 2 centers on the nucleus movement **(Figure 4.7 A 2)**. If the plastid had a stromule, on the other hand, the nucleus moved to the plastid surface; it was defined as category 4, but the stromule appeared in the opposite direction of the nucleus movement; this movement defined us the category number 6 **(Figure 4.7 A 6)**. The numbering and categorization system was defined and established on the observation during the long-term move tracking **(Figure 4.7 A) (Supplementary gif movies submitted with cd in the folder)**. This work is done with the help of Julian Arndt as part of his project study.

When plastid and nucleus interactions in the 15 movies were tracked and sorted into one of the six categories, 947 interactions were recorded (raw data in Supplementary Table 3). Based on the current model, built on ETI-induced plastid relocation, it was surprising that in 679 (72%) cases, nuclei moved towards the plastid, and in only 127 (13%) cases, plastids movement towards nuclei. Even more surprising was that in only 141 (14%) interactions, plastids with stromule were involved (independent of the stromule's direction or which organelle moved) **(Figure 4.7 B)**. However, only 14% (movement 3 and 4 together) of all interactions involved plastids with stromules; in the majority of these interactions, stromules faced the nuclei's direction; in only 3% of all interactions, stromules faced a different direction.

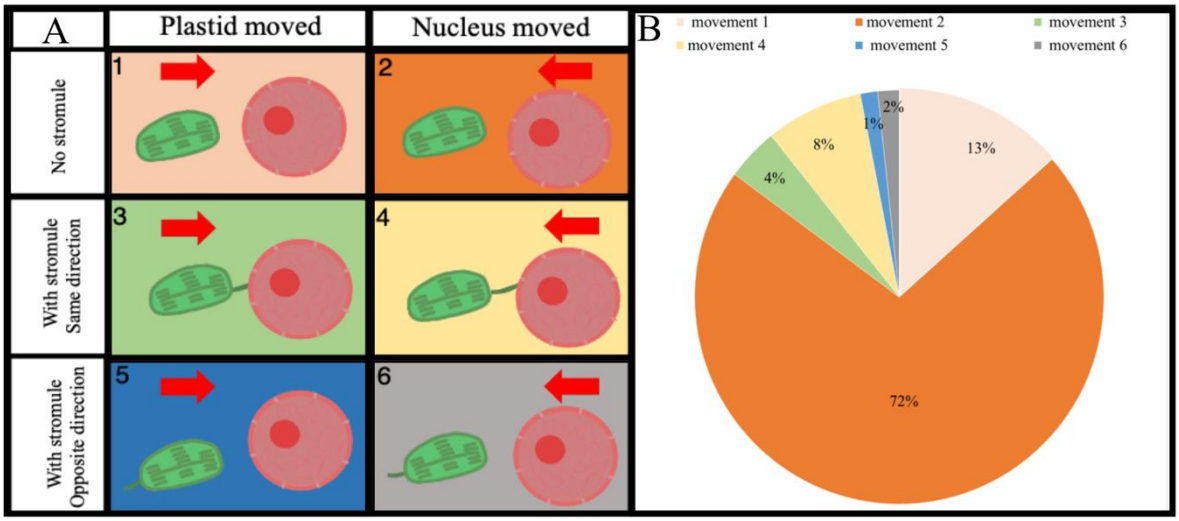

Figure 4.7 A The categorization for plastid nucleus movement in the long-term movie. Each category showed numbers 1- 6. **B** Pie chart shows the distribution of each movement in 15 long-term movies. The nucleus moves 72 % of the movement to contact the plastid nucleus. Red arrow = direction of the organelle.

These data reveal that nuclear movement is critical in bringing plastids in contact with the nucleus under the observed conditions. However, stromules are involved in some of the interactions; they seem not as important as nucleus or plastid movement **(Figure 4.7 B)**. On the other hand, if the stromule played a role in the movement, their direction was most of the time

the movement of the direction of the organelle. Also, considering the plastid-nucleus interaction in the presence of a stromule, nuclear movement is the main guide (8% of movement).

In order to test how reliable this behavior is, the movement for each movie was plotted separately **(Figure 4.8)**. The stacked bar graph showed the interaction category distribution in the majority of the movies. Exemptions are movies 01 and 02, in which nucleus-based movement type 2 is less dominant than in the other 13. However, in summary, the earlier conclusions seem to be rather the rule.

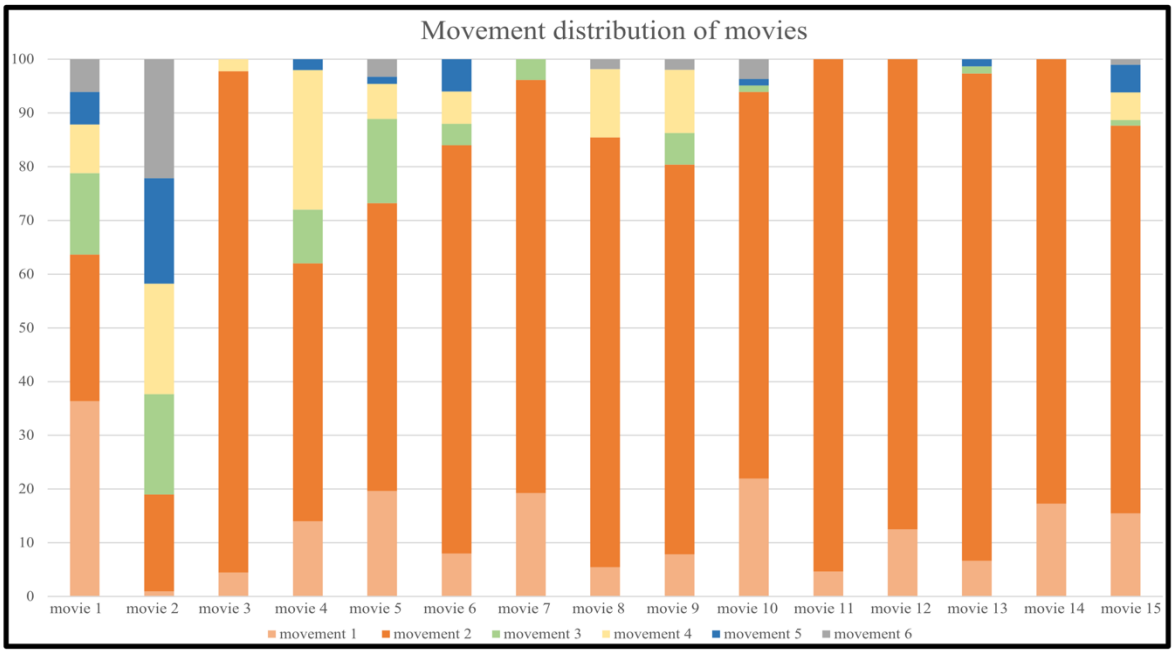

Figure 4.8 Movement distribution for all movies. The bar graph illustrates the distribution of movement for each of the movies in percentage—**raw data in supplementary table 3**.

4.5 The inducer of plastid clustering is not known

Imaging data covering 289 h of nucleus and plastid movements induced by the imaging procedure showed that nucleus movement might be an important driving force for plastid clustering in *N. benthamiana* lower epidermis. However, we still did not know which stress was the reason for the observed clustering. Because nucleus movement seems to be the predominant force during the observed clustering and nucleus repositioning depending on light quality and quantity, light used during imaging could be the cause of plastid clustering or close association around the nucleus (Exposito-Rodriguez et al., 2017). Therefore, the next step was to remove the blue light and see if clustering around nuclei still occurs. Two additional movies without blue light were recorded. To understand the blue-light effect, the 488nm laser was deactivated,

while the rest of the setup was kept unchanged. Since eGFP is used in transgenic plants to label plastids without the 488nm laser, plastid position could be better determined during the movie. First, I quantitatively compared plastid accumulation around the nucleus by checking plastid clustering around the nucleus. I counted the number of plastids around the nucleus at the beginning and end of the movies and compared them with blue light movies (**results in Figure 4.6, raw data in Supplementary table 2**). Control movies with blue light showed an average of 2 plastids in contact with the nucleus and by the end of the movie, this increased to almost 4 plastids (**Figure 4.6**). On the other hand, without blue light, the average number of plastids in contact with the nucleus was 2 at the start of the movie, and at the end of the imaging procedure, this slightly increased to 2.14 plastids in two movies (**Figure 4.9A**). This indicates that blue light might induce plastid accumulation around the nucleus, as removing the 488nm laser showed a significant difference for plastid accumulation around the nucleus. Moreover, this data focuses individually on two movies, and only 14 detectable nuclei were considered in movies without blue light. Furthermore, the data was not statistically different.

To quantitatively compare, nucleus movement was tracked and analyzed (Imaris 9.1). A comparison of nucleus speeds with and without 488nm showed that the average nucleus speed did not change compared to the control movies (with blue light) (**Figure 4.9 B**). Therefore, 488nm light-induced changes to nucleus movement might be responsible for the observed clustering however did not affect the average speed of the nucleus.

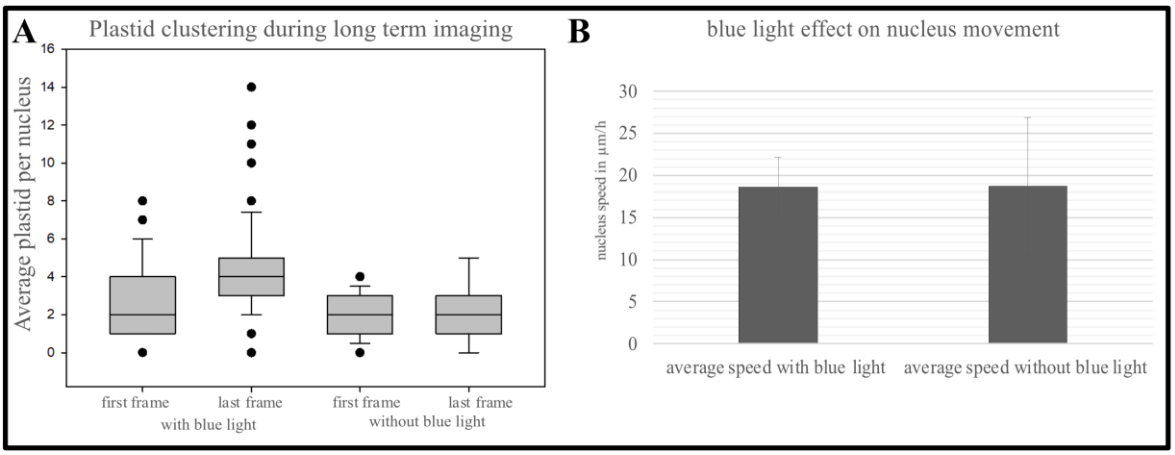

Figure 4.9 Blue light effect on plastid clustering and nucleus speed. The bar graph of the average amount of the plastid around the nucleus in the first and last frames during long-term imaging in the *N. benthamiana* with and without blue light lower epidermis in 15 movies.

In summary, based on the experiments and observations so far, the imaging process via the confocal microscope had an effect on the XopQ expression. XopQ expression appears to be

delayed and stromule induction is inhibited. Thus, this approach is not feasible to shed light on ETI-induced plastid clustering by continues imaging. Alternative approaches will need to be explored, such as using a different microscopic chamber during the treatment of XopQ to reduce delayed expression. On the other hand, different effector proteins for ETI induction can be considered, which initiate the ETI response relatively quickly. Also, using an inducible system for a new approach may be the solution to this challenge.

However, using imaging-induced clustering during long-term imaging provided a unique chance to study plastid-nucleus association/accumulation. The image analysis revealed that nucleus and plastid movement without stromules are sufficient to bring plastids and nuclei in contact. Surprisingly nucleus movement plays a central role in plastid-nucleus associations under imaging conditions. This contradicts what was suggested by published data (Caplan et al., 2015; Sampath Kumar et al., 2018), which indicated that plastid stromules are needed to find the nucleus before the plastid body can associate with nuclei during ETI. Unfortunately, these studies did not cover the whole process, therefore, it is not clear how exactly plastids find the nucleus in these cases worked. It is possible, that also in the cases of ETI induced plastid clustering nucleus movement plays an important role, as seen in our imaging induced clustering. However, clustering could also be mediated by different mechanisms based on the stimuli.

5 Plastid-nucleus interaction during ETI in *A. thaliana*

4.6 Estradiol inducible effector-triggered immunity

Evaluation of XopQ-induced expression in *N. benthamiana* in a transient assay showed me that with this method, it is exceptionally challenging to examine the relationship between the effector-induced stromule formation and plastid-nucleus interactions. The effector expression was not predictable and seemed impacted by the imaging procedure. Furthermore, keeping the exact localization of the *N. benthamiana* plant tissue on the microscope slide during imaging was specifically tricky. Therefore, we decided to test an alternative approach and decided to test an inducible system in our second model plant *A. thaliana.* An inducible system will give us better control of expression time points because the presence of bacteria and T-DNA transfer is not necessary for expression to occur. Among the available inducible vectors systems, I chose an estradiol-based system to understand the role of stromules in the interaction between plastids and nuclei during Effector trigged immunity, which has been used before for a similar experimental setup (Aggarwal et al., 2018; Man Ngou et al., 2020; Zuo et al., 2000). The benefit

of *A. thaliana* as a model system is the substantial amount of available genetic resources. Thus, transferring the system from transient infiltration in *N. benthamiana* to stable expression in *A. thaliana* would allow us to study plastid-nucleus interactions during ETI in different cell biological and signalling mutants, providing important insights into the regulation of observed changes.

4.7 Golden gate construct expresses plastid, nucleus, and inducible AvrRps4

To understand how stromule-mediated plastid-nucleus interactions are formed in response to ETI stress in *A. thaliana*, I needed to establish first the needed molecular tools to inducible trigger the expression of an effector protein, which is recognized by *A. thaliana*, to visualize the plastids (stromule) and to visualize nuclei. Because multiple expression cassettes are needed to be transferred and integrated into the genome of *A. thaliana* plants, transgene stacking seems not feasible within the timeline of the theses. Thus, the aim was to construct a multigene plasmid based on the MoClo System published by (Engler et al., 2014).

A Selection of fluorescence markers in life cell imaging

First, I had to choose the suitable fluorescent protein for each compartment and the effector. Due to the limitations of current microscopy, it is tough to visualize three distinct cell compartments without overlapping wavelengths. Additionally, I had to identify and test a combination of three fluorescence proteins, which can be simultaneously imaged (single track) with standard CLSM setups in green and non-green plant tissues. I needed to avoid shorter excitation wavelengths, limiting the amount of ROS generated by laser light shorter than 488 nm. Additionally, I wanted to combine fluorescence proteins in green tissue, where strong chlorophyll autofluorescence precludes the use of fluorescence proteins in most setups.

Because most standard glass-based beam splitter imaging systems support simultaneous excitation with a 488nm Argon laser and a 561nm diode laser, effective combinations of fluorescence proteins would be excitable at these wavelengths.

Green fluorescence is an essential protein with a maximum excitation value of 488nm. Therefore, it would be convenient to use enhanced GFP to visualize one of the cell compartments. Additionally, I searched for one with a narrow emission spectrum among the available orange fluorescence proteins. This would ensure that the emission spectrums of the eGFP and the orange fluorescence protein overlap only slightly, if at all. Specifically,

mOrange2, mKO2, and mKO&Kappa (from here on referred to as mKOK) appear most appropriate. Despite its widespread use, mOrange2's emission spectrum exhibits a distinct shoulder toward longer wavelengths, resulting in increased crosstalk with red fluorescence proteins. The mKO2 and mKOK, on the other hand, have significantly smaller shoulders and a lower level of crosstalk. As a result, I selected the mKOK (Drobizhev et al., 2011; Mastop et al., 2017) protein to visualize another cell compartment **(Figure 4.10)**.

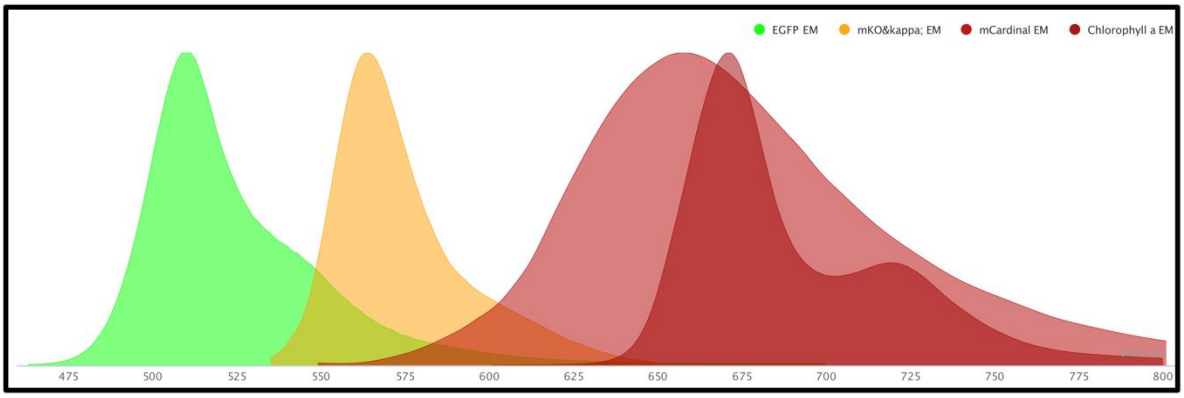

Figure 4.10 Demonstration of spectra view of the selected fluorescent proteins with the fluorescence emission. The emission peak for each chosen protein (eGFP, mKO&Kappa, and mCardinal, respectively) is 475 wavelengths (fpdatabase.org).

I found that specifically, E2-Crimson, mNeptune2.5, and mCardinal emit fluorescence that is shifted toward longer wavelengths, which would lower crosstalk and benefit the spectral separation. However, this protein should still be sufficiently bright, fast-maturing, and bleaching-resistant. Its spectrum should still be separable from the chlorophyll autofluorescence of green tissue, which mainly seems to originate from chlorophyll a **(Figure 4.10)**. E2-Crimson, mNeptune2.5, and mCardinal can cover these requirements even if the E2-Crimson is the brightest of the three, and I preferred to use mCardinal, to avoid potential adverse effects by E2-Crimsons tetrameric nature (Chu et al., 2014). The emission peak of mCardinal is more toward longer wavelengths and deceits right before chlorophyll a. Despite the large overlay of their fluorescence beyond 650nm, the peak of mCardinal fluorescence could be captured with only minor crosstalk with chlorophyll and mKOK **(Figure 4.10)**. Therefore, the combination of a green fluorescence protein (eGFP), an orange mKOK, and a dark red fluorescence protein (mCardinal) would be suitable for microscopy **(Figure 4.10)**. It is noteworthy that the chosen proteins, orange mKOK and dark red fluorescence protein (mCardinal), are yet to be applied to plant cell biology. Testing would have to reveal their usefulness in the planned context. We constructed a set of Golden Gate-compatible molecular building blocks according to the

guidelines outlined in (Engler et al., 2014), enabling the construction of multi-marker plasmids, which allow simultaneous transfer of the inducible effector proteins and all the organelle markers with one T-DNA.

B Creating L1 cloning modules with the MoClo system

Before a multigene construct can be assembled, individual transcription units (L1-modules) have to be created. First, I made a BASTA selection cassette construct for the stable transgenic plant selection. Then the residual modules were cloned. For labelling plastids, I decided to utilize the cauliflower mosaic virus promotor p35S (Brunkard et al., 2016; Erickson et al., 2017; Gray et al., 2011). Based on the reports of (Caplan et al., 2015), which showed stromule induction following inoculation of *A. thaliana* leaf tissue with AvrRps4 transferring *Pseudomonas syringae* cells, I decided to utilize AvrRps4 as the ETI-induced effector also for my constructs. Fortunately, another study used this effector in an inducible setup previously, which utilized the same MoClo cloning strategy. Therefore, I adapted the same estradiol inducible system to express the wild-type *Pseudomonas syringae* pv. *Tomato* (*Pst*) DC3000 AvrRps4 effector, tagged with mKOK as a C- terminal fusion (Engler et al., 2014)(Man Ngou et al., 2020; Zuo et al., 2000) by the planned constructs. The inducible system is composed of the chimeric transactivator XVE (LexA-VP16-ER) and the corresponding LexA-inducible promotor, which drives, in this case, the expression of AvrRps4. As negative controls, two inactive AvrRps4 mutant variants (AvrRps4$^{KRVY\text{-}AAAA}$, and AvrRps4^{E187A}, respectively) were cloned as well. It is known that after -estradiol treatment, the chimeric transcription factor XVE cloned on the driver L1 module binds to the lexA promoter cloned on the reporter L1 module, activating the gene of interest's transcription. Additionally, I also cloned a tag-only control consisting of only mKOK. For nucleus visualization, mCardinal was N-terminally tagged with a NLS-S40 sequence, and C-terminally tagged with a Flag tag. All constructs were created with the golden gate molecular toolbox with a selected promoter and terminator **(Figure 4.11)**.

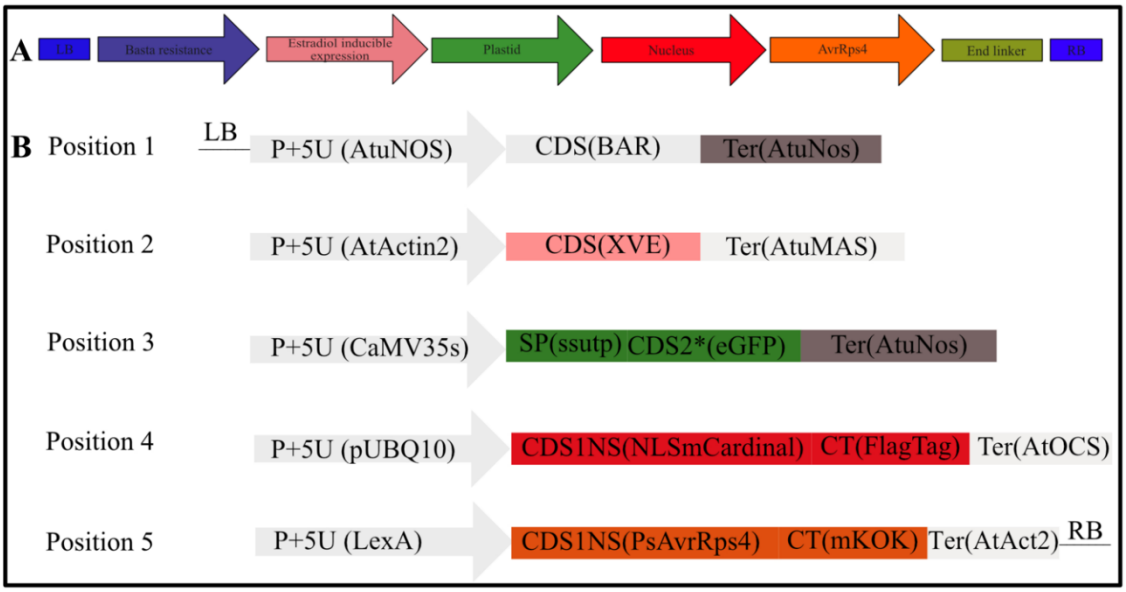

Figure 4.11 A Demonstration of an inducible expression constructs B Positions 1–5 represent the five individual expression units listed as Golden Gate Level 2 METI construct positional components. Position 1 of the Basta selection marker's expression unit. Chimeric transactivator XVE (LexA-VP16-ER) and the consequent LexA-inducible system to express AvrRps4 or its mutant variants in response to -estradiol (E2) in Positions 2 and 5. Positions 3 and 4 include eGFP and mCardinal proteins with transit peptide and C terminal Flag tags. (**Supplementary Tables S3 and S4 contain all the individual units used for construct assembly).**

4.8 Level 1 constructs, test by transient expression in *N. benthamiana*

Before all L1 modules were assembled in a single L2, the individual L1 expression cassettes were tested separately. To verify the developed level 1 constructs, I used a transient expression system in *N. benthamiana* WT by infiltrating agrobacterium that delivers the created T-DNA for expression into lower epidermis cells.

First, I checked the Position 2 and 5 created constructs of L1, encoding the constitutively expressed estradiol receptor and the effector and control proteins under the control of the inducible promoter in *N. benthamiana* lower epidermis. To do that, created L1 constructs for positions 2 and 5 were expressed with the help of the *A. tumefaciens* lab strain GV3101. *N. benthamiana* plants were inoculated with expressed GV3101 containing positions 2 and 5 in two different spots. After 2 days of post-inoculation, 50µm estradiol was used for one spot, and another spot was applied with 0.1% DMSO as a control (see supplementary figure 6). Images show that following induction with estradiol, AvrRps4–mKOK localizes in the nucleus and cytoplasm 24 h after E2 infiltration **(Figure 4.12)**. This localization corresponds to earlier reports of AvrRps4, which localized it to the nucleocytoplasm (Man Ngou et al., 2020). Additionally, AvrRps4KRVY-AAAA and AvrRps4E187A were checked via transient expression as negative signaling controls. KRVYmut and E187A can induce mutant AvrRps4

allele expression but not immunity because the corresponding receptors RRS1 and RPS4 do not recognize these two AvrRps4 alleles.

Surprisingly, control infiltrations show expression of both modules without any prior estradiol exposition. Expression was sporadically and not in each cell **(Figures 4.12 C and E)**. However, we assumed this sporadically expression is a transient expression artefact. Because the expression with estradiol leads to much higher levels and almost all cells compared to the few cells in the non-induced condition, I concluded that the inducible system works as anticipated. Therefore, I used those to create the level 2 construct in the next step. Next, I examined the transient expressions of the plastid construct (position 3). 3 days post infiltration, plastids and stromules were reliably labeled (stroma-targeted transit peptide) with eGFP (**Figure 4.13 A)**. At last, I created the nucleus construct (Position 4) with mCardinal, which showed the nucleus localization in transient expression reliably (**Figure 4.13 B)**.

After successfully verifying each L1 construct, the L2 construct was cloned (**Figure 4.11)**. I named this mega construct (multigene stacking) `Mega ETI' or 'METI' (inspired by (Man Ngou et al., 2020)). The mega construct contains 5; L1 transcription cassettes **(Figure 4.11**) (Engler et al., 2014). The five constructs comprised plant selection cassette Basta, plastid and nucleus visualization markers, and estradiol inducible wild-type *Pseudomonas syringae* pv. *Tomato* (*Pst*) DC3000 carrying the AvrRps4 effector protein with a visualization marker; with this construct, we can observe the interaction between the plastid nucleus and the role of the stromule during ETI.

Before the METI construct was transformed into *A: thaliana* by floral dipping, the created level 2 construct was tested in *N. benthamiana* transient expression assays **(Figure 4.14)**. To see the effector protein AvrRps4 (orange; mKOK), I infiltrated 50 µm estradiol in the same infiltration spot as the construct was infiltrated before 2 dpi. Confocal images showed that in transient expression, each of the created constructs reliably expresses the effector or one of the control proteins, the nucleus, and the plastid marker **(Figure 4.14)**. After this confirmation, transgenic Arabidopsis lines expressing AvrRps4 (METI WT), AvrRps4KRVY-AAAA, and AvrRps4E187A were initiated by floral dipping with Agrobacterium carrying the METI, METI KRVYmut, and METI E187A, respectively.

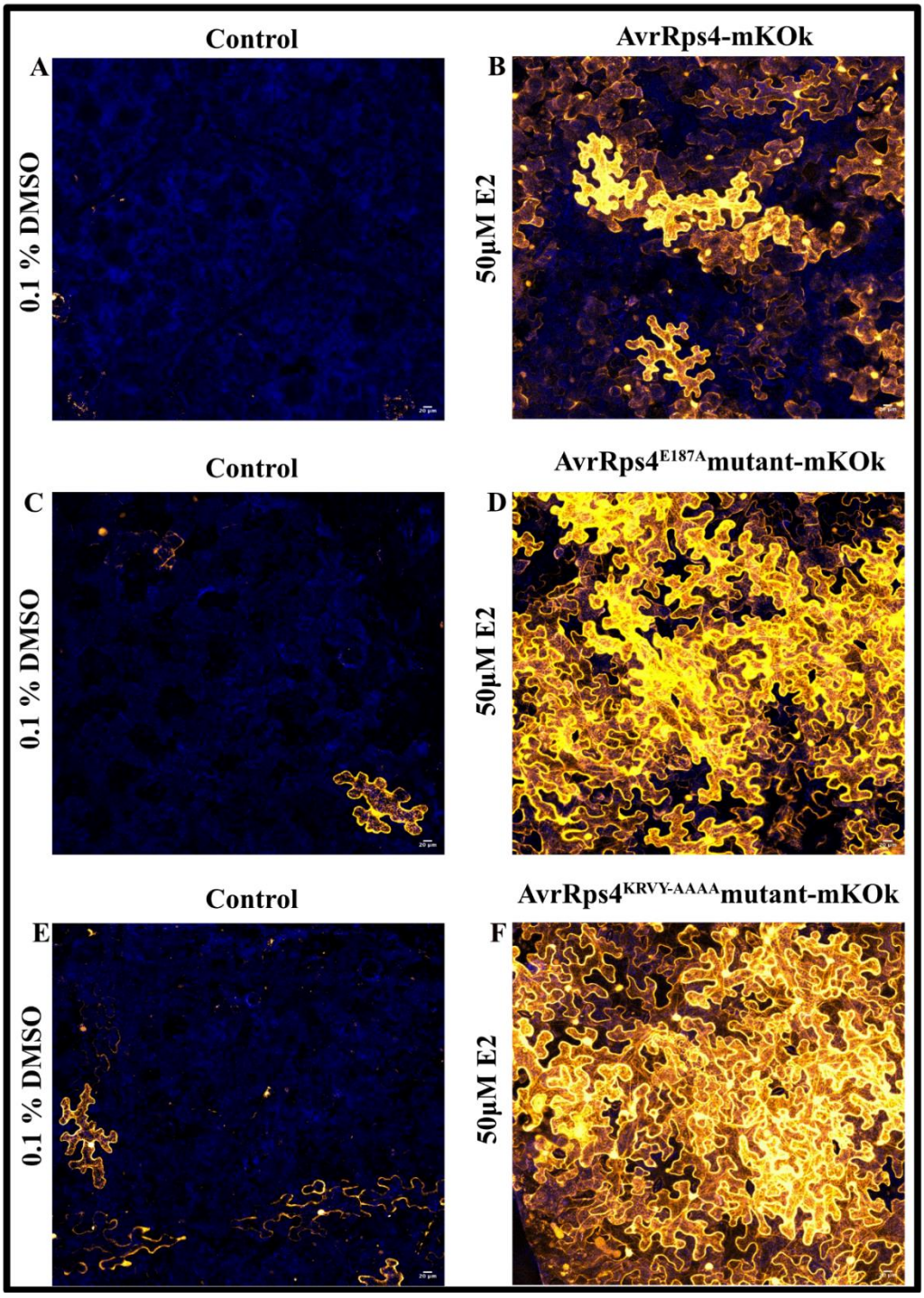

Figure 4.12 Confocal images of estradiol inducible construct with transient expression in *N. benthamiana*
WT lower epidermis at 3dpi. Leaves were infiltrated with Agrobacterium containing position 2-5 constructs together. After two days, leaves were re-treated with **A, C, and E** 0.1% DMSO as a control for each treatment. **B** 50µM E2 for AvrRps4 effector protein construct. **D** AvrRps4E187Amutant-mKOk and **F** AvrRps4KRVY-AAAAmutant-mKOk. The orange channel shows the nucleocytoplasmic localization of AvrRps4–mKok, and blue chlorophyll. Scale bars=20 µm.

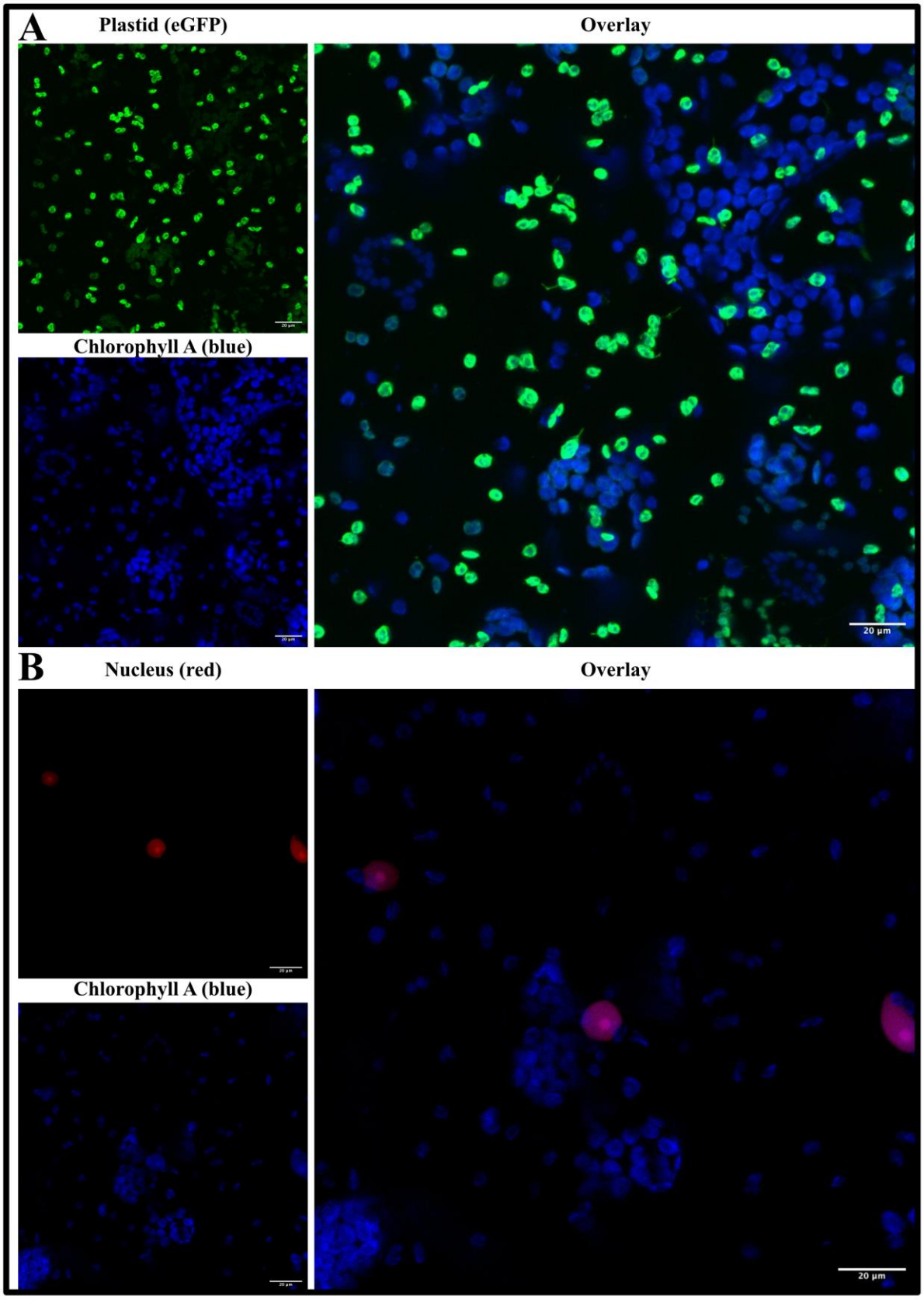

Figure 4.13 Confocal images of plastid and nucleus visualization construct with transient expression in *N. benthamiana* WT lower epidermis at 3dpi. Leaves were infiltrated with Agrobacterium containing created L1 construct. The green Chanel shows the plastid, red Channel nucleus, and blue chlorophyll localization. Scale bars=20 µm.

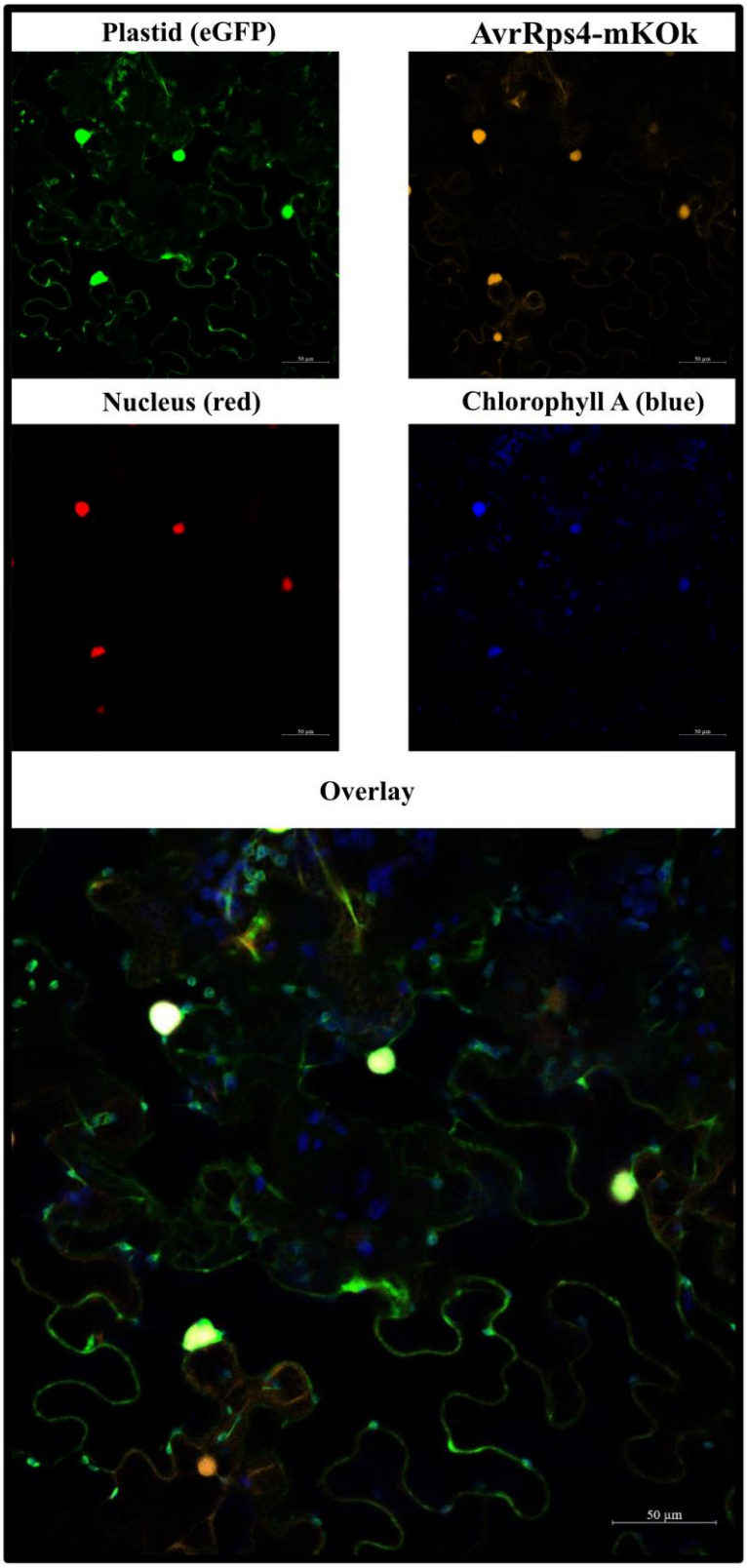

Figure 4.14 Confocal images of plastid, nucleus, and AvrRps4 visualization construct with transient expression in *N. benthamiana* WT lower epidermis at 3dpi. Leaves were infiltrated with Agrobacterium containing created L2 construct. The green Chanel shows the plastid, red channel nucleus, orange channel AvrRps4, and blue chlorophyll localization. Scale bars=50 µm.

4.9 Stable transgenic METI lines

After stable transgenic plant selection with the BASTA treatment, selected METI WT plants were kept in the short-day conditions to screen for expression of the plastid (stromule) and nucleus marker. During the selection process for BASTA-resistant plants and the screen for organelle marker expression, it became obvious that all resistant plants lacking organelle expression showed a normal growth phenotype. However, all plants with organelle marker expression showed a dwarf phenotype. Interestingly, this growth retardation was only observable in the wt AvrRps4 and not in the mutant AvrRps4 containing METI constructs **(Figure 4.15 A)**. The observed growth retardation was reminiscent of plants with a constantly triggered immune system (van Wersch et al., 2016). I suspect that the growth phenotype observed in the AvrRps4-containing plants is due to leaky expression of AvrRps4 by the XVE system, leading to a constant low amount of AvrRps4 constantly triggering ETI **(Figure 4.15 B)**. This idea is supported by the screen of AvrRps4 mutant transgenic plants, which yielded well-expressing plants with no visual growth phenotype. Leaky expression of those proteins will not lead to induced ETI due to the fact that RRS1 and RPS4 do not recognize them. In over 100 screened plants, no plant was found in which good marker expression was paired with a normal growth phenotype **(supplementary table 5)**. I suspect that when the T-DNA inserts into a genome region supporting strong marker expression, the estradiol inducible promotor is leaky, leading to constantly triggered ETI. Thus, it seems combining marker and estradiol expression is not possible from one plasmid. Therefore, a change of strategy seems advisable here. First a line with inducible AvrRps4 expression and no phenotype should be established. Afterwards this line should be super transformed with a marker plasmid. Alternatively, a killer exon (Gonzalez et al. 2015) could be used to create a nonleaky inducible system. Due to time restrictions, exploring these alternative strategies during this thesis was not possible.

Although the behaviour of plastids and nuclei during the switch from unchallenged to ETI induction cannot be observed in the created METI plants a closer inspection of the METI plants of AvrRps4 and its mutant variants might still provide insights into plastid-nucleus interactions under steady, subtle ETI induction.

Before detailed cell biological studies are performed on these lines at first it has to be clarified if those plants face indeed a steadily triggered ETI response by testing the expression of ETI marker genes. If confirmed, plastid-nucleus interactions could be looked at in detail and compared to control lines. Due to time restrictions, this was not possible during this thesis.

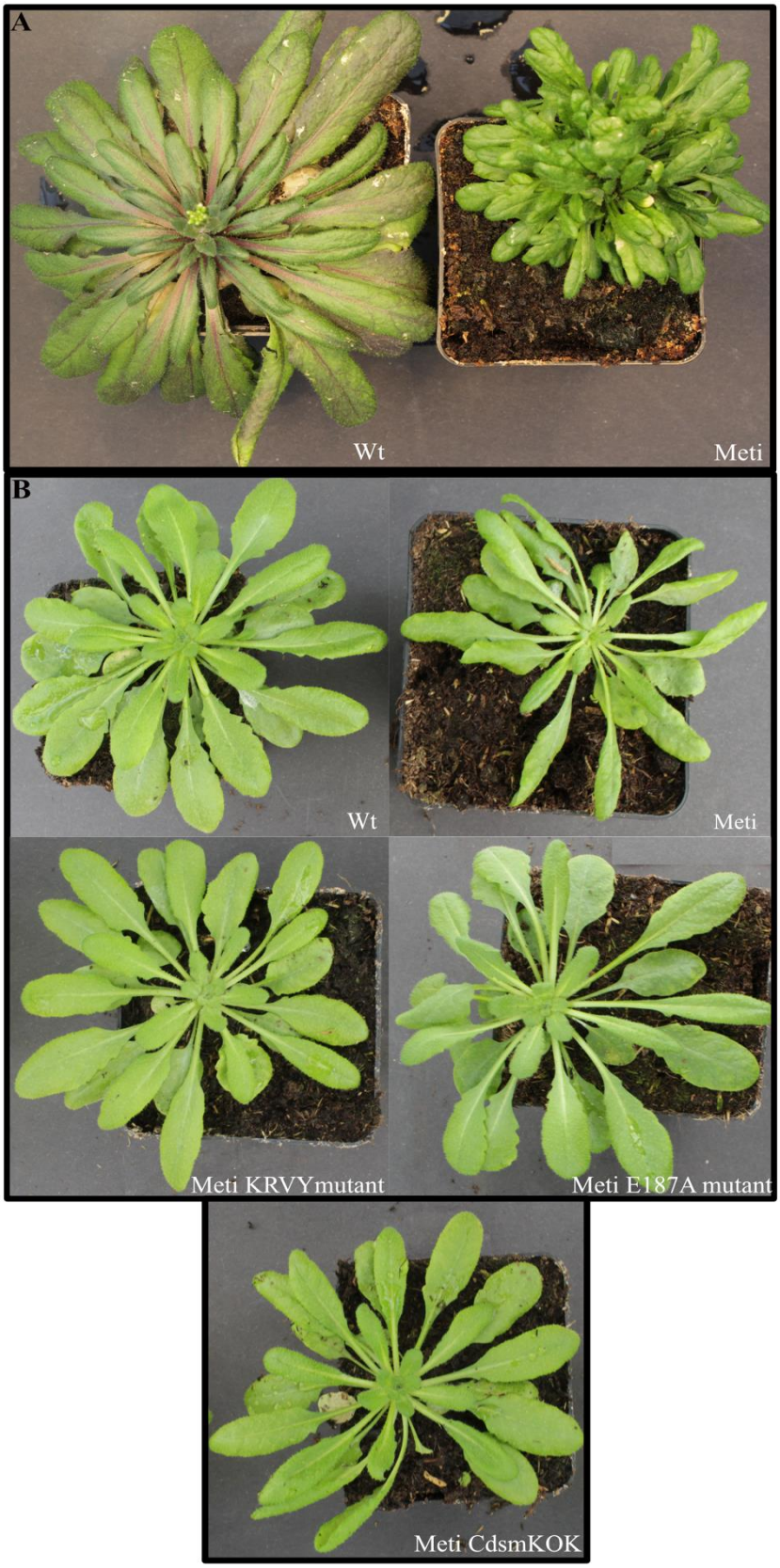

Figure 4.15 A METI selected plants. WT (Col – 0), 8 weeks old (right side), and selected stable transgenic METI plants 8 weeks old (left side). Unexpected dwarf and multiple leaf growth feature in METI plants. **B** Stable transgenic WT (Col – 0), METI wt, and mutant lines 4 weeks old. METI shows a dwarf phenotype; however, mutants of METI do not show a visible phenotype.

4 B Interaction during steady-state conditions in *A. thaliana*

As outlined in the previous paragraphs, attempts to capture and study the change in stromule frequency and plastid position during a triggered immune reaction faced obstacles, which I could not overcome within the time frame of this thesis. However, work from Jolina Marx, Caroline Alfs, and Jessica Erickson showed that in contrast to unchallenged *N. benthamiana* lower epidermis in unchallenged *A. thaliana* upper epidermis plastids and stromules are associated with the nucleus (Erickson et al., 2017). Our lab's former experiments revealed an 8 µm wide stromule "promoting zone" around the nucleus, in which stromule frequency is ten times higher than at greater distances (Erickson et al., 2017). This seemed to confirm the hypothesis established by Caplan et al., 2015 and Kumar et al., 2018, which suggests that stromules reach out to the nucleus to establish signal transfer conduits. However, time series experiments revealed a different behavior than was to be expected based on this model. Stromules were found to form when the nucleus moves away from the stationary plastids. This strong correlation between nucleus movement and stromule formation leads to an alternative hypothesis, which suggests that nucleus movement is the driving force of stromule formation in this tissue and that stromules do not reach out to distant nuclei. Using multiple mutants impacting nucleus movement, Jolina Marx and Jessica Erickson showed that nucleus movement is the driving force of stromule formation within this zone (unpublished data).

Close examination of time-lapse data showed that stromule width changes in the process of nucleus-driven stromule formation, this thinning is known from artificial lipid vesicles forming stromule-like tubules and is interpreted as a result of the limited membrane surface, which restricts the length of formable tubules. When the limit is almost reached, the tension of the formed tubule rises, leading to the observed thinning.

This suggested that in the observed epidermis cells, stromules from stationary plastids get under tension when the nucleus moves away from their body and that the building tension might hinder the nucleus from moving further away (controlling nucleus movement). Thus, I hypothesized that plastids restrict nucleus movement by being attached to the nucleus surface and possessing only a limited membrane area, which restricts stromule length and consequently nucleus movement. If this is true, this formed plastid-nucleus-complex might ensure efficient retrograde signalling in this tissue by low plastid density characterized.

In order to test this hypothesis, I used various mutants to check the impact of different mutations on nucleus speed, which was chosen as an indicator of nucleus movement freedom, among the chosen mutants where mutants affecting plastid morphology, number, and positioning.

4.10 The *msl2-1/msl3-1* mutant lacks stromules and has cells without detectable plastids

First, I decided to test if nucleus movement is indeed impacted by stromule length. If this is indeed the case, then restricting stromule length even more than in the wild type should lead to even more restricted nucleus movement. In order to do this, I focused on an *Arabidopsis thaliana* double mutant called *msl2-1/msl3-1* (phenotype in **Figure 4.16**). It is known that plastid envelope ion channels MSCS-LIKE 2 and MSCS-LIKE 3 (MSL2 and MSL3) from *Arabidopsis thaliana* regulate the plastid's osmatic homeostasis. Furthermore, Arabidopsis plants embracing insertional mutations in both MSL3 and MSL2 display malfunctions in the size and shape of plastids. The double mutant (*msl2-1/msl3-1*) shows blow-up and circular plastids compared to the small, oval-shaped plastids in wild type (Haswell & Meyerowitz, 2006; Veley et al., 2012). The *msl2-1/msl3-1* mutant had abnormal plastids and no stromule formation was visible in plants expressing the prepared plastid marker. (Erickson & Schattat, 2018; Haswell & Meyerowitz, 2006).

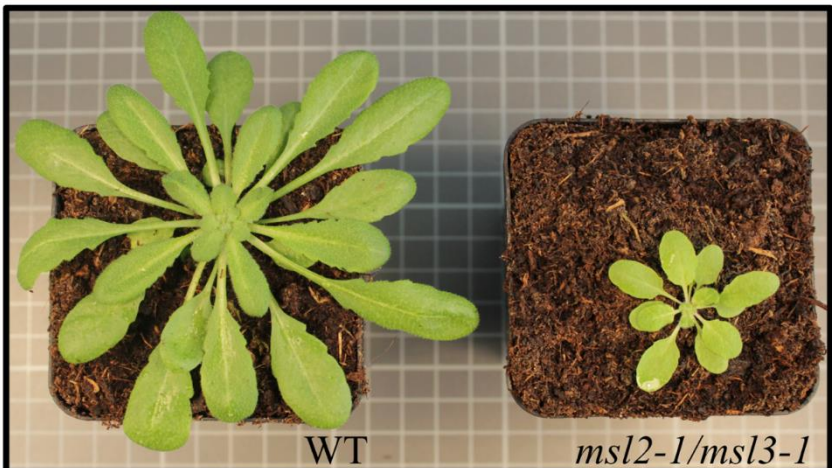

Figure 4.16 Phenotype of *msl2-1/msl3-1* mutant compared to wt (col – 0). 4-6 weeks old *Arabidopsis thaliana* wt and *msl2-1/msl3-1* double mutant.

Whenever water flows into the plastid and is regulated (e.g., by providing osmolytes to double mutants), plastids return to normal size, shape and restore their ability to create stromules in various conditions (Veley et al., 2012). This demonstrates that plastid osmotic control is required to make stromule extensions, and an extra membrane must be provided for the stromules. Moreover, using this mutant will clearly give an idea of how the plastid attachment

on the nucleus movement without stromule formation or no stromule length. In order to observe the effect of these aberrantly inflated plastids on plastid-nucleus interactions, I transformed the *msl2-1/msl3-1* double mutant and the wildtype (col-0) to visualize plastids and nuclei with *pLSU4::pn* (Erickson et al., 2017) (selected lines are listed in **supplementary table 6**). Three primary transgenic plants with sufficiently fluorescence plastids and nuclei were selected for mutant and wt (control). The stable transgenic mutant lines showed inflated plastids **(Figure 4.17)**.

Furthermore, the enlarged plastids were spherical, with no visible stromules (**Figure 4.17**). Only in rare cases was a different morphology observed; in a few instances, I detected plastid membranes seemingly breaking, leading to a fast change from the typical spherical shape to the shape of long tubular plastids with stromules (**Figure 4.18**). Otherwise, almost all the plastids examined in the upper epidermis of mutant leaves had this abnormal morphology, with typically shaped plastids being rare.

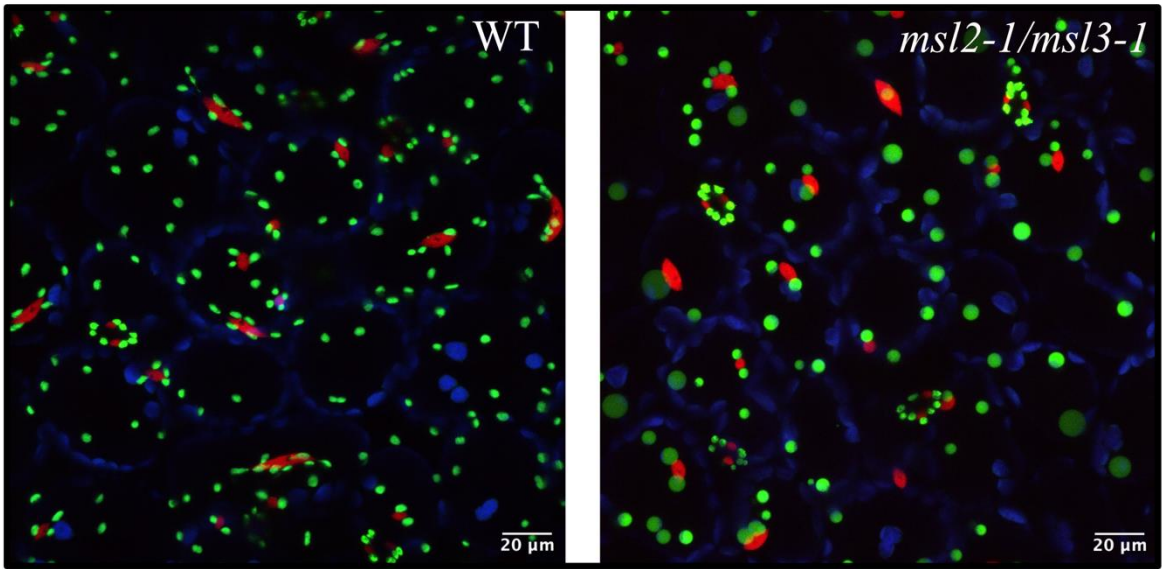

Figure 4.17 Enlarged plastid structure in *msl2-1/msl3-1* pn mutant compared to wt. Z-stack images of wild-type (pLSU4::pn) *Arabidopsis thaliana* upper epidermis 4-6 weeks old (left side) and *msl2-1/msl3-1* pn mutants (right side). The green Chanel shows the plastid, red channel nucleus, and blue shows autofluorescence of chlorophyll A . Scale bars=20 µm.

In addition, images indicated fewer plastids than the wild type **(Figure 4.17)**. The number of plastids and the stromule frequency in *msl2-1/msl3-1* mutants were counted to quantify this. Z-stack images were used to check stromule frequency and the plastid number. The quantification confirmed that the visual impression and plastid number were significantly lower per field of view (8.34 mm2 area) than in the wild-type tissue **(Figure 4.19)**.

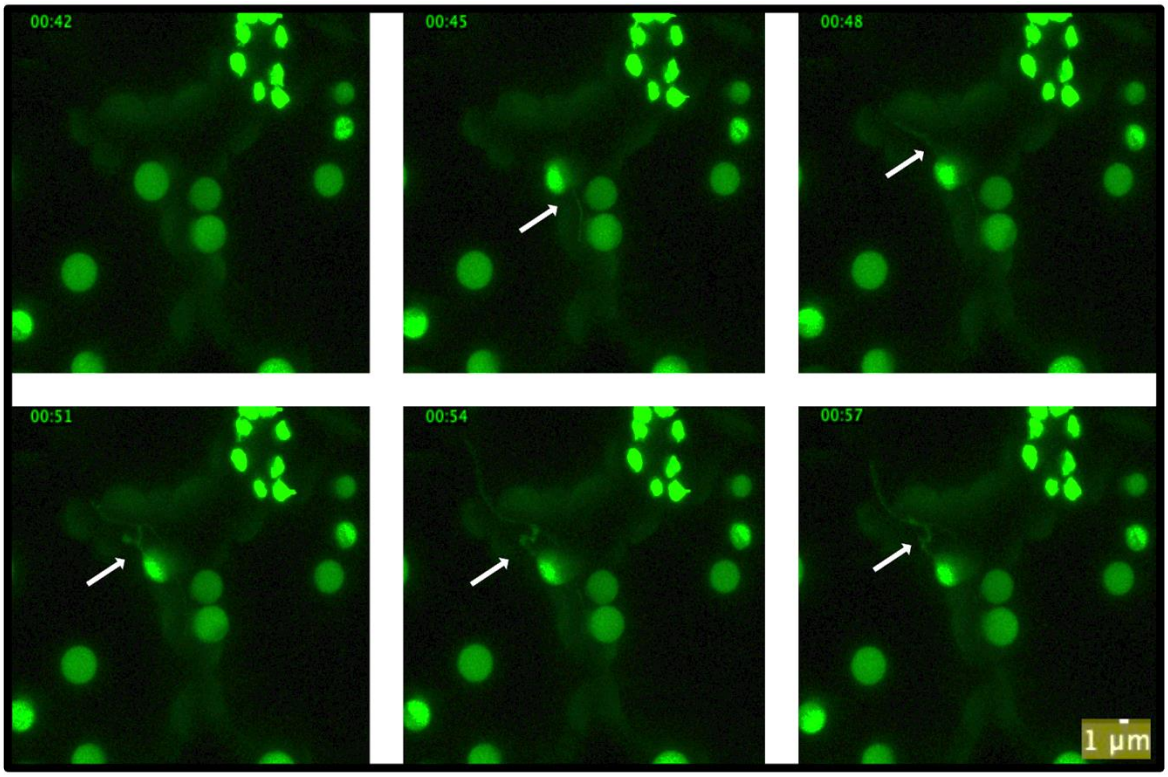

Figure 4.18 Breaking membrane of the circular plastid in *msl2-1/msl3-1* pn mutants. Time series images cropped from time-lapse movies for *msl2-1/msl3-1* pn mutants. Green labeled enlarged plastid, which is typical for the mutant (first image in the middle), was losing osmotic membrane homeostasis and showing stromule formation. The green Chanel shows the plastid, arrow = stromule, and time stamper on top (min). Scale bar =1µm

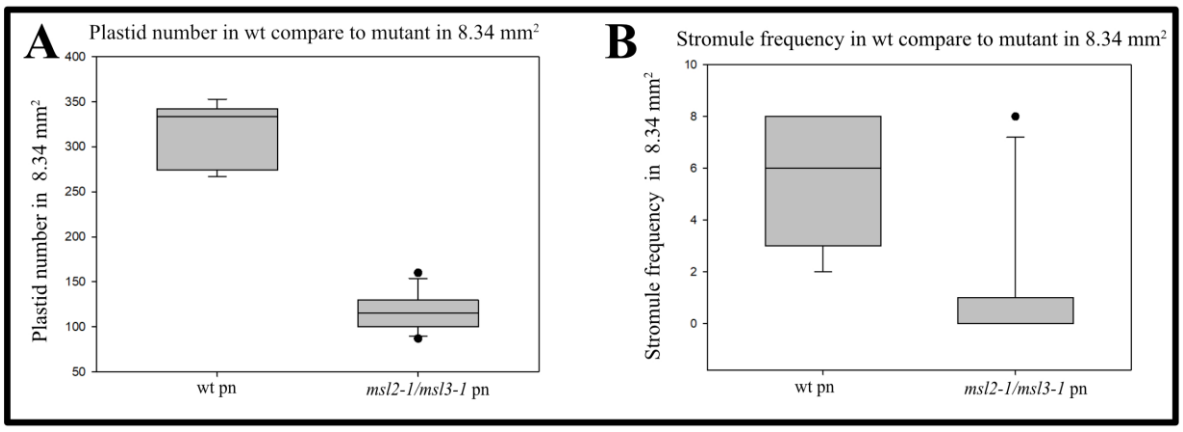

Figure 4.19 Plastid number and stromule frequency in *msl2-1/msl3-1* pn mutants. **A** Box graph shows the amount of the plastid in 8.34 mm^2 for wt pn and *msl2-1/msl3-1* pn. One-way ANOVA test value p=0.001
B Box graph displays stromule frequency in 8.34 mm^2 for wt pn and *msl2-1/msl3-1* pn. Mann-Whitney Rank Sum Test p= 0.002 **(Supplementary table 8-9)**.

In addition, stromule frequency was significantly lower in *msl2-1/msl3-1*. Stromules were observed in the images taken in only a few cases. The occurrence of stromule forming plastids can be explained by breaking of the plastid envelope membranes which was captured and is depicted in **Figure 4.18**. Further, in the upper epidermis of *A. thaliana* wild type and the *msl2-*

1/msl3-1 double mutant plants at least one plastid is close to the nucleus (**Figure 4.17**). However, during quantification of plastid numbers in the double mutant and the wild type, I realized that some cells did not show any detectable plastids, which is rarely reported in plants and only one mutant was found to show such plastid less cells so far (crl mutants, mutants (Chen et al., 2009)).

Furthermore, it has never been reported from wild-type plants. It was generally believed that cells without plastids could not be viable for long. If this mutant indeed has cells without plastids, this would provide a unique opportunity to study nucleus movement in the total absence of plastids, which would no longer hinder nucleus movement.

To clarify whether this was the case for this mutant, Z stack images were taken to see the details of the cell with a confocal microscope (Leica Stellaris 8). Selected *msl2-1/msl3-1* plants from two different primary transgenic lines were used, and cell lines were stained with propidium iodide (PI) to highlight cell boundaries. In the selected example in **Figure 4.20**, highlighted cell displayed a nucleus without any plastid attached (5 out of 120 cells in 2 selected images).

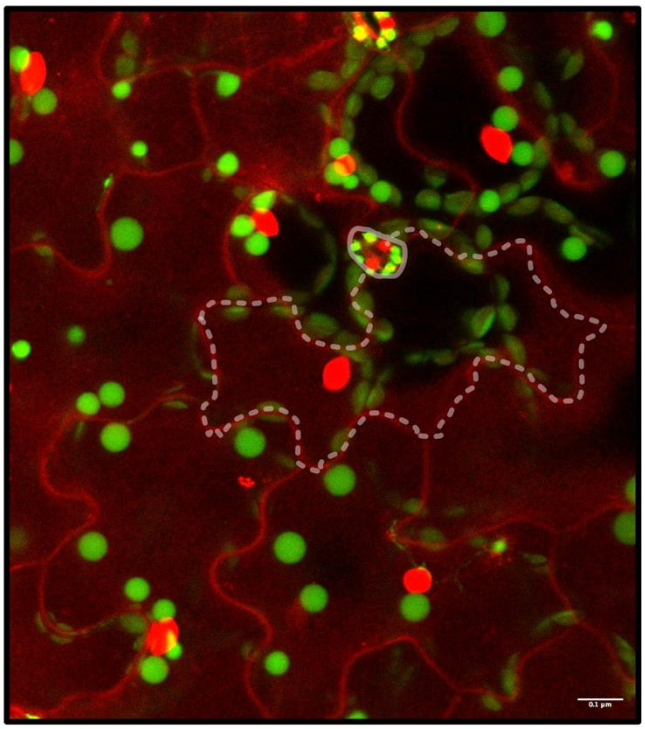

Figure 4.20 Confocal images of m*sl2-1/3-1* pn mutants (*pLSU4::pn)* upper epidermis. An example of a cell without a detectable plastid is outlined. The green Chanel shows the plastid, red Chanel nucleus, and cell line labelled with propidium iodide (red) scale bars=0.1 µm

4.11 Nucleus movement restricted by plastid/stromule attachment

Considering the last observation, this double mutant offers the opportunity to test **a)** if no plastid association leads to more freely moving nuclei and **b)** if plastids without the capability to form

stromules restrict nucleus movement more obvious than in the wild type (with stromules). In order to study nucleus behaviour, time-lapse experiments spanning 1.5h to 2h were conducted in the three selected transgenic mutant and three selected transgenic wild-type lines (Carl Zeiss, LSM). As mentioned before, nucleus velocity was used as a measure for nucleus movement freedom, and nuclei speed was measured in upper-epidermis cells (Imaris 9.6.1) **(Supplementary raw data in folder).**

From previous work by (Erickson et al., 2017), I knew that the upper epidermis of *A. thaliana* consists of cells of very different sizes, which was found to influence nucleus movement. In larger cells, nuclei have more freedom of movement than in small epidermal cells. Therefore, cell size has to be considered when the movement speed data is analysed. Thus, cells were grouped according to the previous work into different size classes; small > 1000um^2, medium = 1000-3000um^2, and large > 3000um^2 (Erickson et al., 2017). Because only a few cells were captured as a whole, cell size was estimated based on nucleus size. This is possible because cell size is correlated with nucleus size in the upper epidermis of *A. thaliana*.

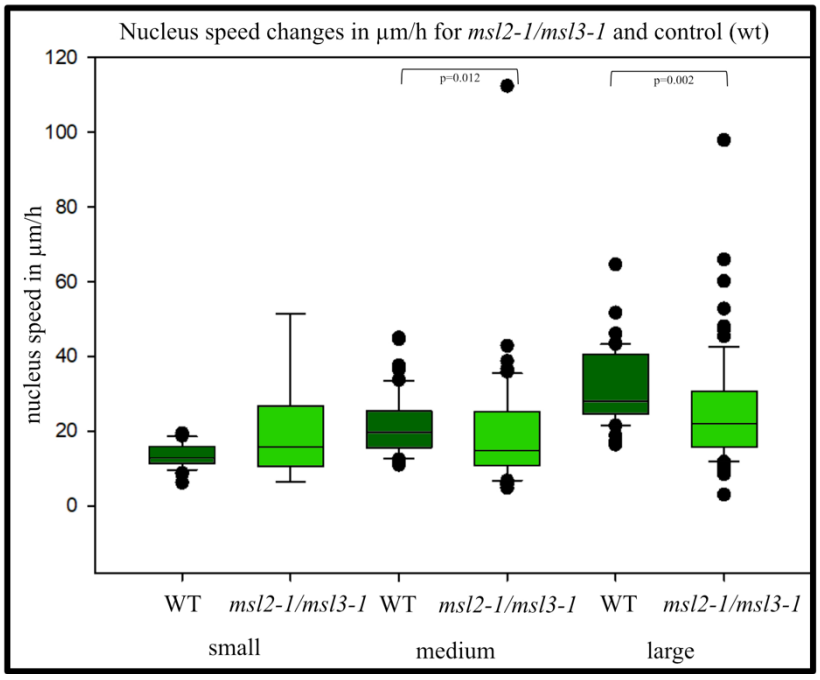

Figure 4.21 Box graph shows nucleus speed changes in µm/h for *msl2-1/msl3-1* and control (wt) based on the size categories. P values resulting from Mann-Whitney U Statistic.

In order to conclude from nucleus size on cell size, the correlation between those two parameters in the *msl2/msl3* double mutant was measured and plotted **(supplementary figure 5)**. A resulting fitting curve was used to obtain an equation describing the correlation between the nucleus and cell size for this mutant. This equation was later used to conclude from nucleus

size on cell size **(supplementary figure 5)**. After cell size categorization for the nucleus, the nucleus speed in small, medium, and large cells was compared between wt (col-0) and *msl2-1/msl3-1*. The box graph indicates a clear and significant drop in nucleus velocity in the *msl2-1/msl3-1* mutant, especially in medium and large cells. No difference seems to exist in small cells **(Figure 4.21**) (for raw data see supplementary folder-raw data velocity *msl*). These results suggested that when plastid stromule formation is prevented, nucleus movement is more restricted.

Furthermore, it was known that wt Arabidopsis upper epidermis cell's nuclei have predominantly 3 or more plastids attached (Erickson et al., 2017). However, nuclei of *msl2-1/msl3-1* mutant differ in the number of attached plastids and fewer nucleus-associated plastids and can range from 0 to 4 **(Figure 4.22)**. Interestingly nucleus behavior seems to change depending on the number of attached plastids, which seems to have a differential impact on nucleus movement. The images from time-series movies show how nucleus movement is affected by the different numbers of attachment plastids in the *msl2-1/msl3-1* mutant **(Figure 4.23- Figure 4.24)**. Images displayed that if the nucleus is not restricted by any plastid, it can move freely during the time – series experiment **(Figure 4.23 A**). One attached plastid caused the nucleus to showed clockwise and anticlockwise movement around the single plastid **(Figure 4.23 B)**. It was observed that as the number of attached plastids increased, the mobility of the nucleus decreased. The **figure 4.24 A** shows that the attachment of a second plastid reduces the movement of the nucleus and becomes a structure that only oscillates to the right and left. In these situations, the plastids seem trap the nucleus. A similar observation was also present when the plastid attachment increased to 3 or more. If plastids surround the nucleus, their movement is restricted; if this limitation is removed, the nucleus seems to start moving again **Figure 4.24 B**.

To test the impact of the number of attached plastids on nucleus velocity, nuclei were sorted into 4 categories (category 1: nucleus without plastid attached, category 2: nucleus with one plastid attached, category: 3: nucleus with two plastids attached, and category 4: nucleus with 3 or more plastids attached). The analysis was done independently as well as dependent on cell size. The result showed that nucleus speed affected each plastid attachment in *msl2-1/msl3-1* **(Figure 4.25)**.

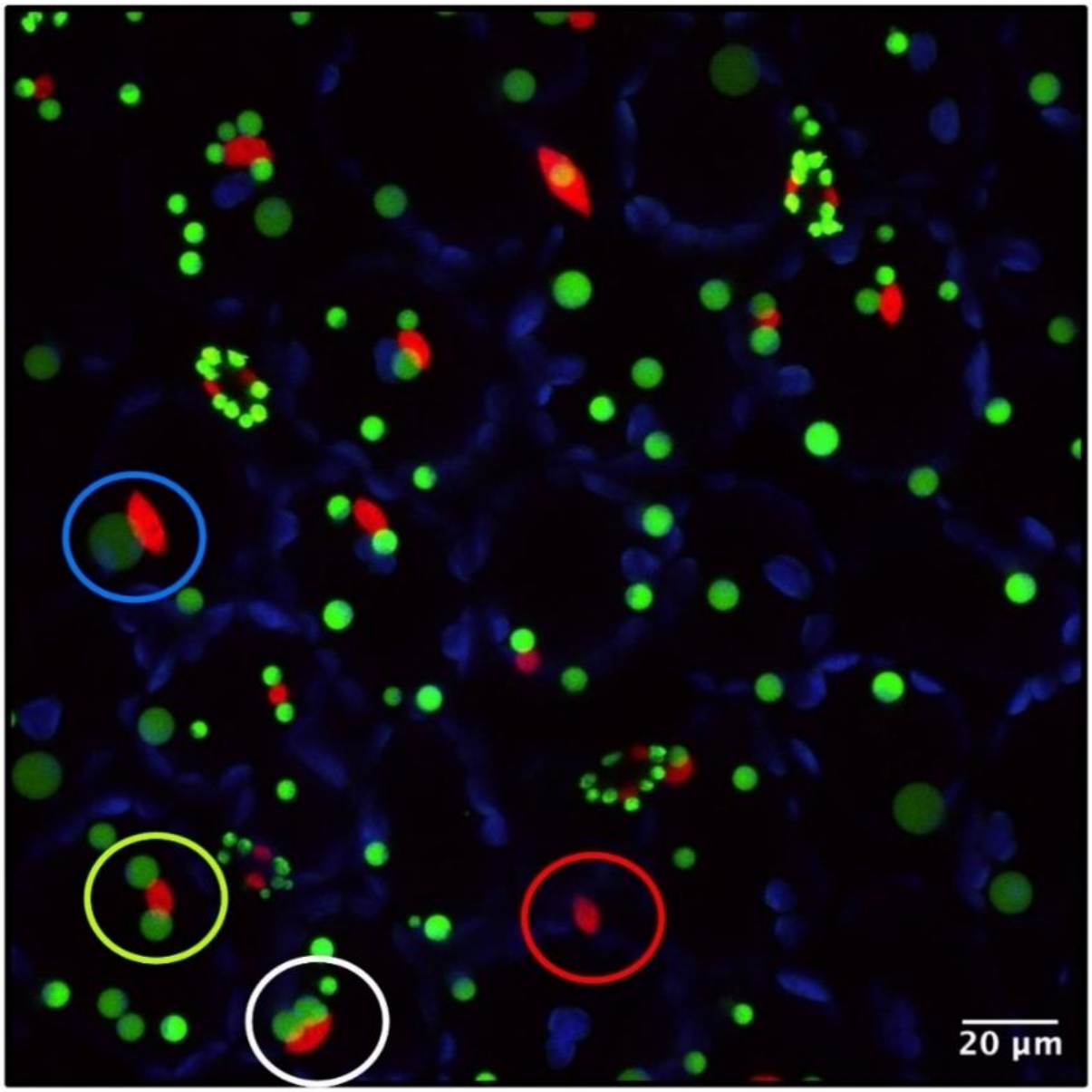

Figure 4.22 Confocal images of nucleus-plastid localization in *msl2-1/msl3-1pn* mutants. Categories were described as follows: 1 (red circle) nucleus without plastid attachment; 2 (blue circle) nuclei with one plastid attached; 3 (yellow circle): nucleus with two plastids attached, and 4 (white circle) nuclei with 3 or more plastids attached and blue = chlorophyll A, scale bars=20 µm

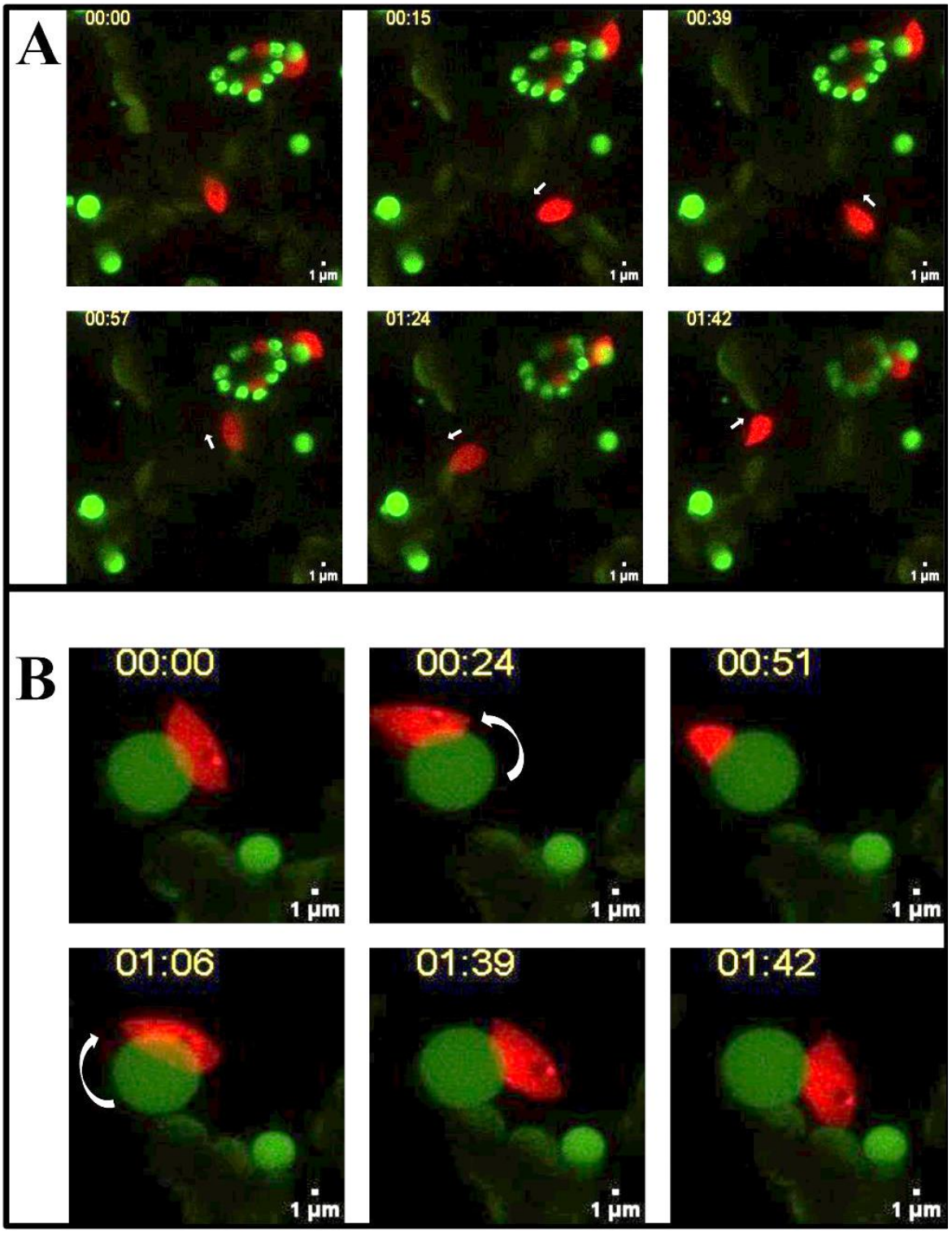

Figure 4.23 Selected time-lapse images of nucleus-plastid localization in *msl2-1/msl3-1pn* mutants. A Image series display the nucleus movement in a double mutant. Red color presents a nucleus without plastid attachment; in the following time series, the nucleus seems to move freely. The white arrow shows the direction of the nucleus movement. **B**. Images show the movement of the nucleus with attachment of 1 plastid. The nucleus might show clock and anticlockwise movement, the green= plastid, red = nucleus, scale bars=1 µm

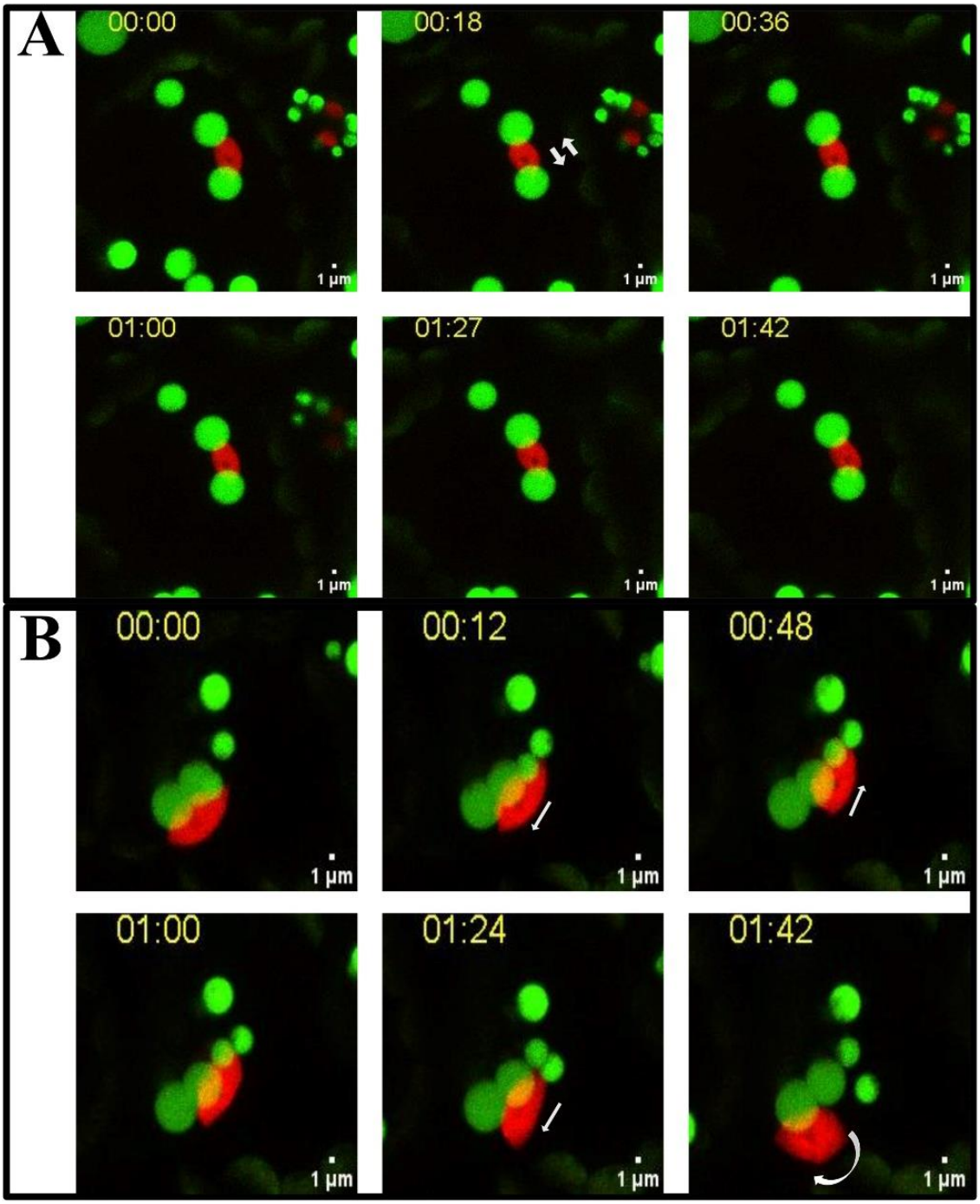

Figure 4.24 Selected time-lapse images of nucleus-plastid localization in *msl2-1/msl3-1pn* mutants with restricted movement. A Image series display the nucleus movement in a double mutant. Red color presents a nucleus; with 2 plastids attach in the following time series, the nucleus movement is restricted. The white arrow shows the direction of the nucleus movement. **B**. Images show the movement of the nucleus with attachment of 3 or more plastids, scale bars=1 µm

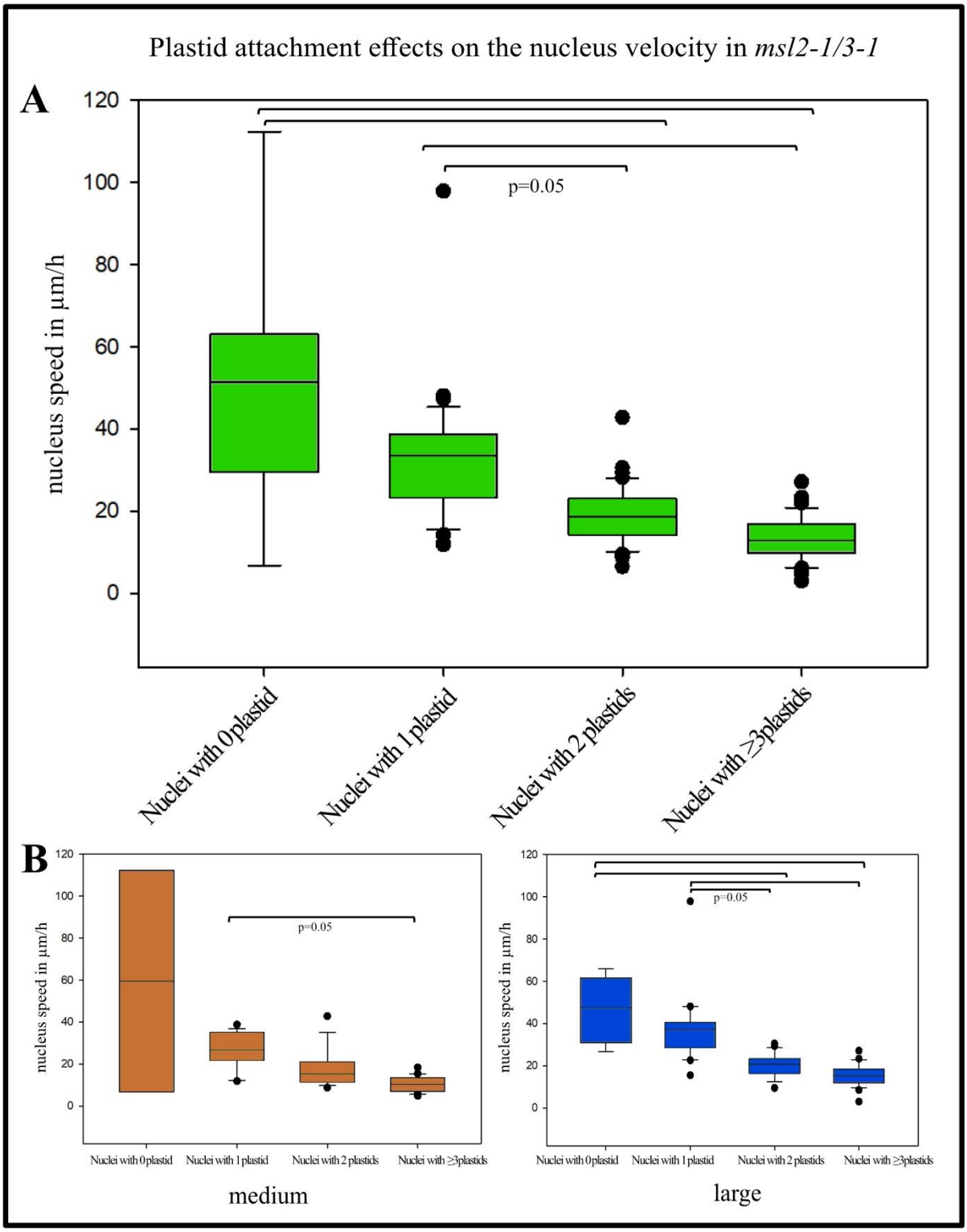

Figure 4.25 Box graph shows nucleus speed changes in µm/h for *msl2-1/msl3-1*. Based on plastid attachment categorization. **A** Nucleus speed changes for all visible plastids on time-lapse movies. **B** Nucleus speed changes for medium and large cells. One-way ANOVA test value p = 0.005

Initially, evaluation was done regardless of cell size (**Figure 4.25 A**). The box graph illustrates that, on average, the fastest nuclei were found in cells devoid of plastids. Moreover, with

increasing numbers of attached plastids, nucleus speed decreased, indicating the restricting impact of stromule-less plastids on nuclei. The nucleus without a plastid attached moved freely, independent of cell size. After that, I considered cell size, and the result of the movement was divided into small, medium, and large cells **(Figure 4.25 B)**. Due to a very restricted number of data points in small cells, data was not included in the analysis **(supplementary raw data folder)**. Medium and large cells demonstrated a similar impact of plastid attachment on the nucleus, even if not all data was statistically significant.

4.12 chup1-3 kac 1-2, kac 2-2 and kac 1-2, kac 2-2

So far, I showed that plastids incapable of forming stromules have a more restrictive effect on nucleus movement than wild-type plastids forming stromules. In addition, I wanted to test my hypothesis with a different set of mutants. Ideally, an Arabidopsis mutant would be tested that misses the plastid anchor point on the nucleus, which is responsible for anchoring the tip of the stromule. In these mutants, plastids should no longer inhibit nucleus mobility, and as a result, nuclei should show a greater movement speed, as seen in the plastid-free cells of the double mutant msl2-1 / msl3-1. Unfortunately, this attachment point is unknown, and its existence is still hypothetical. Therefore, I had to change the strategy. For a plastid to be able to restrict nucleus movement, the plastid body must be kept stationary relative to the nucleus. Therefore, mutants for plastid body anchors should have plastids that do not withstand the pull force of the nuclei and are dragged along with the nucleus. Therefore, I looked at mutants lacking plastid body anchoring to the cell periphery. Plastid localization is known to be facilitated by chloroplast-actin filaments (cp-actin), commonly located on the cell's periphery. CHUP1 is required for the accumulation of chloroplast-actin filaments (cp-actin), and mutants show more mobile plastids and accumulation of perinuclear plastids (Oikawa et al., 2008; Suetsugu et al., 2010).

Further factors in regulating cp-actin filaments are KAC1 and KAC2 (Higa et al., 2014; Suetsugu et al., 2010, 2016). If my hypothesis is true and plastids restrict nucleus movement, removing the plastid anchoring filaments should result in a more freely moving nucleus. Double mutants *kac1/kac2(kk)* and triple mutants *chup1/kac1/kac2(ckk)* were analysed to test if this is the case.

Initially, the *kac1-1*/*kac2-2* double mutant and the triple mutant *chup1-3/kac1-2/kac2-2* were provided by (Suetsugu et al., 2010), and mutants were confirmed with genotyping. To see the effect of the mutants on the plastid and nucleus localization (pn) marker pLSU4:: P35s: FNRtp:

eGFP: t35s: pUBQ10: H2B: mCherry: tNos was transformed into the lines, and at least 3 independent lines were selected based on the brightness of each fluorescence marker **(Supplementary table 10)**. Moreover, propidium iodine was performed to better understand the cell outline for each mutant and the control (wt).

Confocal images amply demonstrated that **(Figure 4.26)** plastid distribution in epidermis cells of the *kac1/kac2* double mutant was distinct from wt (col – 0); even without quantification it is evident that more plastids accumulate at the nucleus. However, some plastids remain not nucleus associated. In the triple *chup1/kac1/kac2* mutant **(Figure 4.26)**, the accumulation of plastids around the nucleus was more prominent, and almost all plastids accumulated at the nucleus **(Figure 4.26)**.

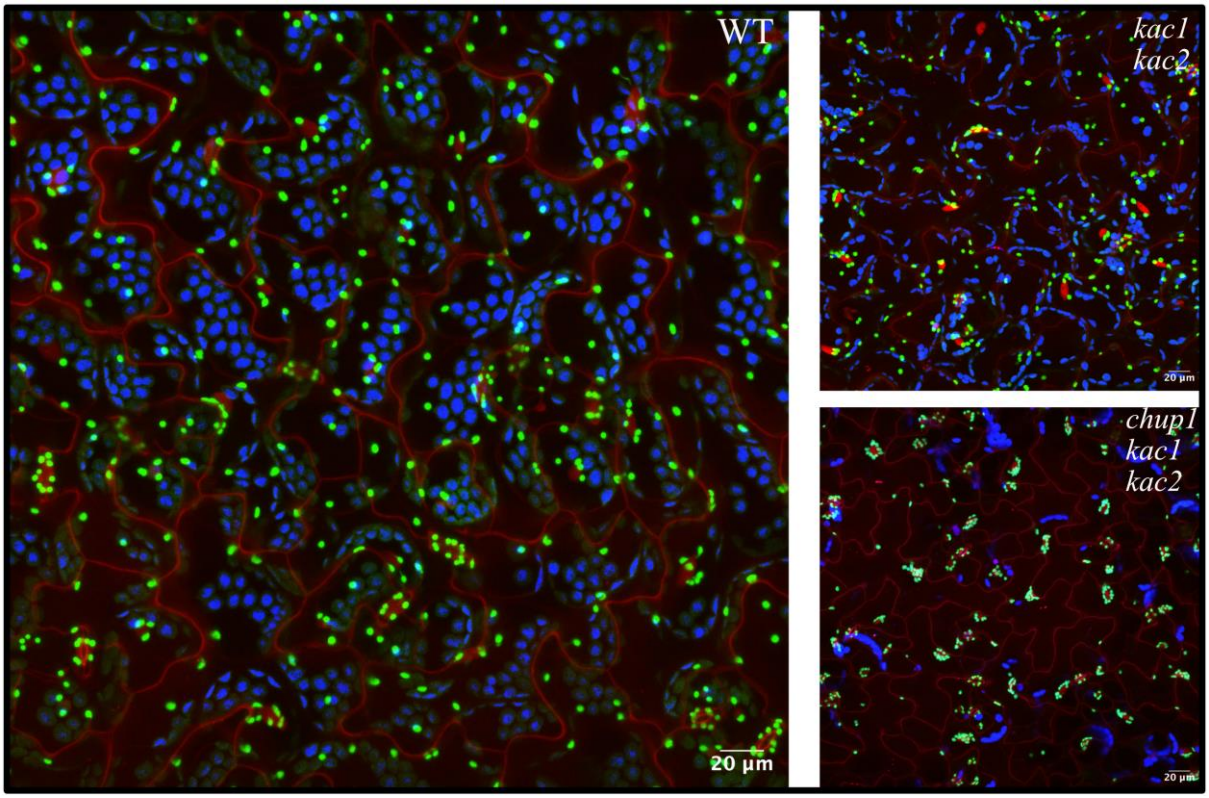

Figure 4.26 Confocal images of wild-type (pLSU4::pn) ***Arabidopsis thaliana*** **upper epidermis** 4-6 weeks old and *kac1/kac2; chup1/kac1/kac2* pn mutants. The green channel shows the plastid, the red channel nucleus, and the blue channel shows autofluorescence of chlorophyll A. Cell lines labelled with Propidium iodide (red) scale bars=20 µm.

In addition, no stromules were observed in selected mutants. In order to quantify the extent of plastid clustering in the selected mutant lines (*kac1/kac2* and *chup1/kac1/kac2)*, the number of nucleus-associated plastids was counted by Fiji for each nucleus in the first frame of the time-lapse movies (**Figure 4.27 A)**. Furthermore, the obtained data were separated into small, medium, and large cells based on the cell size **Figure 4.27 B**.

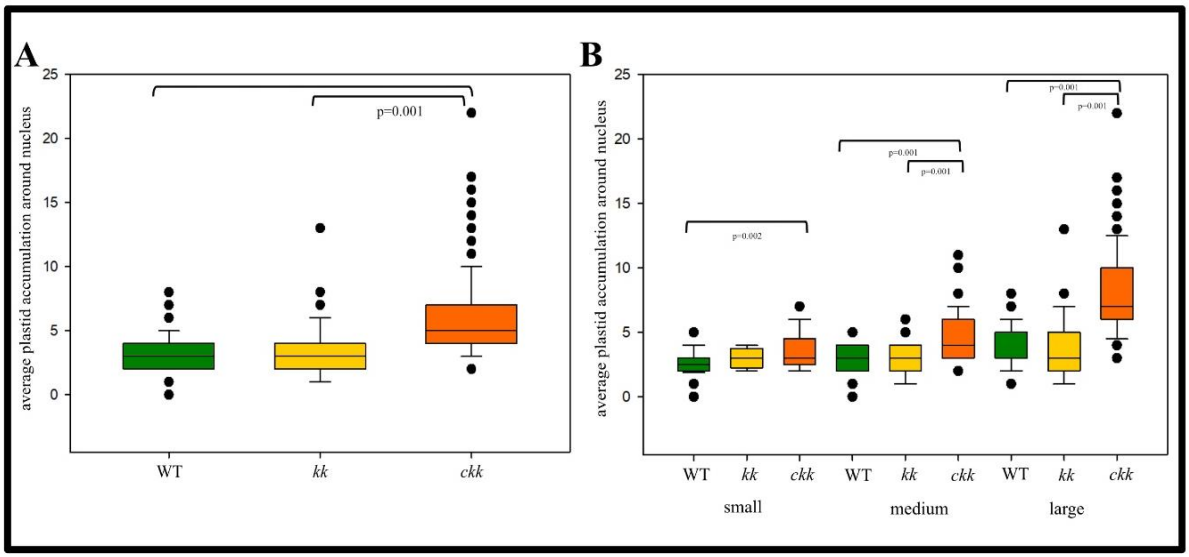

Figure 4.27 Box graph illustrating the average plastid amount around the nucleus. A Average plastid accumulation in wild-type (WT) pn, *kac1/kac2(kk);* and *chup1/kac1/kac2(ckk)* pn mutants in all cell sizes. P values resulting from Mann-Whitney U Statistic. **B** Average plastid amount per nucleus in the small, medium, and large cell in selected mutants. The green box shows the wild type, yellow: *kk*, and orange *ckk*. P values resulting from Mann-Whitney U Statistic.

The double mutant *kk* displayed a similar number of accumulations of plastids compared to the wild type **(Figure 4.27)** wt=3.09 and *kk*= 3.09 average for the plastid around the nucleus. Plastid accumulation around nucleus was higher in the triple mutant *ckk*= 5.06 **(Figure 4.27 A)**. The box graph indicated that the increase in plastid accumulation observed in the *ckk* mutation is likely due to the impact of the mutation.

4.13 If the plastid restriction is removed, the nucleus can move more freely

To test the effect of non-stationary plastids on nucleus dynamics, we examined selected pn marker mutants (*kk* and *ckk)* via time-lapse movies like the other mutants before. Velocity measurements were based on a cell size and separated in small, medium, and large cells and were compared with the respective wild-type results (col-0).

In the upper epidermis of *Arabidopsis thaliana*, the double mutant *kk* exhibited a clear and significant increase in the nucleus velocity, particularly in small and large cell sizes, confirming the restrictive impact of stationary plastids on nucleus movement. Furthermore, the double knockout mutant showed faster movement in cells of any size than wt, while wt showed the lowest nucleus speed in all cell sizes **(Figure 4.28)**

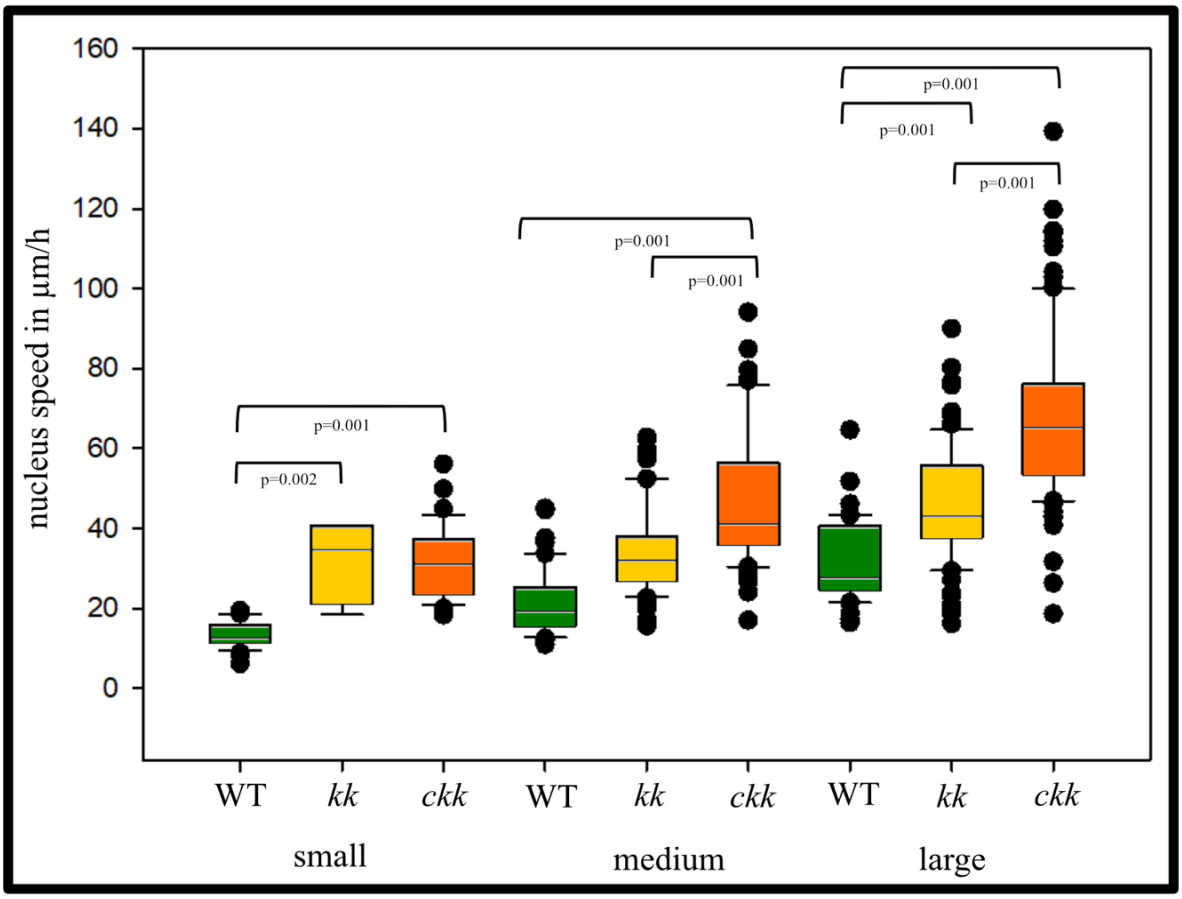

Figure 4.28 Box graph exhibits that nucleus velocity changes in µm/h during time-lapse movies (90mins) for wild-type (col-0), double mutant *kac1kac2* (*kk*), and triple mutant *chup1kac1kac2* (*ckk*) in small, medium and large cell size. P values resulting from Mann-Whitney U Statistic **(raw data in supplementary CD).**

The triple knockout, which did not contain *chup1, kac1,* and *kac2,* exhibited an accelerated nucleus movement in all cell types compared to the wild type. When we compared only the double mutant (*kac1/kac2*) and the triple mutant (*chup1/kac1/kac2),* we observed that the nucleus speed of the double mutant was considerably lower than that of the triple mutant in medium and large cells. Moreover, there was a similar acceleration trend in both cell sizes. Nevertheless, small cells did not show a similar trend. The nucleus speed of the double mutant was higher than that of the wild-type and triple mutant. These results indicated that plastids inhibit the nucleus movement if they are stationary. The nucleus was free in the triple mutant than in the double mutant. If plastids were not stationary in the cell periphery/plasma membrane, they were not halting the nucleus dynamics. Based on the experiment and observation, I hypothesized that plastids are attached to the ever-moving nucleus and are kept stationary, by CHUP1, KAC1 and KAC2. Stromules are formed when the nucleus moves away from the stationary plastids; due to the limited plastid membrane available, stromule length is

restricted and keeps preventing the nucleus from moving further. This results in oscillating nucleus movement.

By manipulating the stromule-forming capabilities and local plastid anchoring with the different mutants. I confirmed our hypothesis; nuclei constantly move in the upper epidermis of *A. thaliana*, and plastids restrict nucleus movement and keep constant physical contact. On the other hand, the plastid should be stationary to hinder the nucleus's movement. The function of this bond between both organelles might be to ensure efficient plastid-to-nucleus signalling. However, in this thesis, I have not checked the effect of tight association between plastid and nucleus on the physiological relevance.

4.14 Cytoskeleton-related plastid nucleus - interaction

Our previous experiments showed us that under normal conditions, the interaction between the plastids and the nucleus was not a coincidence, at least in the upper epidermis of *A. thaliana*. Nuclei constantly moved, and plastids had to be stationary on the plasma membrane or the cell periphery, restricting nucleus movement. As a result, plastids are able to maintain constant physical contact with the nucleus through stromules or by direct contact with the body of the plastid. This assigns a specific function to stromules within the stromule-promoting zone.

What remains open is the question: How are the plastids attached to the nucleus periphery? It has been shown that stromules extend on microtubules, and actin can be an anchor point for the stromule at the nucleus in *N. benthamiana* (Sampath Kumar et al., 2018). To reveal which mechanisms are responsible for plastid-nucleus dynamics in *A. thaliana*, understanding which cytoskeletal element is involved in plastid-nucleus anchoring will help to guide future research efforts for identifying the anchoring complex. In order to test if actin plays a role in stromule anchoring at the nucleus I created stable-transgenic plants to visualize either simultaneously actin, plastids and nuclei or just actin and nuclei.

4.15 An actin cage surrounds the nucleus surface

In *A. thaliana* the movement of the nucleus is known to be driven by actin-based myosin motors (Tamura et al., 2013). Therefore, I suspected that in this species actin would likely encapsulate the nucleus, providing potential anchor points for stromules. To test if this is the case, first, I had to understand the localization of actin filaments in Arabidopsis pavement cells. To examine the expected actin cage around the nucleus, I created stable transgenic Arabidopsis lines expressing a histone marker (H2B:mcherry, citation for H2B as nucleus/chromatin marker) and

an actin marker (p35S:GFP:ABD2:GFP:tNOS) (Wang et al., 2008) (**Figure 4.30**). After selecting a series of primary transgenic lines, one was chosen for CLSM imaging of upper leaf epidermis pavement cell nuclei (4-6 weeks old plants). The z stack images show that thick (bundles) and fine actin longitudinal actin filaments covered the nucleus as a cage. After confirmation that actin forms a cage around the nucleus, I examined the role of actin formation in stromule dynamics during plastid nucleus interaction.

4.16 Actin filaments play a role in stromule morphology/formation

The actin cytoskeleton consists of well-visible filament bundles and very thin filaments, which are difficult to visualize in light microscopy. Therefore, attempts to test if stromule tips are always anchored at actin filaments was inconclusive. To test the involvement of actin in stromule-nucleus anchoring, I aimed to study actin-stromule dynamics and stromule frequency under control conditions and when actin is depolymerized by respective inhibitors. To visualize the dynamics of actin filaments during plastid-nucleus interaction, I created a golden gate L2 construct containing distinct fluorescence markers to visualize plastid, nucleus, and actin filaments **(Figure 4.29 A-B)**. Before cloning, the final L2 construct individual transcription units in L1 vectors were tested for functionality by *N. benthamiana* transient expression. All constructs showed the expected organelle labels and L2 cloning was initiated (data not shown).

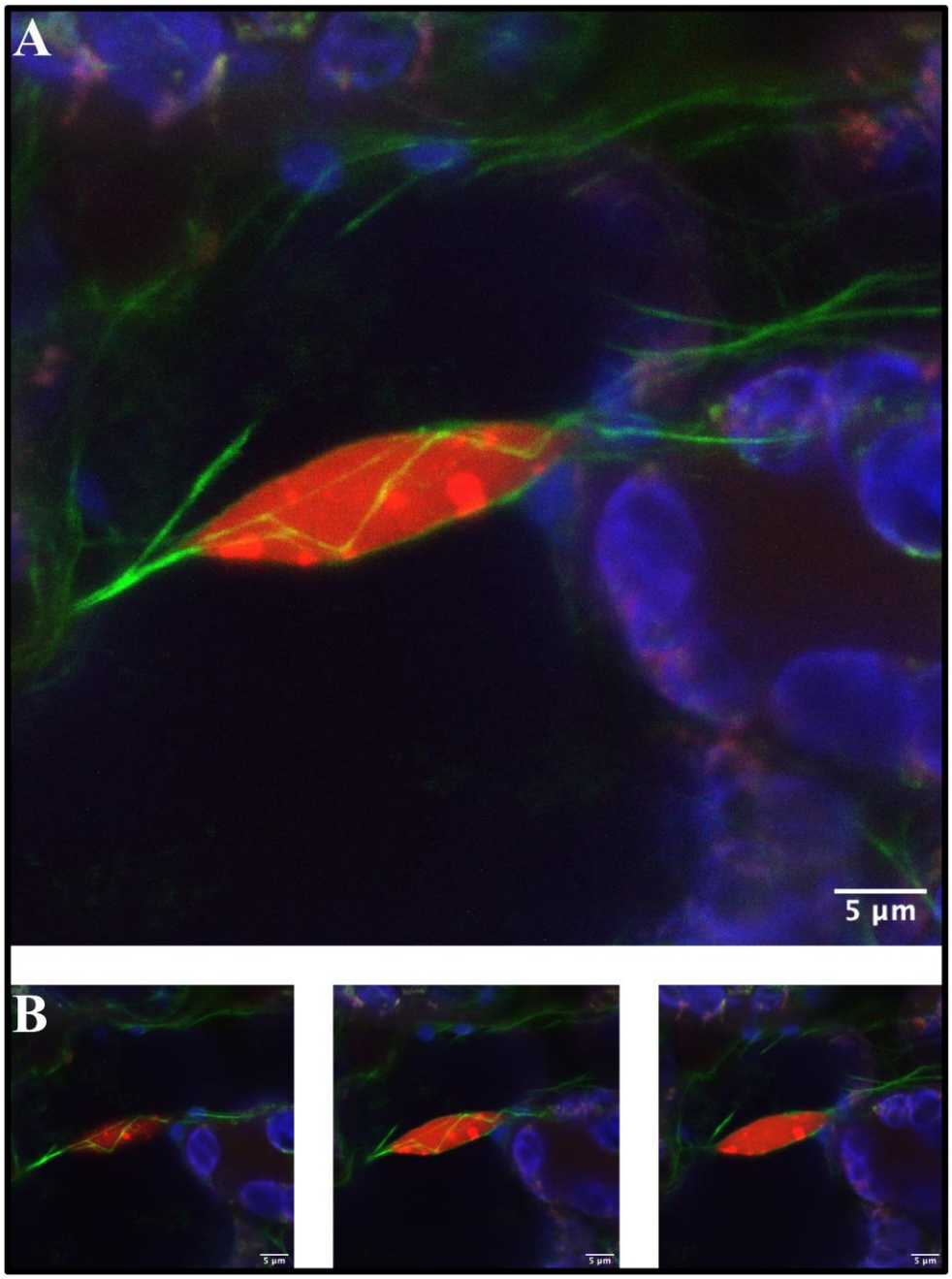

Figure 4.29 Actin bundle around the nucleus in *Arabidopsis thaliana*. A Maximum intensity projection of the Z stack image shows actin filaments in the green channel surrounding the nucleus (red). Blue channels chlorophyll A . **B** Z stack of each of the 8 frames (0-8), (8-16), and (16-24), respectively. Scale bar 5 µm.

The resulting L2 vector was subsequently used to create transgenic *A. thaliana* lines. Transgenic plants showing fluorescence for all three markers were selected and the three best lines were used for further experiments. In order to efficiently disrupt actin efficiently I chose to use Cytochalasin D (CTD). In initial experiments I tested various time points to identify the approximate application time needed for complete actin disruption to take place. The initial experiment showed that CTD application (4µm) started depolymerase actin filaments after 45

min. However, complete disruption was achieved approximately after two h of (4µM) CTD application. Based on these findings all subsequent experiments were executed with 4µM CTD after 2 hours **(Figure 4.31)**.

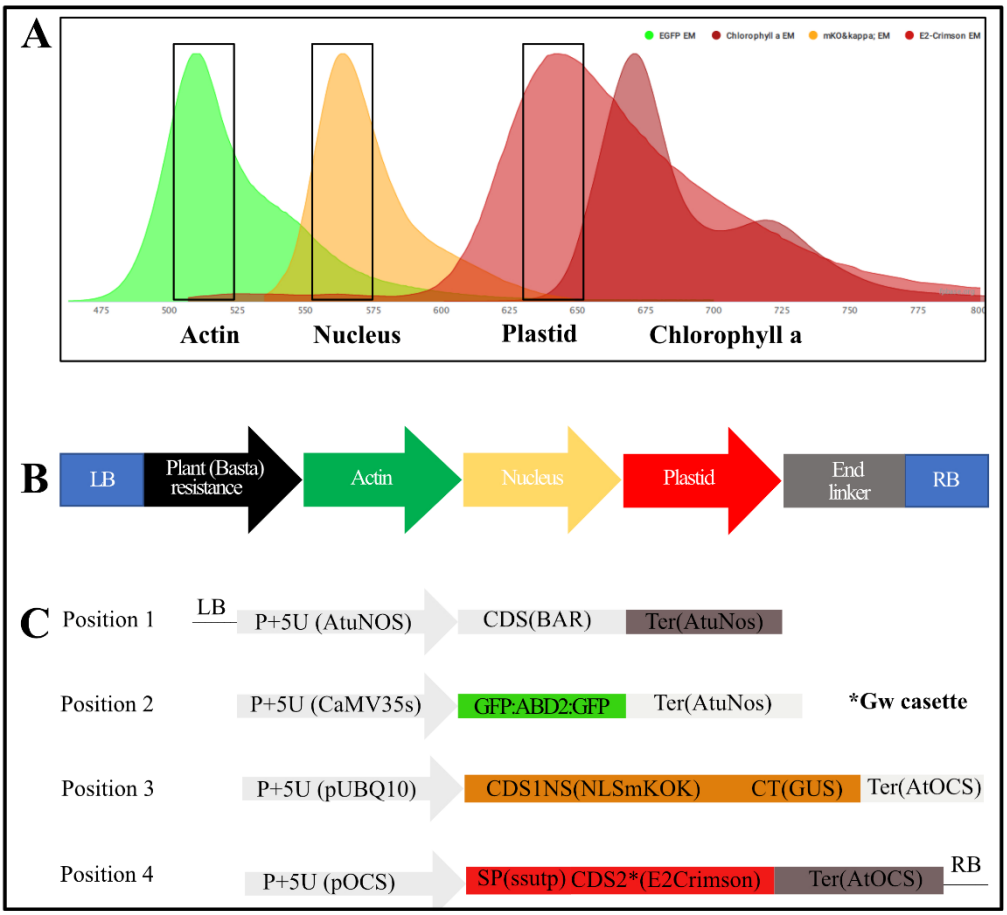

Figure 4.30 Actin construct A chosen fluorescent protein for actin, plastid, and nucleus visualization (**fpbase.org**). **B** Created cassette for all constructs. **C** Positions 1– 4 represent the four individual expression units listed as Golden Gate Level 2 construct positional components. Position 1 of the Basta selection marker's expression unit. Position 2 shows the actin labeling cassette (created via the gateway) (Wang et al., 2004), labelling the nucleus C terminal GUS and for plastid E2-Crimson protein with the transit peptide.

If indeed stromules are anchored on nucleus associated actin, than depolymerising actin should result in a collapse of nucleus associated stromules when CTD is applied to the leaf samples. To determine the role of the actin on stromule formation, created stable lines were treated with CTD, and snapshot images were taken after 2h of incubation. In these images it is visible that after 2h of treatment, long actin filaments disappeared completely in almost all observed cells **(Figure 4.31)**. In order to test the impact, the treatment had on stromule frequency, stromules where quantified in CTD - and mock (DMSO 0.1%) treatments for three different plant lines and for each line in 3 replicates **(Figure 4.32)**. The box graph demonstrates that stromule frequency dropped significantly following CTD treatment **(Figure 4.32 replicate 1 and 2)**.

These results show that indeed actin plays a role in stromule formation or stability. Interestingly, some cells still showed actin filaments, indicating that the drug's effect on actin filaments is not 100% disruptive. This could potentially explain why not all stromules disappeared and few remained. Although this result confirms the role of actin filaments in stromule morphology and frequency and confirms earlier reports (Kwok & Hanson, 2003, 2004a; Sampath Kumar et al., 2018); it is at this point not clear yet if the reduced stromule frequency is due to loss of stromule anchors at the nucleus. In order to take further steps towards understanding the importance of actin for stromule-nucleus-anchoring I focused in the next step on testing specifically the impact of actin depolymerisation on nucleus movement and stromule frequency.

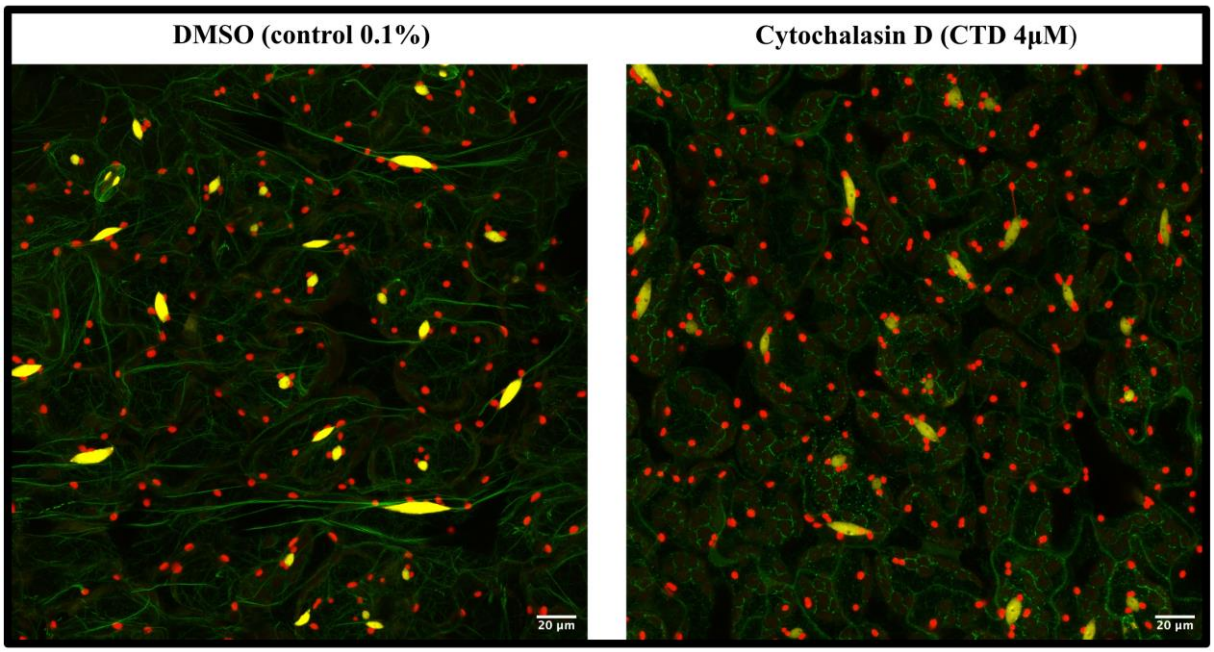

Figure 4.31 Actin disruption with cytochalasin D (CTD) treatment on Arabidopsis upper epidermal cells after 2h. Snap-shot images of plastid-nucleus and actin 2h post-treatment with 4µm of actin inhibitor cytochalasin D (CTD) or DMSO (control) on the leaf of the stable transgenic *A. thaliana*. The experiments were repeated three times with 3 replicates per treatment. The green channel shows the actin, the red channel is plastid, and the yellow channel shows the nucleus. The scale bar equals 20 µm.

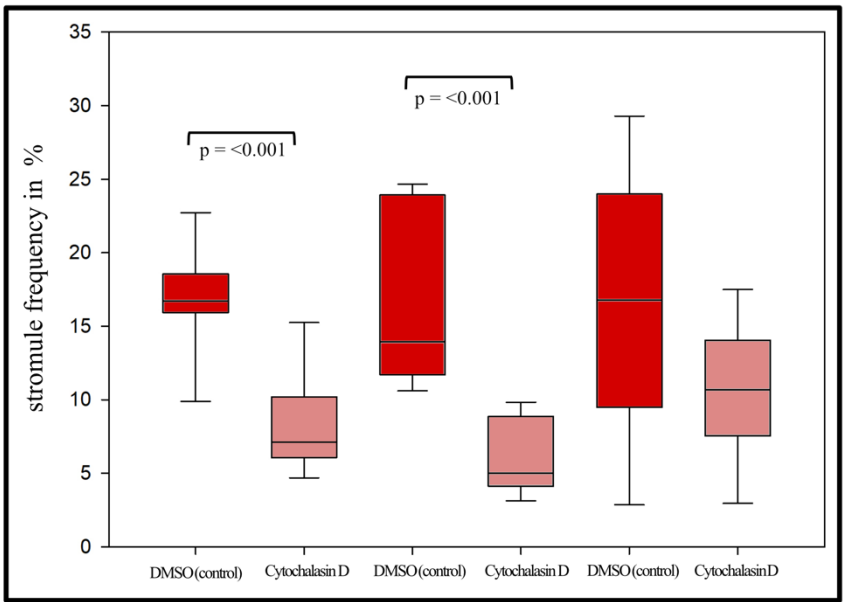

Figure 4.32 Stromule frequency in % with actin inhibitor cytochalasin D (CTD) 4µm and control (DMSO) in A*rabidopsis thaliana* upper epidermis. The experiments were repeated three times with 3 replicates per treatment.

4.17 Nucleus speed decreases with Cytochalasin D

By closer inspection of images taken after 2h of CTD treatment it became clear that in some cell's actin filaments did not completely depolymerize by the chosen treatment. Because the above-described results where snapshot data it is not clear if actin depolymerisation is sufficient to stop actin depending on processes. In order to have a better idea how well the treatment impacts actin related processes I wanted to test if nucleus movement, a process strongly depending on actin (Higa et al., 2014) is impacted by CTD and how stromule frequency behaves when actin is removed. Two time-lapse movies were taken of upper epidermis cells following mock (DMSO 0.1%) or CTD treatment for approximately 120 min using a confocal microscope (Leica), using the same triple marker lines. Movies were started immediately after each treatment mock (DMSO 0.1%) and with CTD. It is nicely visible that at the beginning of the movie in the CTD as well as the control treatment actin is still visible as fibres. In the course of the experiment actin filaments started to disappear in the CTD treatment forming short point like aggregates. However, few actin filaments in some cells remained visible

Nucleus speed was measured in time-lapse movies with and without treatment via Imaris 9.6.1, and data were analysed via excel. The box graph showed that with DMSO control, the average nucleus speed was 18 µm/h in tracked 16 nuclei, while the average speed of the cytochalasin D treatment was approximately 4 µm/h (n = 16 nuclei) during 2h of the time-lapse movie (**Figure 4.33**; p = 0.001; p values mann whitney sum test **(Supplementary raw data folder)**. The box

graph demonstrated that the nucleus speed decreased considerably with cytochalasin D treatment. Although residual small fragments of actin filaments are still visible, the slowed down nucleus speed shows that the treatment impacts actin related processes significantly.

I moved on to have a closer look at the impact CTD had on stromules. When it is true that plastids are attached to actin at the tip of their stromules depolymerisation of actin should remove those anchors and should lead to the frequent collapse of stromules shortening their persistence. In order to test if stromule stability is impacted by CTD treatments I revisited the movies and observed the formation of stromules during the 2 h movies. I wanted to understand if I could see stromule behavioural changes during the depolymerisation of actin. For this I looked in both experimental conditions for stromules which were in contact with the nucleus and observed them over the whole time of the experiment. With the CTD treatment 9 out of 11 stromules and 15 out of 22 stromules retracted within the duration the 2 movies **(Figure 4.34)**. I recorded stromule retraction movements outside with no nucleus context for 1 out of 11 stromules in movie 1 for 4 out of 22 stromules in movie 2 (raw data in the supplementary). This result showed average stromule retraction movement around the nucleus with cytochalasin D was 75% and only 25% of stromules stayed persistent within the 2h of observation. One example for stromule retraction in a CTD experiment is shown in figure 4.35. The selected image showed that in the first frame of the movie stromule attached to the nucleus, moreover during the movie with the treatment of Cytochalasin D, the stromule seemed chopped off from the attachment point of the nucleus (might be surface) and showed retraction movement **(Figure 4.35)**.

In contrast to the CTD treatment stromules persistence was different for the control treatment. Interestingly persistence of stromules without nucleus context was as low as for the CTD treatment, I observed 14 out of 18 stromules to retract **(Figure 4.36)**. However, I barely observed any stromule collapse around the nucleus in the control treatment, only 4 out of 18 stromules collapsed within the 2h. Moreover, I never followed the retraction movement during the time-lapse movies, not around the nucleus. This data showed that with drug treatment, cytochalasin D stromule stability dropped in the *A. thaliana*; this clearly demonstrated that when actin filaments were removed from the cell, stromules were not stable (not staying over time) anymore. Furthermore, the movement of retraction was dominated by drug treatment when actin draws; the stromule showed retraction (pulled back to the plastid body, it does, it does not extend and stays on the cell). On the other hand, control treatment showed that the stromule did not show the retraction.

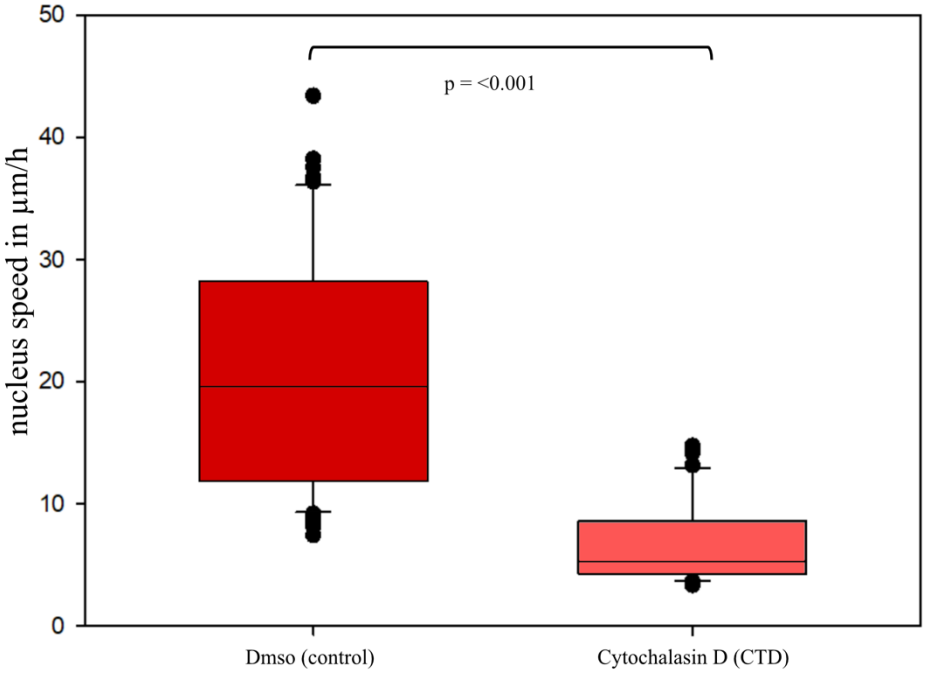

Figure 4.33 Nucleus speed changes in 90 mins time-lapse movies with CTD treatment. Box graph demonstrated the velocity of a nucleus in Arabidopsis upper epidermis with actin depolymerization drug treatment CTD (4 µM) and Control (DMSO 0.1 %) 90 mins time-lapse movies.

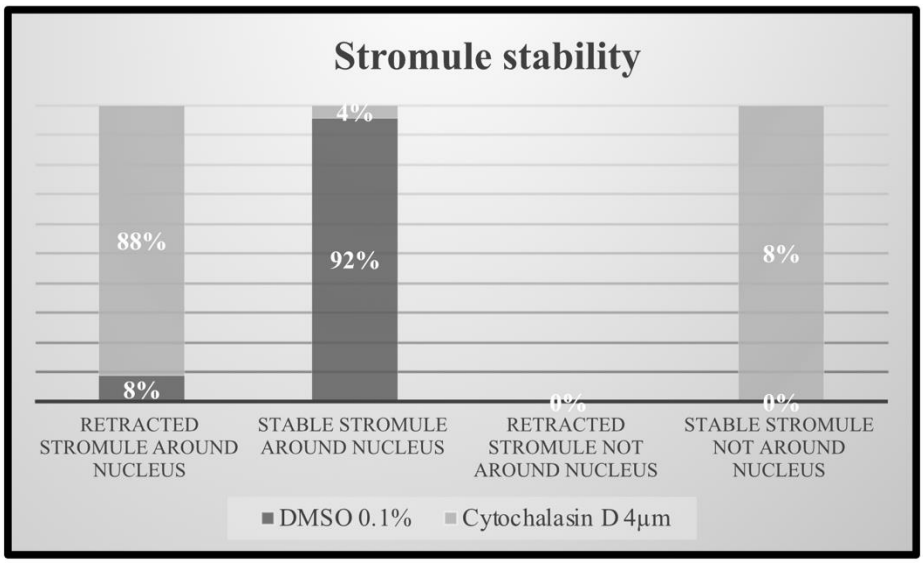

Figure 4.34 Stromule stability changes in 2h time-lapse movie, drug treatment with Cytochalasin D (4 µM) and Control (DMSO 0.1 %) 90 mins time-lapse movies.

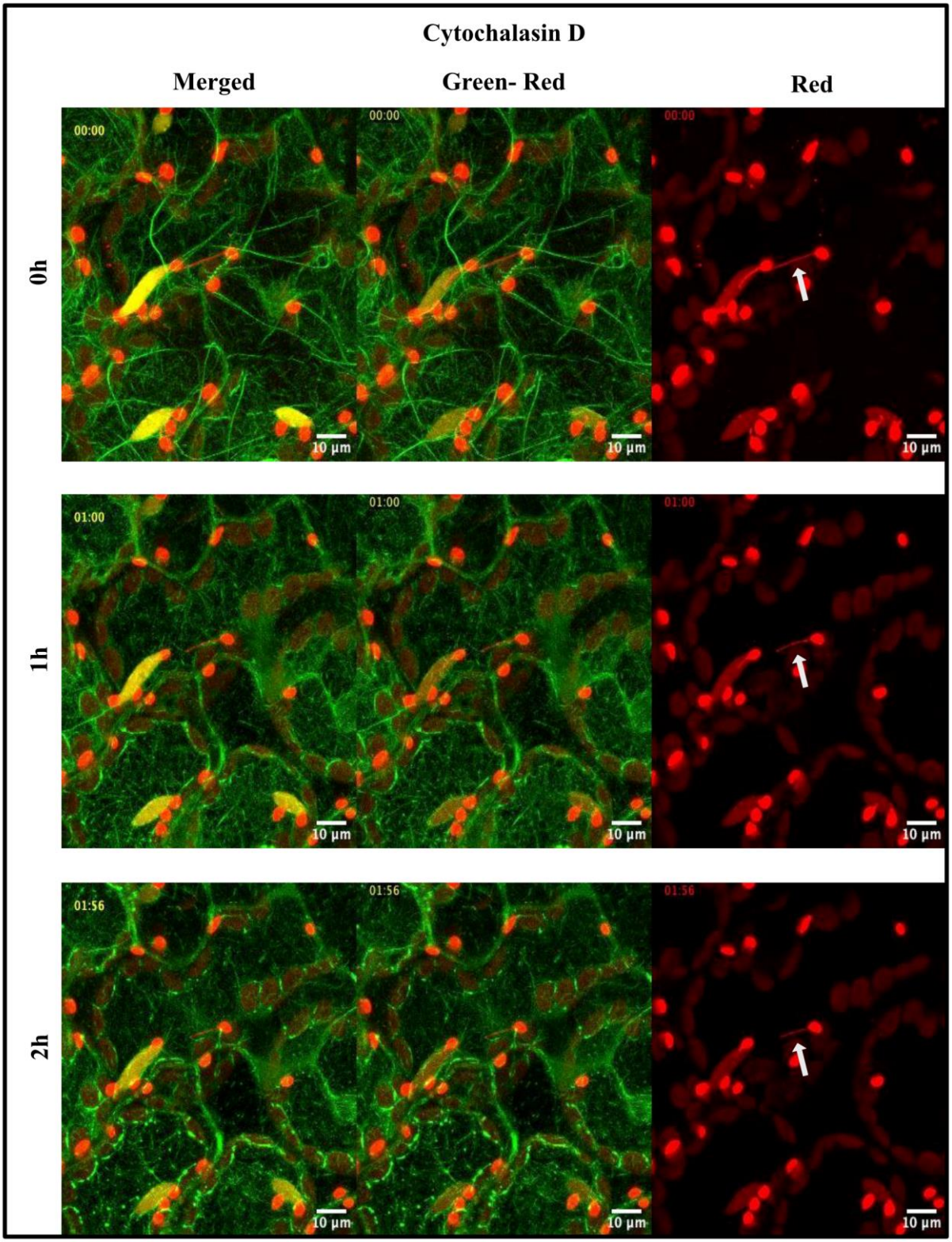

Figure 4.35 Stromule retraction movement around the nucleus. The image shows stromule retraction with Cytochalasin D treatment during 2h of the time-lapse movie (0h-1h-2h). The white arrow demonstrates stromule formation in the merge, green-red, and only red channels. The green channel shows the actin, the red channel is plastid, and the yellow channel shows the nucleus. The scale bar equals 10 µm

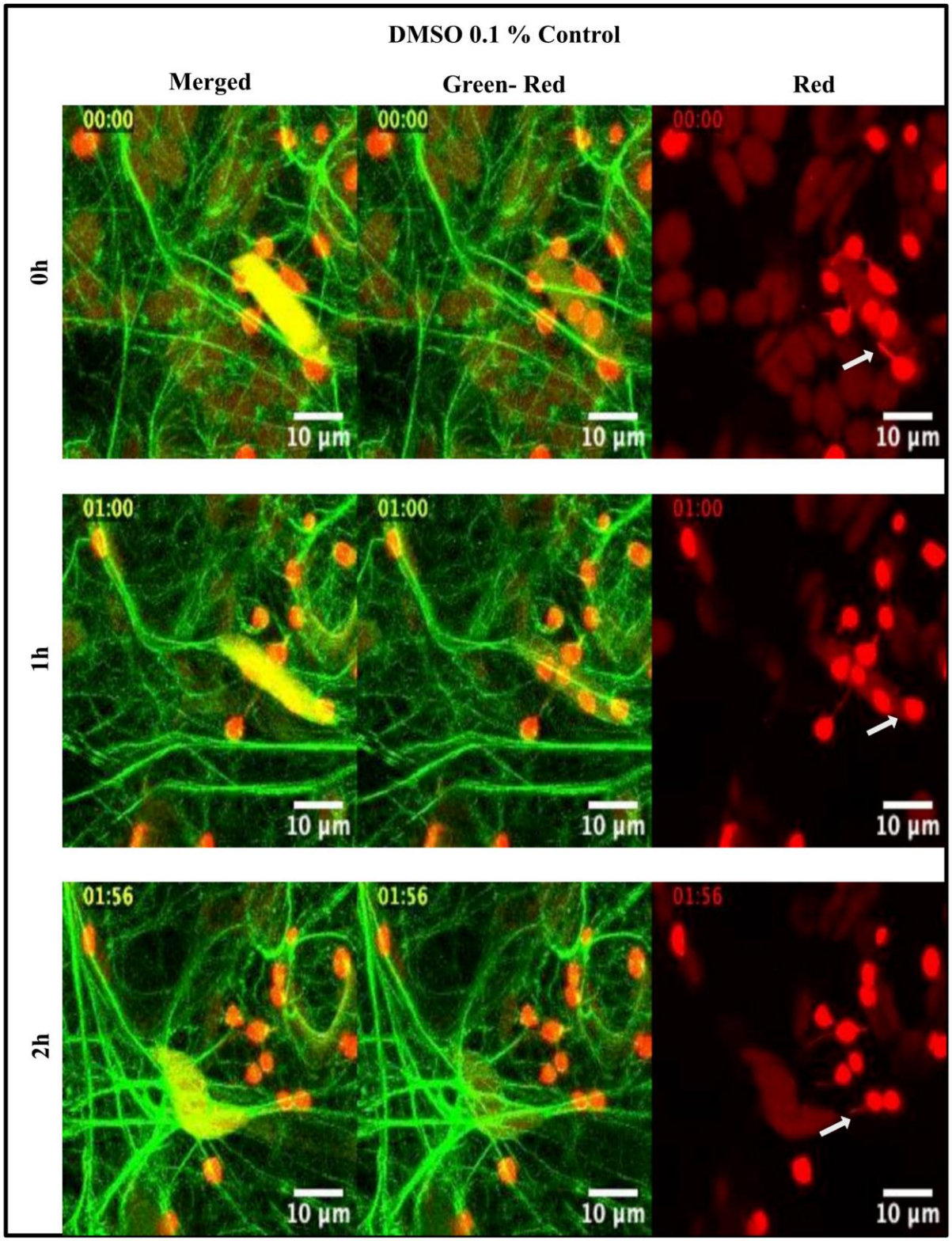

Figure 4.36 Stable stromule formation around the nucleus. Image shows stromule formation around the nucleus with DMSO (0.1 % control) treatment during 2h of a time-lapse movie (0h-1h-2h). The white arrow demonstrates stromule formation in a merge, green-red, and only red channels. The green channel shows the actin, the red channel is plastid, and the yellow channel shows the nucleus. The scale bar equals 10 µm

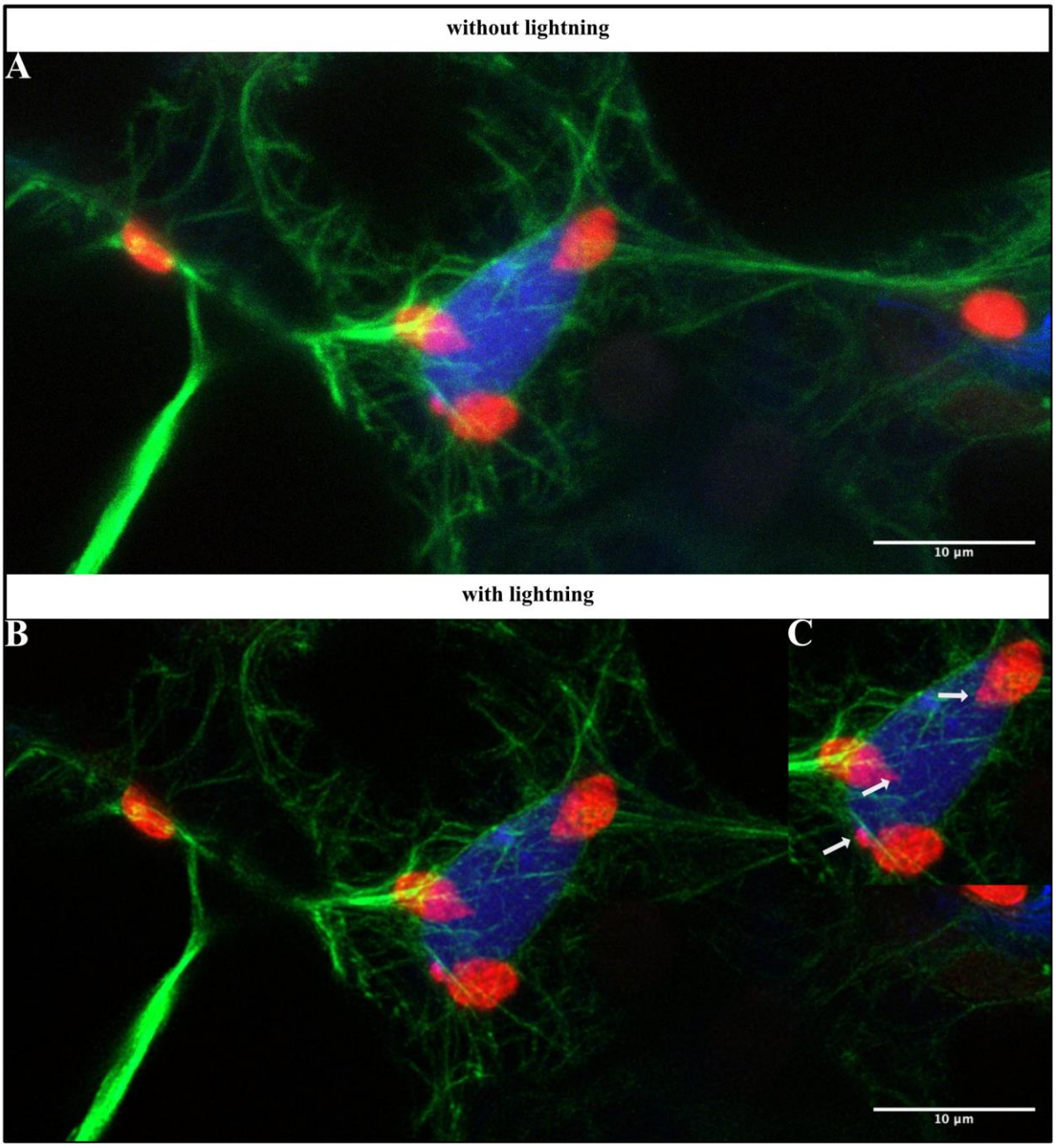

Figure 4.37 Snap-shot images of Actin-nucleus stromule localization in Arabidopsis leaf with and without lightning technique (improvement of the image). **A** Image shows stromule formation around the nucleus without lightning image resolution correction. **B** image shows lightning improvement. **C** The white arrow demonstrates stromule formation. The green channel shows the actin, the red channel is plastid, and the blue channel shows the nucleus. The scale bar equals 10 µm

The movement, even if they moved during the time-lapse movie. Stromule formation was stable over time, but they can still move around the nucleus and change direction. These results have confirmed the actin filaments on the stability of the nucleus; additionally, nucleus movement in the Arabidopsis also depends on the actin formation. However, observing the anchor point of the stromule on the nucleus surface via actin was not possible with basic microscopy technics and the confocal imaging detection limit. Snap shops or time-lapse movies did not have a

reasonable resolution to demonstrate the anchor point. Therefore, I changed the microscopy mode, which might help my resolution problem so far. I decided to use the LIGHTNING Mode in the Leica microscope to maximize the information from my specimen and get an in-depth answer. It is known that lightning detection dynamically calculates the important information for each image spot to provide higher outcomes. Hence, I can get more detailed images to see the exact localization of stromule extension on the nucleus surface. To get the improved images, I took the serial snap-shot images with selected stable transgenic lines **(Figure 4.37)**. Snap-shots showed comparatively improved resolution with the lightning mode **(Figure 4.37 A-B)**.

V. Discussion

5.1 Short summary of goals and results

Despite the commendable progress, which has been made to understand different aspects of plastid to nucleus signalling it is still not clear if specific mechanisms facilitate the transfer of plastid signals through the cytoplasm to the nucleus. At the beginning of my thesis, experiments performed manly in *N. benthamiana* (Caplan et al., 2015; Sampath Kumar et al., 2018) were used to form a model, which suggested that plastid stromules are send (e.g. as response to a triggered ETI response) out by plastids to "seek" for the nucleus, guiding plastid body movement towards the nucleus upon anchoring of the stromule tip at the nucleus. It was further suggested that this interaction and movement is supporting the respective stress response. Because literature research revealed that for full support of this hypothesis information is missing, I set my self-three goals to close these gaps.

A) Test if the proposed model in *N. benthamiana* holds true or has to be refined.

B) Investigate the Similarity of Plastid and Nuclear behaviour during ETI Responses in *A. thaliana* and *N. benthamiana*.

C) Use time-lapse imaging in *A. thaliana* mutants to understand the mechanics of nucleus-plastid interactions in upper epidermis cells in this species in more detail.

In the following paragraphs I want to discuss the challenges I faced as well as my findings described in the results section and how they extend the currently available knowledge, providing at the same time suggestions for future directions.

5.2 Long-term time-lapse imaging to capture the full ETI induced plastid reaction. (B)

Imaging ETI induced sub-cellular dynamics is still an unsolved challenge: As mentioned before, because the currently available imaging data does not cover the actual movement of plastids to the nucleus in total during an ETI response in *N. benthamiana*, my first aim was to fill this gap with imaging data covering the complete process. This would allow me to proof or disproof the current hypothesis and gain a more detailed insight into how plastids and stromules

find the nucleus. In preparation for the long-term time-lapse imaging part of this thesis, I tested in which time scale following *A. tumefaciens* infiltration the XopQ effector protein, used to induce effector-triggered immunity, would accumulate in the cells and induce the ETI reaction. The experiments showed that this takes place between 16-24 hours post-inoculation and a subsequent rapid increase of accumulation was visible within the following 24 hours, as observed in snapshot experiments **(Figure 4.2)**. These preliminary results should have enabled me to determine the optimal time frame for full time-lapse experiments, which I determined to be between 24-48 hours post-inoculation. However, transient expression of XopQ and subsequent imaging proved to be difficult. For example, long-term movies and repeated snapshots experiments demonstrated that the timing of XopQ expression was not very well to predict. I came to the conclusion that the continuous illumination during the imaging process might suppressed the accumulation of XopQ and in conclusion supresses the development of the ETI reaction (**Figure 4.3**). This idea is supported by the observation that XopQ induced cell death is stronger when the inoculated leaf is wrapped in aluminium foil, blocking light from reaching the inoculation spots. This seems indeed a common practice for this effector (Lapin et al., 2019; Qi et al., 2018). Although it is not clear why exactly this is the case for XopQ, it is an emerging concept that light exposure and perception have an impact on the plants immune system (Kim MG et al., 2021). This lends support for the idea that the light used during the imaging impacts the expression and action of XopQ in *N. benthamiana* cells, leading to a reduced ETI reaction. Hormone inducible expression systems as they are now widely used (Borghi, 2010) might provide a future solution to this problem. As described earlier in this thesis with such systems expression can be induced by the application of a mammalian hormone, such as Dexamethasone, to the plant tissue. The activated hormone receptor subsequently acts as a transcription factor, inducing the transcription of the target protein, for example XopQ. Protein production should start within a few hours of hormone application making the time of XopQ expression with these systems better predictable. However, if this will solve the issue is not clear, because still XopQ activity could be hindered by illumination. For this the hormone expression system could be combined with the use of different ETI inducing effectors, which show a more robust expression and ETI response even when illuminated, such as AvrBs2 (Caplan et al., 2015). It has to be taken into consideration that the corticoid hormone inducible systems have been reported to show in some cases low background expression, despite the absence of the respective hormone. Because effector protein perception is very sensitive and even small amounts of protein cause cellular reactions,

this 'leakiness' can cause problems in stable transgenic plants (Gonzalez et al., 2015), resulting in autoimmune phenotypes as also reported here for the METI construct. An interesting option which could be explored in future is the combination of an inducible system with a suicide exon and a specific splicing factor. Such a system has been successfully used to establish an inducible effector expressing *N. benthamiana* plant line, showing hormone inducible ETI ((Gonzalez et al., 2015); for more details see also discussion part B).

A different issue I faced was that *N. benthamiana* tissue continues to expand during long term imaging (20-30 h), resulting in significant drift. I suspect that this is due to the uptake of water, used as mounting medium, by the leaf cells. Although the drifting issue can be compensated to some degree by drift correction procedures in Imaris and Fiji, making it possible to extract numerical data, the quantity of extractable data suffered significantly. Here in future the further optimisation could help to increase the imaging data quality. This could be done by the use of different imaging chambers or the use of a medical adhesive to glue the leaf in place on the coverslip.

Control imaging conditions allow to study plastid nucleus interactions in *N. benthamiana*:

Following my initial experiments I came to the conclusion, that especially due to the unreliable expression of XopQ it was not possible to further follow my original goal to observe plastids and nuclei throughout a XopQ induced ETI response. However, some of the obtained imaging data I was still able to use to learn more about plastid-nucleus interaction in *N. benthamiana*.

During my analysis of long-term movies, I made a surprising observation: under control conditions (no XopQ, just the mounting medium), time lapse movies showed clustering and stromule formation **(Figure 4.5)**. The most likely cause of this is light stress resulting from continuous imaging. It is known that laser scanning microscopy is not only a strong blue light source, being probably perceived as strong blue light by respective photoreceptors, but it is at the same time the cause of H_2O_2 production in epidermis chloroplasts (Dopp et al., 2023; Ugalde et al., 2021). Although the later was shown for 405 nm excitation in combination with 488 nm, it is likely that 488 nm light alone has similar effects. Thus, my imaging conditions most likely represent a combination of a strong blue light signal and the release of H_2O_2 from plastids. Interestingly, H_2O_2 is known to induce stromule formation as well as plastid clustering at the nucleus (Caplan et al., 2015; Ding et al., 2019). Further, strong blue light is known to induce plastid avoidance movement(Sztatelman et al., 2016). Although in my experiments I could not provide direct experimental proof for these stresses to be present, it is likely that both processes in combination are the reason for the observed plastid behaviour in my control

movies: 1) induced stromule formation and plastid clustering along with 2) plastids avoiding the centre of the cell, moving towards the anticlinal (side) cell walls. Although here no ETI was triggered these movies provided the unexpected opportunity to study stromule formation and plastid clustering in continuous movies, likely in response to strong blue light and H_2O_2 production by the plastids. In order to test the stromule guided plastid to nucleus association model I collected quantitative data on plastid nucleus interactions in these movies.

Nuclei are mobile and have to be considered in plastid-nucleus interaction studies: Because no long-term imaging data of nuclei in *N. benthamiana* is available it was surprising to find the nucleus in *N. benthamiana* lower epidermis to be highly mobile. In many cells nuclei were observed, moving throughout the cell, covering larger areas of the cell. In contrast to nuclei in *A. thaliana* upper epidermis, which show a more localized oscillating motion, nuclei in the lower epidermis of *N. benthamiana* seem to move more freely. Because nucleus position in *A. thaliana* is known to be impacted by blue light (Higa et al., 2014; Suetsugu et al., 2016). I tested whether this observed movement was induced by the 488 nm laser light, used to excite the plastid EGFP marker, I recorded control movies without the use of this blue laser line. Surprisingly, I found nucleus speed to be similar in movies with and without 488 nm laser light. Therefore, the observed movement is not light induced. If nuclei move as observed in cells, not currently under imaging is hard to say, because preparing leaf discs for imaging in imaging chambers will induce a number of physiological reactions, which could also impact nucleus mobility. The reason why the mobility of nuclei was a surprising finding is that none of the previous studies, which looked into plastid-nucleus interactions (Caplan et al., 2015; Sampath Kumar et al., 2018) covered longer time scales and were restricted to few minutes. In the light of my observations this is too short realise the actual nucleus moving behaviour. Longer time frames (hours) are needed to appreciate the complex nucleus behaviour. Hours seems also to be the time frame, which is needed for a plastid accumulation response to take place in transient expression experiments (Caplan et al., 2015; Sampath Kumar et al., 2018). Thus, my results clearly show that when plastid nucleus interactions have to be followed over such long-time spans to analyse conclusively analyse plastid nucleus interactions.

Stromules play a minor role in plastid-nucleus interactions during light stress: The quantitative analysis of plastid nucleus interactions by the use of a scoring system, representing different mode of interactions, showed that nucleus movement plays a more important role in plastid-nucleus interactions than plastid movement. Meaning that in most cases nuclei moved toward the plastid and not as suggested by the model *vice versa*. Additionally, stromules had a

small role in making first contact. This is one of the key findings of these experiments, because this contradicts the current model, which suggested that stromules grow towards the nucleus, which allows the plastid body to later follow the stromule toward the nucleus. My analysis shows that such movements indeed exist, but that the majority of interactions is independent of stromules and are mostly driven by nucleus movement. Thus, a different mechanism must be responsible for plastid-nucleus accumulation or at least a stromule intendent second mechanism contributes to it in majority. This is in agreement with findings of (Prautsch et al., 2022), which also collected evidence for plastid accumulation at the nucleus and stromule formation during an ETI, showing that even without the induction of ETI induced stromule formation efficient plastid clustering takes place. It is worth noting, that these observations were made in the context of light stress and not ETI. Therefore, it remains a possibility that plastid-nucleus interactions during ETI responses follow the model suggested by (Caplan et al., 2015). If this would hold true it would suggest that there are stress specific ways for plastids to interact with the nucleus. This, will have to remain open until ways have been found to overcome the above-described imaging obstacles.

Stromule formation seems intensified close to the nucleus: So how is plastid clustering happening than? In some cases, it appeared that plastids coming in close proximity to the moving nucleus became more stromule-forming active, an effect, which was observed before in *A. thaliana* upper epidermis cells by (Erickson et al., 2017). The authors showed that in a several µm wide zone around the nucleus stromule formation is very frequent resulting in a concentration of stromules in this zone. The time laps data shown in this publication show stromules to be connected to the nucleus periphery moving in concert, indicating a connection between both organelles. Also, in my movies stromules were visible to follow the nucleus movement in a similar manor. In contrast to *A. thaliana* in *N. benthamiana* plastid bodies often started to follow the nucleus through the cell, giving the impression that the nucleus collects plastids on its way, forming nucleus associated plastid clusters. In the way the nucleus collected plastids, it also frequently left plastids behind, a situation, which was not as often observed in *A. thaliana*. Further in *A. thaliana* plastid clusters seems always present, even at the beginning of observations. In *N. benthamiana* the stromule promoting zone and clusters were established in response to the imaging conditions. In conclusion *A. thaliana* and *N. benthamiana* share similarities in plastid nucleus interactions, but also show differences. Unfortunately, it was not possible in the time frame of this theses to collect quantitative data to support these

observations and this could be an interesting future direction for research. This would help to understand if stromule formation and behaviour is uniform or specific to tissue and/or species. **In conclusion:** Based on the current model, the initial expectation was that the plastid would establish contact with the nucleus by growing stromules, followed by movement of the plastid body towards the nucleus. However, the specific imaging setup used in this study did not support these expectations, indicating that the current model may not fully explain the process of plastid-nucleus cluster formation in *N. benthamiana*. This suggests the need to either modify the existing ETI model or consider stress-specific mechanisms that influence plastid-nucleus interactions. Interestingly, I observed that nucleus movement, although not readily apparent in short-duration movies, emerged as a significant factor over longer time scale. Therefore, I propose that future studies investigating plastid-nucleus interactions, particularly in response to ETI in N. benthamiana, should consider the role of nucleus movement. It is important to note that continuous imaging data is crucial for understanding the clustering process in response to ETI. Overcoming the limitations associated with imaging ETI processes will be essential for gaining a deeper understanding of this phenomenon. As a result, it remains unclear whether the current model requires a general reconsideration or if the mechanisms by which plastids locate the nucleus are stress-specific. Further research is needed to address these questions and to unravel the complexities of plastid-nucleus interactions during ETI.

5.3 Plastid nucleus interactions in *A. thaliana* as responds to ETI (B)

The behaviour of plastids and nuclei in *A. thaliana* in response to ETI is unknown: The proposed model of stromule-mediated nucleus-plastid clustering was established through observations in transient expression assays using *N. benthamiana* (Caplan et al., 2015; Sampath Kumar et al., 2018). While stromule formation in response to infiltration with ETI-inducing *P. syringae* strains was also observed in *A. thaliana*, there is currently no available information on how this specific ETI response affects the interaction between plastids and nuclei in this species. Therefore, it remains unknown whether plastids and nuclei react similarly during triggered ETI in *A. thaliana* as they do in *N. benthamiana*. To address this knowledge gap, our objective was to employ a hormone-inducible expression system to trigger ETI in *A. thaliana* while simultaneously visualizing organelle dynamics for a comprehensive understanding of their dynamic interactions, following ETI induction. There are several reasons for choosing a hormone-inducible system to study effector-triggered immunity in this context: **1. Improved control of effector expression time points:** By using a hormone-inducible system, the timing

of ETI onset can be better regulated compared to other methods such as transient expression in *N. benthamia* (see previous discussion point). **2. Continues imaging with imaging chambers:** The implementation of microscope flow chambers provides a valuable method for inducing ETI and conducting continuous imaging experiments concurrently, using a hormone-inducible system. This allows for the application of expression-triggering hormone during imaging while maintaining the ongoing imaging experiment. This setup would allow to cover the whole process, from preinduction to post induction = ETI reaction. **3. Ability to differentiate between PTI and ETI reactions:** With the use of a hormone-inducible system, it becomes possible to induce only ETI responses without triggering pathogen-associated molecular pattern-triggered immunity, which is always triggered when bacteria are present, allowing for focused investigation on the ETI specific immune pathways.

The METI strategy failed to provide usable plant lines: A crucial aspect of studying the interactions between plastids and the nucleus in *A. thaliana* involves developing the molecular tool, which allows to effectively visualize organelles and to express the effector protein. To establish such a system in *Arabidopsis thaliana*, I adopted a modified version of the SETI system developed by (Man Ngou et al., 2020). This new approach, which I called METI, includes two marker genes for organelle visualization along with the SETI system to simplify visualization and analysis of plastids and nuclei. Through the integration of these organelle markers into the inducible effector system, METI was meant to enable me to transform all components needed for analysis in one single transformation event, making it specifically useful for the analysis of plant lines with multiple mutations. As outlined in the results section I was able to design and clone various iterations of the METI system. Regrettably, there was a challenge in obtaining plant lines with satisfactory marker expression while simultaneously maintaining normal plant growth characteristics. Conversely, there was an association between organelle marker expression levels and hindered plant growth. It appears that this outcome is likely attributable to the incomplete suppression of gene expression within the estradiol system, which relies on the core 35S promoter sequence. Thus, the initial approach appears to have been unsuccessful, indicating that a change of strategy may be warranted in this case.

Alternative strategy 1: As already mentioned, research by (Man Ngou et al., 2020) showed, it is generally feasible to establish lines with inducible effector-triggered immunity without any growth-related effects. However, as I have found this may not be possible when strong expressing organelle markers are included as part of the selection process. As an alternative

strategy, one could consider first establishing a line with inducible AvrRps4 expression and no observable phenotypic changes or straight away utilize the ETI-inducing lines already developed by (Man Ngou et al., 2020). Those could be used to introduce a marker plasmid, carrying the plastid and nucleus marker, through super transformation. This would provide 'wildtype lines' for the study of nucleus plastid interactions, with no growth phenotype. If analysis in mutant backgrounds is needed it would be the most efficient to introduce necessary mutations into this original 'wildtype line' by using CRISPR techniques. As demonstrated by (Ordon et al., 2021) even the creation of multiple mutant alleles in a single transformation event could be created this way.

Alternative strategy 2: Alternatively, addressing leaky expression can be achieved through the strategic utilization of a synthetic variant of the suicide exon P5SM (Gonzalez et al., 2015), Hyp5SM (Hickey et al., 2012). This innovative strategy is based on the interplay of the ribosomal protein L5, which plays a pivotal role in ribosomal RNA maturation in all plants, with the specific secondary structure of the P5SM exon. In instances where the ribosomal protein L5 is present, the exon is effectively skipped during mRNA maturation, resulting in the production of accurate mRNA. However, in cases where the ribosomal protein L5 is either absent or present in limited quantities, the exon remains retained within the mRNA. This inclusion of the exon introduces a premature stop codon into the mRNA sequence, rendering it susceptible to degradation via the nonsense-mediated decay pathway (Hammond et al., 2009). Hyp5SM represents a synthetic chimeric exon, which only can be bound by rice OsL5. This characteristic allows for the effective splicing of the Hyp5SM exon in dicot species, such as *A. thaliana* and *N. benthamiana*, only when co-expressed with OsL5. The collaborative arrangement between an inducible effector housing the Hyp5SM exon and the inducible expression of the ribosomal protein OsL5 emerges as a robust mechanism to counteract inadvertent background expression stemming from leaky inducible promoters. This system has already demonstrated its efficacy in establishing inducible AvrBs2 expression in *N. benthamiana* (Gonzalez et al., 2015). Even in the presence of Dex promoter leakiness, the resulting AvrBs2 coding mRNA retains the Hyp5SM exon, promptly invoking a premature stop codon and subsequent mRNA decay. Successful skipping of the exon and AvrBs2 production is achieved only when Dex is employed to simultaneously induce the expression of AvrBs2 and ribosomal protein OsL5, thereby ensuring a sufficient concentration of OsL5 for exon skipping. This framework holds potential for adapting AvrRps4 expression in *A. thaliana*.

However, it's important to acknowledge the challenge posed by the integration of the exon into the gene of interest. Careful integration is essential to ensure that exon skipping occurs while maintaining the correct reading frame in the resulting mRNA. Unfortunately, due to time limitations, exploring these alternative strategies was regrettably beyond the scope of this thesis.

5.4 Mechanics of nucleus-plastid interactions in upper epidermis of *A. thaliana* (C)

What is the significance of the stromule promoting zone in *A. thaliana* upper epidermis? Attempts to study the change in stromule frequency and plastid position during a triggered immune reaction faced challenges that couldn't be addressed within the thesis timeframe. However, previous research by previous students in the Schattat lab (J. Marx, C. Alfs, and J. L. Erickson) demonstrated that in *A. thaliana* upper epidermis, unlike unchallenged *N. benthamiana* lower epidermis, plastids and stromules are associated with the nucleus, even in unchallenging conditions. Our lab's experiments revealed a stromule-promoting zone around the nucleus, where stromule frequency is significantly higher (Erickson et al., 2017). This supported the hypothesis that stromules reach out to the nucleus for signal transfer, as proposed by (Caplan et al., 2015) and (Sampath Kumar et al., 2018). However, time series experiments unveiled unexpected behaviour of nuclei and stromules. Stromules formed when the nucleus moved away from the stationary plastids, indicating a strong correlation between nucleus movement and stromule formation. Based on this observation, an alternative hypothesis emerged, suggesting that **nucleus movement drives stromule formation** in this tissue, rather than stromules reaching out to distant nuclei. Multiple mutants affecting nucleus movement, studied by J. Marx and J. L. Erickson, supported this hypothesis (unpublished data). Analysis of time-lapse data revealed that stromule width changes during nucleus-driven stromule formation, a phenomenon similar to the thinning observed in artificial lipid vesicles forming stromule-like tubules. This thinning is attributed to the limited membrane surface, which restricts the length of the tubules. When the limit is nearly reached, tension builds up in the tubule, resulting in the observed thinning.

Do plastids really restrict nucleus movement? Based on these findings, it was hypothesized **that plastids, attached to the nucleus surface with limited membrane area, restrict nucleus movement** and generate tension in stromules when the nucleus moves away, resulting in a plastid-nucleus complex, **which potentially could ensure efficient retrograde signalling** in this tissue, characterized by low plastid density. Therefore, I focused on examining whether

plastids indeed impose restrictions on nucleus movement and if a close and significant association exists between these two organelles. To address this, I pursued two distinct lines of inquiry.

1st: I explored the possibility of changing a plastids' capability to form stromules by reducing the potential length of stromules. This line of investigation aimed to assess the impact of altered stromule extension on the movement of nuclei, which would help to asses if indeed nucleus movement is restricted by plastid attachment and the limited stromule length. The results obtained from the *msl2_msl3* mutant lines (stronger restriction of nucleus movement than wildtype), are complementary to results obtained in the group of M. Schattat on plastid division mutants. Those mutants have less but larger plastids than wildtype (Haswell & Meyerowitz, 2006) and their stromules are generally longer due to an access of membrane (Haswell & Meyerowitz, 2006). J. Marx could show that nuclei in these mutants are more mobile due to the extra-long stromules (unpublished). Taken together the collected evidence clearly indicates that nucleus movement is restricted by plastid attachment in wildtype plants.

2nd: In order to further complement the experiments, I aimed into identifying ways to sever the connection between the stationary plastids and nuclei. Ideally, a mutant missing protein forming the hypothetical attachment complex between stromules and the nucleus would be optimal for this purpose. Regrettably, such mutants are not currently available due to the elusive nature of this complex. Given the limitations in directly targeting the attachment complex, I used an alternative approach involving mutants deficient in plastid positioning. In these mutants (*chup1, kac1_kac2, chup1_kac1_kac2*), plastids lack a fixed anchoring position and are instead carried along passively with the nucleus during movement, thus not applying restricting forces on the nucleus. The outcomes from both experimental directions yielded with much faster nuclei complementary results for results obtained in the 1st direction, lending further support to the hypothesis of restricted nucleus movement due to plastid interactions.

Although the absence of mutants directly deficient in stromule-nucleus attachment was a challenge, the findings presented here provide robust backing for the initially proposed hypothesis.

What is the biological meaning of plastid restricted nucleus movement? I propose that the close association observed between plastids and the nucleus might have functional implications for plastid-to-nucleus signalling. This proximity could potentially facilitate efficient signal transduction, including molecules like H_2O_2, as demonstrated by (Exposito-Rodriguez et al., 2017). This might be specifically important in the sparsely populated epidermis cells in which

signal transfer from few plastids in the lager cells might be supported by additional mechanisms, such as close proximity. The anchoring of plastids to the nucleus would ensure the constant contact of the nucleus to a sufficient number of plastids. Thus, my findings contribute significantly to our understanding of the dynamic interplay between these organelles and hint at potential functional implications in retrograde signalling.

What could be future directions? The next important step would be to test if indeed plastid attachment supports plastid nucleus signalling. My experimental findings suggest a possible indirect linkage between the plastid envelope and the nucleus, possibly mediated through the association with actin fibers surrounding the nucleus. Therefore, one potential avenue involves the exploration of mutants lacking the stromule anchoring complex, resulting in a nucleus capable of free movement without associated plastids. This would fill in the last gap of the so far used mutant analysis. These mutants could be further subjected to stress conditions known to trigger retrograde signalling. If the plastid-nucleus interaction is indeed physiologically relevant, these mutants should display deficiencies in response to such stressors. Additionally, mutants with larger plastid nucleus clusters (e.g. *chup1*) could complement those experiments, nicely and should show stronger reactions to these conditions. In order to unveil the enigmatic anchoring complex, basis of creating such mutants, close proximity labelling methods, such as split turbo ID (Cho et al., 2020) could be employed to identify proteins that interact with both actin and the outer envelope membrane. Further, members of the not completely analysed NET-Protein family are promising candidates for such mediating anchors (Deeks et al., 2012). This protein family is characterised by possessing an actin binding domain as well as a membrane anchor (Deeks et al., 2012). Specifically interesting is the member Net3A, which has been shown to label in BY2 cells actin filaments as well as dot like structures on actin filaments. Some of those dots even have been seen nucleus associated, providing a labelling patter expected of a potential stromule tip anchor. Co-localisation experiments of stromule tips and Net3A and mutant analysis could be of use to test if Net3A is involved in stromule anchoring. Independent of these stress experiments, a way to test if indeed plastid association has an impact on plastid to nucleus signal transfer could be based on the work of (Exposito-Rodriguez et al., 2017), which used Hyper probes to show that strong light exposure results in H_2O_2 production in epidermis plastids and to its transfer to the nucleus. The addition of mutants with altered plastid nucleus association would add the possibility to this setup to decipher the impact of plastid nucleus clusters in H_2O_2 transfer from plastids to nuclei. Mutants with less plastids

at the nucleus should show slower H_2O_2 accumulation and mutants with higher plastid accumulation should show faster H_2O_2 accumulation.

5.5 Are there species-specific differences in nucleus plastid interactions?

As outlined at the beginning of the discussion at the beginning of my thesis, it was suggested that nucleus distant plastids form stromules to reach out and search for nuclei using resulting stromule nucleus contacts to guide plastid movement (Sampath Kumar et al., 2018). This model was based on experiments in *N. benthamiana* in response to ETI induction, showing stromule frequency increases as well as formed plastid clusters (Caplan et al., 2015). It occurred to me that it was not discussed in the respective publications if this is specific to *N. benthamiana* and ETI or if this is general and also applies to *A. thaliana* (Caplan et al., 2015; Sampath Kumar et al., 2018). In deed in the respective publication stromule increase in *A. thaliana* was shown in response to ETI inducing conditions, but data on relative position of plastids and stromule relative to the nucleus was not collected. So, it is not only important to test if this stromule guidance model is true in *N. benthamiana*, but also if this is a general phenomenon or if this is species or even tissue specific. As already discussed at least for light stress induced clustering in *N. benthamiana* stromule play a minor role and the model from *N. benthamiana* would have to be changed in this regard, taking into consideration that also ETI stromules and clustering are similar to light stress induced interactions. Additionally, experiments collected in my thesis indicate important Differences between *A. thaliana* and *N. benthamiana* in plastid nucleus interactions. Comparing plastid nucleus relations in unstressed cells show that in the upper epidermis of *A. thaliana* plastids are clustered around the nucleus and stromules are attached to it. In *N. benthamiana* plastid clusters at the nucleus are rare and most nuclei have one or two plastids associated or even none. So, in *N. benthamiana* the plastid-nucleus complex is a response to stress conditions, where as it seems in *A. thaliana* to constantly established. Additionally, I was not able to find any literature reporting plastid cluster formation in response to stress for *A. thaliana*. Only in the curse of plastid division as seen in dividing protoplasts plastid accumulation at the nucleus was observed (Sheahan et al., 2004, 2020). Interestingly, also similarities can be seen between both species. In the course of imaging *N. benthamiana* plastids and nuclei I observed the onset and continues stromule formation and nucleus association of stromules in close proximity of the nucleus. Although, quantitative data was not recorded in my thesis, this behaviour was reminiscent of the stromule promoting zone in *A. thaliana* upper epidermis cells, except that it was induced by imaging.

One has to keep in mind while comparing the here presented results from *A. thaliana* and *N. benthamiana* that in *A. thaliana* we focused on the upper epidermis and in *N. benthamiana* on the lower epidermis, which could impact organelle behaviour.

In conclusion: It is striking that there are no studies on stromule and nucleus interactions available, which provide a side-by-side analysis of *A. thaliana* and *N. benthamiana*. Instead findings from different species and tissues are used to conclude on general brought concepts of stromule function. Also, in my thesis this comparison is missing, in the future this should be done, because my results indicate a potential difference between species and or tissue type.

Despite the lacking ideal tissue and species comparing experiments in this thesis, it is reasonable to conclude that in both species plastid nucleus complexes exist and that nucleus movement is an important aspect of organelle interaction within this complex and that stromules associated with the nucleus periphery play a role. However, both species developed different strategies to enforce plastid nucleus complexes. Whereas in *A. thaliana* the complexes exist and are responsible for restricted nucleus movement ensuring a constant high contact between both, *N. benthamiana* establishes the complexes only when needed during stress.

5.6 Does the here reported nucleus movement behaviour contradict existing reports?

So far most of the studies focusing on nucleus movement in *A. thaliana* consider blue light to be the trigger for nucleus movement (Higa et al., 2014; Suetsugu et al., 2016). Hence, my control experiments testing if blue light (488 nm) drives the observed nucleus movement. Surprisingly, blue light had no beneficial effect on nucleus speed in my experiments. Although only exposed to red light the nuclei continued to move, even with faster speed. This seems to contradict literature reports. It was reported that nucleus movement is mediated by nucleus associated plastid movement (Higa et al., 2014) in which plastids guide (drag) the nucleus away from strong blue light sources, the anticline cell wall in *A. thaliana* pavement cells (Higa et al., 2014). This makes the moving plastids the active part of this nucleus movement and repositioning. In my experiments however I found the nucleus in *A. thaliana* to be actively moving on its own and the plastids to be rather stationary. The reason for this might be that in the study of (Higa et al., 2014) plastids and nuclei where locally illuminated by higher blue light intensities, inducing plastid strong light avoidance movement. In my movies the scanning laser illuminates a larger area covering whole cells, which corresponded more to the natural situation. That indeed nuclei move without any plastids help is demonstrated by my observations in the *msl2_msl3* mutant plants in which I found cells with no plastids and thus

also nuclei without any plastid attached. In these cells nuclei moved freely and even with the highest speeds I measured during my thesis. I hypothesis at this point that in general nuclei perform an oscillating movement in *N. benthamiana* and *A. thaliana* and that this movement is not supported by plastid movement. Only under a strong blue light imbalance induced plastid plastid avoidance movement over writes the normal behaviour and drags the nucleus out of the strongly illuminated cell parts.

5.7 How do actin and/or MT contribute to stromule formation?

Currently, our understanding points to the vital role of microtubules as well as actin filaments, in maintaining wild-type stromule levels and forms. Although the involvement and impact of microtubules on stromule formation seem to diverge across tissues, plastid types and even potentially species (Erickson et al., 2018; Holzinger, Wasteneys, et al., 2007; Kwok & Hanson, 2003; Natesan et al., 2009; Sampath Kumar et al., 2018) the consensus is clearer regarding actin's significance. Evidence indicates that actin filaments play a broader and more widely acknowledged role. Indeed, a variety of tissues, such as the *N. tabacum* hypocotyl epidermis (Kwok & Hanson, 2003) *Oxyria digyna* mesophyll (Holzinger, Wasteneys, et al., 2007), *N. benthamiana* lower leaf epidermis peels (Natesan et al., 2009) and onion bulb epidermal cells (Holzinger, Wasteneys, et al., 2007) have demonstrated the essentiality of actin in stromule frequency and shape maintenance. In a pivotal study by (Kwok & Hanson, 2003), treatment with microfilament inhibitor Cytochalasin D (CTD) and actin polymerization inhibitor Latrunculin B (LatB) yielded significant insights. Stromule frequency was notably reduced post-treatment, with the remaining stromules exhibiting a distinctive shorter and thicker morphology compared to untreated tissue. Intriguingly, a subset of stromules that persisted following CD and LatB treatment displayed loop-like structures, evoking the notion of anchoring, extension, and subsequent release from actin. This dynamic leads to the formation of a relaxed membrane loop at the plastid surface, akin to the "remnant loop" phenomenon described by Gunning in Iris unguicularis petals (2005) (Gunning, 2005). Notably, the outcomes observed upon exposure to actin inhibitor treatments strongly suggest a tethering effect between stromules and actin, stabilizing stromule dimensions, abundance, movement, and overall dynamics. This association with actin as anchor points was also supported by (Sampath Kumar et al., 2018).

The role of microtubules in stromule formation is support by less studies and was not clear until stromule tip growth was observed to take place along microtubules in lower epidermis

cells of *N. benthamiana* (Erickson et al., 2018; Sampath Kumar et al., 2018). This suggested that kinesins as motor proteins are involved in stromule formation in a microtubule's dependent manor. The observations seem to put now kinesins and microtubules in the centre of attention. However, (Erickson et al., 2018) clearly showed by depolymerising microtubules, that also microtubule independent stromule initiation and extension takes place, making microtubules based stromule formation only one of potentially multiple ways for forming a stromule, even in *N. benthamiana*. It is noteworthy that similar visualizations of stromule growth on microtubules has not been done in *A. thaliana* leaving it open to speculations if also in this species microtubules play an active role in elongation.

One reason for why stromules are preferentially abundant when plastids are near to the nucleus is the unequal distribution of actin throughout the cell. If actin is important for stromule elongation, then more actin around the nucleus may contribute to a greater number of possible stromule anchor or initiation sites, increasing the likelihood that the plastid will begin a stromule. This theory is supported by the presence of large actin concentrations in *A. thaliana* mesophyll cells adjacent to the nucleus (Kandasamy & Meagher, 1999). Cryofixation of leaves, followed by actin immunofluorescence localization, demonstrates the presence of a dense basket of thin actin filaments around the nucleus (Kandasamy & Meagher, 1999). The nucleus is connected with thicker actin bundles that extend down the length of the cell in both pavement and mesophyll cells (Higa et al., 2014; Kandasamy & Meagher, 1999). A number of tiny actin filaments stretch in random directions into the cell cortex from these bundles (Kandasamy & Meagher, 1999). Assuming that the chance of generating a stromule is proportional to the number of actins contact sites, the lower actin density in this location might, at least in part, induce a drop in stromule appearance in the cell cortex. According to time-lapse movie data, the abundance of stromules around the nucleus appears to be aided by both a highly mobile nucleus and, maybe, a high actin density in this location. In other words, inside the stromule-promoting zone, there are many possible actin-anchoring sites accessible for plastids, and the movement of both the nucleus and the surrounding actin generates the "force" required to make stromules. Pavement cell live-cell imaging revealed that the actin basket encircling the nucleus, together with the encaged nucleus and closely linked plastids, is continually moving (Higa et al., 2014). This arduous nucleus migration is confirmed in films. Based on the data from the movies, it is reasonable to assume that when plastids do not instantly follow the moving nuclei, plastid-actin contact points are shifted away from the plastid body, causing stromules to "pull" out.

In conclusion the results of my thesis support the idea that there are different stromule forming mechanisms at play, which might imply that stromules also have different functions and different regulating mechanisms. My results provide additional evidence for involvement of actin (possible also myosin) in stromule formation in an indirect way by moving the nucleus and by this pulling out stromules at plastid-actin-nucleus anchor sites, a process independent of microtubules.

VI. Literature

Aggarwal, P., Challa, K. R., Rath, M., Sunkara, P., & Nath, U. (2018). Generation of inducible transgenic lines of arabidopsis transcription factors regulated by microRNAs. In *Methods in Molecular Biology* (Vol. 1830). https://doi.org/10.1007/978-1-4939-8657-6_4

Avendaño-Vázquez, A. O., Cordoba, E., Llamas, E., San Román, C., Nisar, N., De la Torre, S., Ramos-Vega, M., de la Luz Gutiérrez-Nava, M., Cazzonelli, C. I., Pogson, B. J., & León, P. (2014). An uncharacterized apocarotenoid-derived signal generated in ζ-carotene desaturase mutants regulates leaf development and the expression of chloroplast and nuclear genes in Arabidopsis. *Plant Cell*, *26*(6). https://doi.org/10.1105/tpc.114.123349

Bobik, K., & Burch-Smith, T. M. (2015). Chloroplast signaling within, between and beyond cells. In *Frontiers in Plant Science* (Vol. 6, Issue OCTOBER). Frontiers Research Foundation. https://doi.org/10.3389/fpls.2015.00781

Borghi, L. (2010). Inducible gene expression systems for plants. *Methods in Molecular Biology (Clifton, N.J.)*, *655*. https://doi.org/10.1007/978-1-60761-765-5_5

Breuers, F. K. H., Bräutigam, A., Geimer, S., Welzel, U. Y., Stefano, G., Renna, L., Brandizzi, F., & Weber, A. P. M. (2012). Dynamic remodeling of the plastid envelope membranes - A tool for chloroplast envelope in vivo localizations. *Frontiers in Plant Science*, *3*(JAN). https://doi.org/10.3389/fpls.2012.00007

Brunkard, J. O., Runkel, A. M., & Zambryski, P. (2016). Visualizing Stromule Frequency with Fluorescence Microscopy. *J. Vis. Exp*, *117*, 54692. https://doi.org/10.3791/54692

Brunkard, J. O., Runkel, A. M., & Zambryski, P. C. (2015). Chloroplasts extend stromules independently and in response to internal redox signals. *Proceedings of the National Academy of Sciences of the United States of America*, *112*(32). https://doi.org/10.1073/pnas.1511570112

Caplan, J. L., Kumar, A. S., Park, E., Padmanabhan, M. S., Hoban, K., Modla, S., Czymmek, K., & Dinesh-Kumar, S. P. (2015). Chloroplast Stromules Function during Innate Immunity. *Developmental Cell*, *34*(1). https://doi.org/10.1016/j.devcel.2015.05.011

Caplan, J. L., Mamillapalli, P., Burch-Smith, T. M., Czymmek, K., & Dinesh-Kumar, S. P. (2008). Chloroplastic Protein NRIP1 Mediates Innate Immune Receptor Recognition of a Viral Effector. *Cell*, *132*(3). https://doi.org/10.1016/j.cell.2007.12.031

Caspar, T., Huber, S. C., & Somerville, C. (1985). Alterations in Growth, Photosynthesis, and Respiration in a Starchless Mutant of Arabidopsis thaliana (L.) Deficient in Chloroplast Phosphoglucomutase Activity . *Plant Physiology*, *79*(1). https://doi.org/10.1104/pp.79.1.11

Chan, K. X., Phua, S. Y., Crisp, P., McQuinn, R., & Pogson, B. J. (2016). Learning the Languages of the Chloroplast: Retrograde Signaling and beyond. In *Annual Review of Plant Biology* (Vol. 67). https://doi.org/10.1146/annurev-arplant-043015-111854

Chen, Y., Asano, T., Fujiwara, M. T., Yoshida, S., MacHida, Y., & Yoshioka, Y. (2009). Plant cells without detectable plastids are generated in the crumpled leaf mutant of arabidopsis thaliana. *Plant and Cell Physiology*, *50*(5), 956–969. https://doi.org/10.1093/pcp/pcp047

Cho, K. F., Branon, T. C., Udeshi, N. D., Myers, S. A., Carr, S. A., & Ting, A. Y. (2020). Proximity labeling in mammalian cells with TurboID and split-TurboID. *Nature Protocols*, *15*(12). https://doi.org/10.1038/s41596-020-0399-0

Chu, J., Haynes, R. D., Corbel, S. Y., Li, P., González-González, E., Burg, J. S., Ataie, N. J., Lam, A. J., Cranfill, P. J., Baird, M. A., Davidson, M. W., Ng, H. L., Garcia, K. C., Contag, C. H., Shen, K., Blau, H. M., & Lin, M. Z. (2014). Non-invasive intravital imaging of cellular differentiation with a bright red-excitable fluorescent protein. *Nature Methods*, *11*(5). https://doi.org/10.1038/nmeth.2888

Daniell, H., Lin, C. S., Yu, M., & Chang, W. J. (2016). Chloroplast genomes: Diversity, evolution, and applications in genetic engineering. In *Genome Biology* (Vol. 17, Issue 1). https://doi.org/10.1186/s13059-016-1004-2

Davis, A. M., Hall, A., Millar, A. J., Darrah, C., & Davis, S. J. (2009). Protocol: Streamlined sub-protocols for floral-dip transformation and selection of transformants in arabidopsis thaliana. *Plant Methods*, *5*(1). https://doi.org/10.1186/1746-4811-5-3

Deeks, M. J., Calcutt, J. R., Ingle, E. K. S., Hawkins, T. J., Chapman, S., Richardson, A. C., Mentlak, D. A., Dixon, M. R., Cartwright, F., Smertenko, A. P., Oparka, K., & Hussey, P. J. (2012). A superfamily of actin-binding proteins at the actin-membrane nexus of higher plants. *Current Biology*, *22*(17). https://doi.org/10.1016/j.cub.2012.06.041

Ding, X., Jimenez-Gongora, T., Krenz, B., & Lozano-Duran, R. (2019). Chloroplast clustering around the nucleus is a general response to pathogen perception in Nicotiana benthamiana. *Molecular Plant Pathology*, *20*(9). https://doi.org/10.1111/mpp.12840

Dopp, I. J., Kalac, K., & Mackenzie, S. A. (2023). Hydrogen peroxide sensor HyPer7 illuminates tissue-specific plastid redox dynamics. *Plant Physiology*. https://doi.org/10.1093/plphys/kiad307

Drobizhev, M., Makarov, N. S., Tillo, S. E., Hughes, T. E., & Rebane, A. (2011). Two-photon absorption properties of fluorescent proteins. In *Nature Methods* (Vol. 8, Issue 5). https://doi.org/10.1038/nmeth.1596

Dyall, S. D., Brown, M. T., & Johnson, P. J. (2004). Ancient Invasions: From Endosymbionts to Organelles. In *New Series* (Vol. 304, Issue 5668).

Engler, C., Youles, M., Gruetzner, R., Ehnert, T. M., Werner, S., Jones, J. D. G., Patron, N. J., & Marillonnet, S. (2014). A Golden Gate modular cloning toolbox for plants. *ACS Synthetic Biology*, *3*(11). https://doi.org/10.1021/sb4001504

Erickson, J. L., Adlung, N., Lampe, C., Bonas, U., & Schattat, M. H. (2018). The Xanthomonas effector XopL uncovers the role of microtubules in stromule extension and dynamics in Nicotiana benthamiana. *Plant Journal*, *93*(5). https://doi.org/10.1111/tpj.13813

Erickson, J. L., Kantek, M., & Schattat, M. H. (2017). Plastid-nucleus distance alters the behavior of stromules. *Frontiers in Plant Science*, *8*. https://doi.org/10.3389/fpls.2017.01135

Erickson, J. L., & Schattat, M. H. (2018). Shaping plastid stromules — principles of in vitro membrane tubulation applied in planta. In *Current Opinion in Plant Biology* (Vol. 46). https://doi.org/10.1016/j.pbi.2018.07.003

Erickson, J. L., Ziegler, J., Guevara, D., Abel, S., Klösgen, R. B., Mathur, J., Rothstein, S. J., & Schattat, M. H. (2014). Agrobacterium-derived cytokinin influences plastid morphology and starch accumulation in Nicotiana benthamiana during transient assays. *BMC Plant Biology*, *14*(1). https://doi.org/10.1186/1471-2229-14-127

Estavillo, G. M., Crisp, P. A., Pornsiriwong, W., Wirtz, M., Collinge, D., Carrie, C., Giraud, E., Whelan, J., David, P., Javot, H., Brearley, C., Hell, R., Marin, E., & Pogson, B. J. (2011). Evidence for a SAL1-PAP chloroplast retrograde pathway that functions in drought and high light signaling in Arabidopsis. *Plant Cell*, *23*(11). https://doi.org/10.1105/tpc.111.091033

Exposito-Rodriguez, M., Laissue, P. P., Yvon-Durocher, G., Smirnoff, N., & Mullineaux, P. M. (2017). Photosynthesis-dependent H2O2 transfer from chloroplasts to nuclei provides a high-light signalling mechanism. *Nature Communications*, *8*(1). https://doi.org/10.1038/s41467-017-00074-w

Fester, T., & Hause, G. (2005). Accumulation of reactive oxygen species in arbuscular mycorrhizal roots. *Mycorrhiza*, *15*(5). https://doi.org/10.1007/s00572-005-0363-4

Fester, T., Strack, D., & Hause, B. (2001). Reorganization of tobacco root plastids during arbuscule development. *Planta*, *213*(6). https://doi.org/10.1007/s004250100561

Gonzalez, T. L., Liang, Y., Nguyen, B. N., Staskawicz, B. J., Loqué, D., & Hammond, M. C. (2015). Tight regulation of plant immune responses bycombining promoter and suicide exon elements. *Nucleic Acids Research*, *43*(14). https://doi.org/10.1093/nar/gkv655

Gray, J. C., Hansen, M. R., Shaw, D. J., Graham, K., Dale, R., Smallman, P., Natesan, S. K. A., & Newell, C. A. (2012). Plastid stromules are induced by stress treatments acting through abscisic acid. *Plant Journal*, *69*(3). https://doi.org/10.1111/j.1365-313X.2011.04800.x

Gray, J. C., Sullivan, J. A., Hibberd, J. M., & Hansen, M. R. (2001). Stromules: Mobile protrusions and interconnections between plastids. In *Plant Biology* (Vol. 3, Issue 3). https://doi.org/10.1055/s-2001-15204

Gray, J. C., Sullivan, J. A., & Newell, C. A. (2011). Visualisation of stromules on arabidopsis plastids. *Methods in Molecular Biology*, *774*. https://doi.org/10.1007/978-1-61779-234-2_5

Gunning, B. E. S. (2005). Plastid stromules: Video microscopy of their outgrowth, retraction, tensioning, anchoring, branching, bridging, and tip-shedding. *Protoplasma*, *225*(1–2). https://doi.org/10.1007/s00709-004-0073-3

Hammond, M. C., Wachter, A., & Breaker, R. R. (2009). A plant 5S ribosomal RNA mimic regulates alternative splicing of transcription factor IIIA pre-mRNAs. *Nature Structural and Molecular Biology*, *16*(5). https://doi.org/10.1038/nsmb.1588

Hanson, M. R., & Conklin, P. L. (2020). Stromules, functional extensions of plastids within the plant cell. In *Current Opinion in Plant Biology* (Vol. 58). https://doi.org/10.1016/j.pbi.2020.10.005

Hanson, M. R., & Hines, K. M. (2018). Stromules: Probing formation and function. In *Plant Physiology* (Vol. 176, Issue 1). https://doi.org/10.1104/pp.17.01287

Hanson, M. R., & Sattarzadeh, A. (2008). Dynamic morphology of plastids and stromules in angiosperm plants. In *Plant, Cell and Environment* (Vol. 31, Issue 5). https://doi.org/10.1111/j.1365-3040.2007.01768.x

Haswell, E. S., & Meyerowitz, E. M. (2006). MscS-like proteins control plastid size and shape in Arabidopsis thaliana. *Current Biology*, *16*(1), 1–11. https://doi.org/10.1016/j.cub.2005.11.044

Hickey, S. F., Sridhar, M., Westermann, A. J., Qin, Q., Vijayendra, P., Liou, G., & Hammond, M. C. (2012). Transgene regulation in plants by alternative splicing of a suicide exon. *Nucleic Acids Research*, *40*(10). https://doi.org/10.1093/nar/gks032

Higa, T., Suetsugu, N., Kong, S.-G., & Wada, M. (2014). Actin-dependent plastid movement is required for motive force generation in directional nuclear movement in plants. *Proceedings of the National Academy of Sciences*, *111*(11).

Hoekema, A., Hirsch, P. R., Hooykaas, P. J. J., & Schilperoort, R. A. (1983). A binary plant vector strategy based on separation of vir- and T-region of the Agrobacterium tumefaciens Ti-plasmid. *Nature*, *303*(5913). https://doi.org/10.1038/303179a0

Holzinger, A., Buchner, O., Lütz, C., & Hanson, M. R. (2007). Temperature-sensitive formation of chloroplast protrusions and stromules in mesophyll cells of Arabidopsis thaliana. *Protoplasma*, *230*(1–2). https://doi.org/10.1007/s00709-006-0222-y

Holzinger, A., Kwok, E. Y., & Hanson, M. R. (2008). Effects of arc3, arc5 and arc6 mutations on plastid morphology and stromule formation in green and nongreen tissues of arabidopsis Thaliana. *Photochemistry and Photobiology*, *84*(6). https://doi.org/10.1111/j.1751-1097.2008.00437.x

Holzinger, A., Wasteneys, G. O., & Lütz, C. (2007). Investigating cytoskeletal function in chloroplast protrusion formation in the arctic-alpine plant Oxyria digyna. *Plant Biology*, *9*(3). https://doi.org/10.1055/s-2006-924727

Inaba, T. (2010). Bilateral communication between plastid and the nucleus: Plastid protein import and plastid-to-nucleus retrograde signaling. In *Bioscience, Biotechnology and Biochemistry* (Vol. 74, Issue 3). https://doi.org/10.1271/bbb.90842

Inaba, T., Yazu, F., Ito-Inaba, Y., Kakizaki, T., & Nakayama, K. (2011). Retrograde Signaling Pathway from Plastid to Nucleus. In *International Review of Cell and Molecular Biology* (Vol. 290). https://doi.org/10.1016/B978-0-12-386037-8.00002-8

Isemer, R., Mulisch, M., Schäfer, A., Kirchner, S., Koop, H. U., & Krupinska, K. (2012). Recombinant Whirly1 translocates from transplastomic chloroplasts to the nucleus. *FEBS Letters*, *586*(1). https://doi.org/10.1016/j.febslet.2011.11.029

Ishida, H., Yoshimoto, K., Izumi, M., Reisen, D., Yano, Y., Makino, A., Ohsumi, Y., Hanson, M. R., & Mae, T. (2008). Mobilization of Rubisco and stroma-localized fluorescent proteins of chloroplasts to the vacuole by an ATG gene-dependent autophagic process. *Plant Physiology*, *148*(1). https://doi.org/10.1104/pp.108.122770

Ishikawa, H., Yasuzawa, M., Koike, N., Sanjaya, A., Moriyama, S., Nishizawa, A., Matsuoka, K., Sasaki, S., Kazama, Y., Hayashi, Y., Abe, T., Fujiwara, M. T., & Itoh, R. D. (2020). Arabidopsis PARC6 Is Critical for Plastid Morphogenesis in Pavement, Trichome, and Guard Cells in Leaf Epidermis. *Frontiers in Plant Science*, *10*. https://doi.org/10.3389/fpls.2019.01665

Jones, J. D. G., & Dangl, J. L. (2006). The plant immune system. In *Nature* (Vol. 444, Issue 7117). https://doi.org/10.1038/nature05286

Kandasamy, M. K., & Meagher, R. B. (1999). Actin-Organelle Interaction: Association With Chloroplast in Arabidopsis Leaf Mesophyll Cells. In *Cell Motil. Cytoskeleton* (Vol. 44).

Khan, M., Subramaniam, R., & Desveaux, D. (2016). Of guards, decoys, baits and traps: Pathogen perception in plants by type III effector sensors. In *Current Opinion in Microbiology* (Vol. 29). https://doi.org/10.1016/j.mib.2015.10.006

Kim MG, Macoy DM, Lee JY, Cha JY, & Kim WY. (2021). Interactions between Plant Immunity, Temperature, Light, and Circadian Rhythm. *J Plant Biochem Physiol.*, *9:262.*

Klement, Z., & Goodman, R. N. (1967). The Hypersensitive Reaction to Infection by Bacterial Plant Pathogens. *Annual Review of Phytopathology*, *5*(1). https://doi.org/10.1146/annurev.py.05.090167.000313

Köhler, R. H., Cao, J., Zipfel, W. R., Webb, W. W., & Hanson, M. R. (1997). Exchange of protein molecules through connections between higher plant plastids. *Science*, *276*(5321). https://doi.org/10.1126/science.276.5321.2039

Köhler, R. H., & Hanson, M. R. (2000). Plastid tubules of higher plants are tissue-specific and developmentally regulated. *Journal of Cell Science*, *113*(1). https://doi.org/10.1242/jcs.113.1.81

Köhler, R. H., Schwille, P., Webb, W. W., & Hanson, M. R. (2000). Active protein transport through plastid tubules: Velocity quantified by fluorescence correlation spectroscopy. *Journal of Cell Science*, *113*(22). https://doi.org/10.1242/jcs.113.22.3921

Koncz, C., & Schell, J. (1986). The promoter of TL-DNA gene 5 controls the tissue-specific expression of chimaeric genes carried by a novel type of Agrobacterium binary vector. *MGG Molecular & General Genetics*, *204*(3). https://doi.org/10.1007/BF00331014

Krause, K., & Krupinska, K. (2009). Nuclear regulators with a second home in organelles. *Trends in Plant Science*, *14*(4). https://doi.org/10.1016/j.tplants.2009.01.005

Krause, K., Oetke, S., & Krupinska, K. (2012). Dual targeting and retrograde translocation: Regulators of plant nuclear gene expression can be sequestered by plastids. In *International Journal of Molecular Sciences* (Vol. 13, Issue 9). https://doi.org/10.3390/ijms130911085

Krenz, B., Jeske, H., & Kleinow, T. (2012). The induction of stromule formation by a plant DNA-virus in epidermal leaf tissues suggests a novel intra- and intercellular macromolecular trafficking route. *Frontiers in Plant Science*, *3*(DEC). https://doi.org/10.3389/fpls.2012.00291

Krenz, B., Neugart, F., Kleinow, T., & Jeske, H. (2011). Self-interaction of Abutilon mosaic virus replication initiator protein (Rep) in plant cell nuclei. *Virus Research*, *161*(2). https://doi.org/10.1016/j.virusres.2011.07.020

Krenz, B., Windeisen, V., Wege, C., Jeske, H., & Kleinow, T. (2010). A plastid-targeted heat shock cognate 70kDa protein interacts with the Abutilon mosaic virus movement protein. *Virology*, *401*(1). https://doi.org/10.1016/j.virol.2010.02.011

Kwok, E. Y., & Hanson, M. R. (2003). Microfilaments and microtubules control the morphology and movement of non-green plastids and stromules in Nicotiana tabacum. *Plant Journal*, *35*(1), 16–26. https://doi.org/10.1046/j.1365-313X.2003.01777.x

Kwok, E. Y., & Hanson, M. R. (2004). In vivo analysis of interactions between GFP-labeled microfilaments and plastid stromules. *BMC Plant Biology*, *4*. https://doi.org/10.1186/1471-2229-4-2

Lapin, D., Kovacova, V., Sun, X., Dongus, J. A., Bhandari, D., Von Born, P., Bautor, J., Guarneri, N., Rzemieniewski, J., Stuttmann, J., Beyer, A., & Parker, J. E. (2019). A coevolved EDS1-SAG101-NRG1 module mediates cell death signaling by TIR-domain immune receptors. *Plant Cell*, *31*(10). https://doi.org/10.1105/tpc.19.00118

Man Ngou, B. P., Ahn, H. K., Ding, P., Redkar, A., Brown, H., Ma, Y., Youles, M., Tomlinson, L., & Jones, J. D. G. (2020). Estradiol-inducible AvrRps4 expression reveals distinct properties of TIR-NLR-mediated effector-triggered immunity. *Journal of Experimental Botany*, *71*(6). https://doi.org/10.1093/jxb/erz571

Martin, W., Rujan, T., Richly, E., Hansen, A., Cornelsen, S., Lins, T., Leister, D., Stoebe, B., Hasegawa, M., & Penny, D. (2002). Evolutionary analysis of Arabidopsis, cyanobacterial, and chloroplast genomes reveals plastid phylogeny and thousands of cyanobacterial genes in the nucleus. *Proceedings of the National Academy of Sciences of the United States of America*, *99*(19). https://doi.org/10.1073/pnas.182432999

Mastop, M., Bindels, D. S., Shaner, N. C., Postma, M., Gadella, T. W. J., & Goedhart, J. (2017). Characterization of a spectrally diverse set of fluorescent proteins as FRET acceptors for mTurquoise2. *Scientific Reports*, *7*(1). https://doi.org/10.1038/s41598-017-12212-x

Mathur, J. (2021). Organelle extensions in plant cells. *Plant Physiology*, *185*(3), 593–607. https://doi.org/10.1093/PLPHYS/KIAA055

McFadden, G. I. (2001). Chloroplast origin and integration. *Plant Physiology*, *125*(1). https://doi.org/10.1104/pp.125.1.50

Mielecki, J., Gawroński, P., & Karpiński, S. (2020). Retrograde signaling: Understanding the communication between organelles. In *International Journal of Molecular Sciences* (Vol. 21, Issue 17). https://doi.org/10.3390/ijms21176173

Mullineaux, P. M., Exposito-Rodriguez, M., Laissue, P. P., Smirnoff, N., & Park, E. (2020). Spatial chloroplast-to-nucleus signalling involving plastid–nuclear complexes and stromules. In *Philosophical Transactions of the Royal Society B: Biological Sciences* (Vol. 375, Issue 1801). Royal Society Publishing. https://doi.org/10.1098/rstb.2019.0405

Natesan, S. K. A., Sullivan, J. A., & Gray, J. C. (2005). Stromules: A characteristic cell-specific feature of plastid morphology. In *Journal of Experimental Botany* (Vol. 56, Issue 413). https://doi.org/10.1093/jxb/eri088

Natesan, S. K. A., Sullivan, J. A., & Gray, J. C. (2009). Myosin XI is required for actin-associated movement of plastid stromules. *Molecular Plant*, *2*(6). https://doi.org/10.1093/mp/ssp078

Nott, A., Jung, H. S., Koussevitzky, S., & Chory, J. (2006). Plastid-to-nucleus retrograde signaling. In *Annual Review of Plant Biology* (Vol. 57, pp. 739–759). https://doi.org/10.1146/annurev.arplant.57.032905.105310

Oikawa, K., Yamasato, A., Kong, S. G., Kasahara, M., Nakai, M., Takahashi, F., Ogura, Y., Kagawa, T., & Wada, M. (2008). Chloroplast outer envelope protein Chup1 is essential for chloroplast anchorage to the plasma membrane and chloroplast movement. *Plant Physiology*, *148*(2), 829–842. https://doi.org/10.1104/pp.108.123075

Ordon, J., Martin, P., Erickson, J. L., Ferik, F., Balcke, G., Bonas, U., & Stuttmann, J. (2021). Disentangling cause and consequence: genetic dissection of the DANGEROUS MIX2 risk locus, and activation of the DM2h NLR in autoimmunity. *Plant Journal*, *106*(4). https://doi.org/10.1111/tpj.15215

Park, E., Caplan, J. L., & Dinesh-Kumar, S. P. (2018). Dynamic coordination of plastid morphological change by cytoskeleton for chloroplast-nucleus communication during plant immune responses. *Plant Signaling and Behavior*, *13*(8). https://doi.org/10.1080/15592324.2018.1500064

Prautsch, J., Erickson, J. L., Özyürek, S., Gormanns, R., Franke, L., Lu, Y., Marx, J., Niemeyer, F., Parker, J. E., Stuttmann, J., & Schattat, M. H. (2022). Effector XopQ-induced stromule formation in *Nicotiana benthamiana* depends on ETI signaling components ADR1 and NRG1. *Plant Physiology*. https://doi.org/10.1093/plphys/kiac481

Pyke, K. A. (1999). Plastid division and development. *Plant Cell*, *11*(4). https://doi.org/10.1105/tpc.11.4.549

Qi, T., Seong, K., Thomazella, D. P. T., Kim, J. R., Pham, J., Seo, E., Cho, M. J., Schultink, A., & Staskawicz, B. J. (2018). NRG1 functions downstream of EDS1 to regulate TIR-NLR-mediated plant immunity in Nicotiana benthamiana. *Proceedings of the National Academy of Sciences of the United States of America*, *115*(46). https://doi.org/10.1073/pnas.1814856115

Ramel, F., Birtic, S., Ginies, C., Soubigou-Taconnat, L., Triantaphylidès, C., & Havaux, M. (2012). Carotenoid oxidation products are stress signals that mediate gene responses to singlet oxygen in plants. *Proceedings of the National Academy of Sciences of the United States of America*, *109*(14), 5535–5540. https://doi.org/10.1073/pnas.1115982109

Roux, A. (2013). The physics of membrane tubes: Soft templates for studying cellular membranes. In *Soft Matter* (Vol. 9, Issue 29). https://doi.org/10.1039/c3sm50514f

Ruegger, M., Dewey, E., Hobbie, L., Brown, D., Bernasconi, P., Turner, J., Muday, G., & Estelle, M. (1997). Reduced naphthylphthalamic acid binding in the tir3 mutant of arabidopsis is associated with a reduction in polar auxin transport and diverse morphological defects. *Plant Cell*, *9*(5). https://doi.org/10.1105/tpc.9.5.745

Sampath Kumar, A., Park, E., Nedo, A., Alqarni, A., Ren, L., Hoban, K., Modla, S., McDonald, J. H., Kambhamettu, C., Dinesh-Kumar, S. P., & Lewis Caplan, J. (2018). *Stromule extension along microtubules coordinated with actin-mediated anchoring guides perinuclear chloroplast movement during innate immunity*. https://doi.org/10.7554/eLife.23625.001

Schattat, M., Barton, K., Baudisch, B., Klösgen, R. B., & Mathur, J. (2011). Plastid stromule branching coincides with contiguous endoplasmic reticulum dynamics. *Plant Physiology*, *155*(4). https://doi.org/10.1104/pp.110.170480

Schattat, M., Barton, K., & Mathur, J. (2011). Correlated behavior implicates stromules in increasing the interactive surface between plastids and ER tubules. *Plant Signaling and Behavior*, *6*(5). https://doi.org/10.4161/psb.6.5.15085

Schattat, M. H., Barton, K. A., & Mathur, J. (2015). The myth of interconnected plastids and related phenomena. *Protoplasma*, *252*(1). https://doi.org/10.1007/s00709-014-0666-4

Schattat, M. H., Griffiths, S., Mathur, N., Barton, K., Wozny, M. R., Dunn, N., Greenwood, J. S., & Mathur, J. (2012). Differential coloring reveals that plastids do not form networks for exchanging macromolecules. *The Plant Cell*, *24*(4). https://doi.org/10.1105/tpc.111.095398

Schattat, M. H., & Klösgen, R. B. (2011). Induction of stromule formation by extracellular sucrose and glucose in epidermal leaf tissue of Arabidopsis thaliana. *BMC Plant Biology*, *11*. https://doi.org/10.1186/1471-2229-11-115

Schattat, M. H., Klösgen, R. B., & Mathur, J. (2012). New insights on stromules: Stroma filled tubules extended by independent plastids. *Plant Signaling and Behavior*, *7*(9). https://doi.org/10.4161/psb.21342

Schindelin, J., Arganda-Carreras, I., Frise, E., Kaynig, V., Longair, M., Pietzsch, T., Preibisch, S., Rueden, C., Saalfeld, S., Schmid, B., Tinevez, J. Y., White, D. J., Hartenstein, V., Eliceiri, K., Tomancak, P., & Cardona, A. (2012). Fiji: An open-source platform for biological-image analysis. In *Nature Methods* (Vol. 9, Issue 7). https://doi.org/10.1038/nmeth.2019

Schnurr, J. A., Shockey, J. M., De Boer, G. J., & Browse, J. A. (2002). Fatty acid export from the chloroplast. Molecular characterization of a major plastidial acyl-

coenzyme A synthetase from Arabidopsis. *Plant Physiology*, *129*(4). https://doi.org/10.1104/pp.003251

Schultink, A., Qi, T., Lee, A., Steinbrenner, A. D., & Staskawicz, B. (2017). Roq1 mediates recognition of the Xanthomonas and Pseudomonas effector proteins XopQ and HopQ1. *Plant Journal*, *92*(5). https://doi.org/10.1111/tpj.13715

Schulze, S., Kay, S., Büttner, D., Egler, M., Eschen-Lippold, L., Hause, G., Krüger, A., Lee, J., Müller, O., Scheel, D., Szczesny, R., Thieme, F., & Bonas, U. (2012). Analysis of new type III effectors from Xanthomonas uncovers XopB and XopS as suppressors of plant immunity. *New Phytologist*, *195*(4). https://doi.org/10.1111/j.1469-8137.2012.04210.x

Sheahan, M. B., Collings, D. A., Rose, R. J., & McCurdy, D. W. (2020). ACTIN7 is required for perinuclear clustering of chloroplasts during arabidopsis protoplast culture. *Plants*, *9*(2). https://doi.org/10.3390/plants9020225

Sheahan, M. B., Rose, R. J., & McCurdy, D. W. (2004). Organelle inheritance in plant cell division: The actin cytoskeleton is required for unbiased inheritance of chloroplasts, mitochondria and endoplasmic reticulum in dividing protoplasts. *Plant Journal*, *37*(3). https://doi.org/10.1046/j.1365-313X.2003.01967.x

Sohn, K. H., Zhang, Y., & Jones, J. D. G. (2009). The Pseudomonas syringae effector protein, AvrRPS4, requires in planta processing and the KRVY domain to function. *Plant Journal*, *57*(6). https://doi.org/10.1111/j.1365-313X.2008.03751.x

Strand, Å., Asami, T., Alonso, J., Ecker, J. R., & Chory, J. (2003). Chloroplast to nucleus communication triggered by accumulation of Mg-protoporphyrinix. *Nature*, *421*(6918). https://doi.org/10.1038/nature01204

Suetsugu, N., Higa, T., Gotoh, E., & Wada, M. (2016). Light-induced movements of chloroplasts and nuclei are regulated in both cp-actin-filament-dependent and -independent manners in arabidopsis thaliana. *PLoS ONE*, *11*(6). https://doi.org/10.1371/journal.pone.0157429

Suetsugu, N., Yamada, N., Kagawa, T., Yonekura, H., Uyeda, T. Q. P., Kadota, A., & Wada, M. (2010). Two kinesin-like proteins mediate actin-based chloroplast movement in Arabidopsis thaliana. *Proceedings of the National Academy of Sciences*, *107*(19), 8860–8865. https://doi.org/10.1073/PNAS.0912773107

Sun, X., Feng, P., Xu, X., Guo, H., Ma, J., Chi, W., Lin, R., Lu, C., & Zhang, L. (2011). A chloroplast envelope-bound PHD transcription factor mediates chloroplast signals to the nucleus. *Nature Communications*, *2*(1). https://doi.org/10.1038/ncomms1486

Sztatelman, O., Łabuz, J., Hermanowicz, P., Banaś, A. K., Bazant, A., Zgłobicki, P., Aggarwal, C., Nadzieja, M., Krzeszowiec, W., Strzałka, W., & Gabryś, H. (2016). Fine tuning chloroplast movements through physical interactions between phototropins. *Journal of Experimental Botany*, *67*(17). https://doi.org/10.1093/jxb/erw265

Tamura, K., Iwabuchi, K., Fukao, Y., Kondo, M., Okamoto, K., Ueda, H., Nishimura, M., & Hara-Nishimura, I. (2013). Myosin XI-i links the nuclear membrane to the cytoskeleton to control nuclear movement and shape in arabidopsis. *Current Biology*, *23*(18). https://doi.org/10.1016/j.cub.2013.07.035

Toruño, T. Y., Stergiopoulos, I., & Coaker, G. (2016). Plant-Pathogen Effectors: Cellular Probes Interfering with Plant Defenses in Spatial and Temporal Manners. In *Annual Review of Phytopathology* (Vol. 54). https://doi.org/10.1146/annurev-phyto-080615-100204

Ugalde, J. M., Fuchs, P., Nietzel, T., Cutolo, E. A., Homagk, M., Vothknecht, U. C., Holuigue, L., Schwarzländer, M., Müller-Schüssele, S. J., & Meyer, A. J. (2021). Chloroplast-derived photo-oxidative stress causes changes in H2O2 and EGSH in other subcellular compartments. *Plant Physiology*, *186*(1). https://doi.org/10.1093/plphys/kiaa095

Van Norman, J. M., Zhang, J., Cazzonelli, C. I., Pogson, B. J., Harrison, P. J., Bugg, T. D. H., Chan, K. X., Thompson, A. J., & Benfey, P. N. (2014). Periodic root branching in Arabidopsis requires synthesis of an uncharacterized carotenoid derivative. *Proceedings of the National Academy of Sciences of the United States of America*, *111*(13). https://doi.org/10.1073/pnas.1403016111

van Wersch, R., Li, X., & Zhang, Y. (2016). Mighty dwarfs: Arabidopsis autoimmune mutants and their usages in genetic dissection of plant immunity. In *Frontiers in Plant Science* (Vol. 7, Issue NOVEMBER2016). https://doi.org/10.3389/fpls.2016.01717

Veley, K. M., Marshburn, S., Clure, C. E., & Haswell, E. S. (2012). Mechanosensitive channels protect plastids from hypoosmotic stress during normal plant growth. *Current Biology*, *22*(5), 408–413. https://doi.org/10.1016/j.cub.2012.01.027

Wang, Y. S., Motes, C. M., Mohamalawari, D. R., & Blancaflor, E. B. (2004). Green fluorescent protein fusions to Arabidopsis Fimbrin 1 for spatio-temporal imaging of F-actin dynamics in roots. *Cell Motility and the Cytoskeleton*, *59*(2). https://doi.org/10.1002/cm.20024

Waters, M. T., Fray, R. G., & Pyke, K. A. (2004). Stromule formation is dependent upon plastid size, plastid differentiation status and the density of plastids within the cell. *Plant Journal*, *39*(4). https://doi.org/10.1111/j.1365-313X.2004.02164.x

Woodson, J. D., Perez-Ruiz, J. M., & Chory, J. (2011). Heme synthesis by plastid ferrochelatase i regulates nuclear gene expression in plants. *Current Biology*, *21*(10). https://doi.org/10.1016/j.cub.2011.04.004

Xiao, Y., Savchenko, T., Baidoo, E. E. K., Chehab, W. E., Hayden, D. M., Tolstikov, V., Corwin, J. A., Kliebenstein, D. J., Keasling, J. D., & Dehesh, K. (2012). Retrograde signaling by the plastidial metabolite MEcPP regulates expression of nuclear stress-response genes. *Cell*, *149*(7). https://doi.org/10.1016/j.cell.2012.04.038

Yang, F., Xiao, K., Pan, H., & Liu, J. (2021). Chloroplast: The Emerging Battlefield in Plant–Microbe Interactions. In *Frontiers in Plant Science* (Vol. 12). https://doi.org/10.3389/fpls.2021.637853

Yong Jik Lee, Dae Heon Kim, Kim, Y. W., & Hwang, I. (2001). Identification of a signal that distinguishes between the chloroplast outer envelope membrane and the endomembrane system in vivo. *Plant Cell*, *13*(10). https://doi.org/10.1105/tpc.13.10.2175

Zuo, J., Niu, Q. W., & Chua, N. H. (2000). An estrogen receptor-based transactivator XVE mediates highly inducible gene expression in transgenic plants. *Plant Journal*, *24*(2). https://doi.org/10.1046/j.1365-313X.2000.00868.x

VII. Supplementary Information

7.1 Imaging in *N. benthamiana* pn lines results section (A)

Stock number	Strain	Background	Name of plastid	Transfered DNA	Plant resistance	Line numbers
Nb069	*Nicotiana benthamiana*	WT	plsu4-pn	p35S::FNReGFP + pAtUBQ10::H2Bmcherry	HygR	Nb-pn>WT-04-01
Nb070	*Nicotiana benthamiana*	WT	plsu4-pn	p35S::FNReGFP + pAtUBQ10::H2Bmcherry	HygR	Nb-pn>WT-04-02
Nb071	*Nicotiana benthamiana*	WT	plsu4-pn	p35S::FNReGFP + pAtUBQ10::H2Bmcherry	HygR	Nb-pn>WT-07-01
Nb072	*Nicotiana benthamiana*	WT	plsu4-pn	p35S::FNReGFP + pAtUBQ10::H2Bmcherry	HygR	Nb-pn>WT-07-02
Nb073	*Nicotiana benthamiana*	WT	plsu4-pn	p35S::FNReGFP + pAtUBQ10::H2Bmcherry	HygR	Nb-pn>WT-07-03
Nb074	*Nicotiana benthamiana*	WT	plsu4-pn	p35S::FNReGFP + pAtUBQ10::H2Bmcherry	HygR	Nb-pn>WT-07-04
Nb075	*Nicotiana benthamiana*	WT	plsu4-pn	p35S::FNReGFP + pAtUBQ10::H2Bmcherry	HygR	Nb-pn>WT-07-05
Nb076	*Nicotiana benthamiana*	WT	plsu4-pn	p35S::FNReGFP + pAtUBQ10::H2Bmcherry	HygR	Nb-pn>WT-11-01
Nb077	*Nicotiana benthamiana*	WT	plsu4-pn	p35S::FNReGFP + pAtUBQ10::H2Bmcherry	HygR	Nb-pn>WT-11-02
Nb078	*Nicotiana benthamiana*	WT	plsu4-pn	p35S::FNReGFP + pAtUBQ10::H2Bmcherry	HygR	Nb-pn>WT-11-03
Nb079	*Nicotiana benthamiana*	WT	plsu4-pn	p35S::FNReGFP + pAtUBQ10::H2Bmcherry	HygR	Nb-pn>WT-11-04
Nb080	*Nicotiana benthamiana*	WT	plsu4-pn	p35S::FNReGFP + pAtUBQ10::H2Bmcherry	HygR	Nb-pn>WT-11-05
Nb081	*Nicotiana benthamiana*	WT	plsu4-pn	p35S::FNReGFP + pAtUBQ10::H2Bmcherry	HygR	Nb-pn>WT-11-06

Supplementary table 1: List of *N. benthamiana* transgenic pn lines screened and used for life imaging

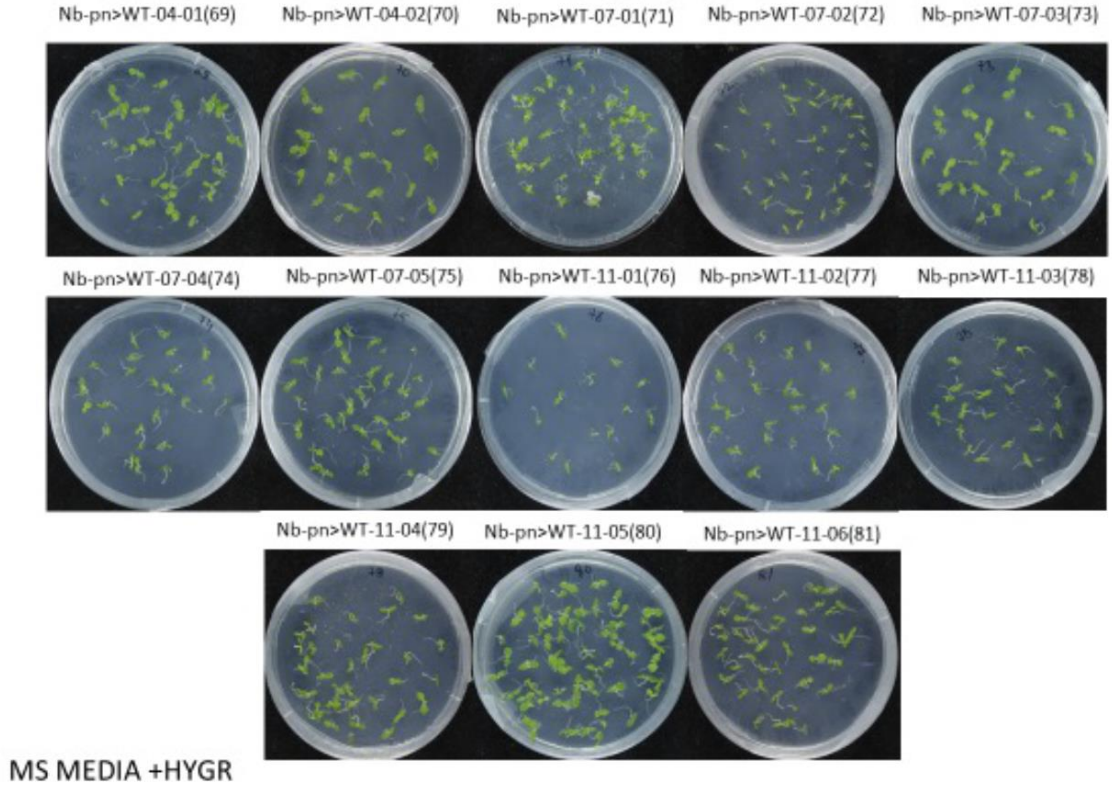

Supplementary figure 1: *N. Benthamiana* (Nb) wild type (WT) background pn lines seeds on MS Media with selected antibiotics. 69-81 Stock Numbers

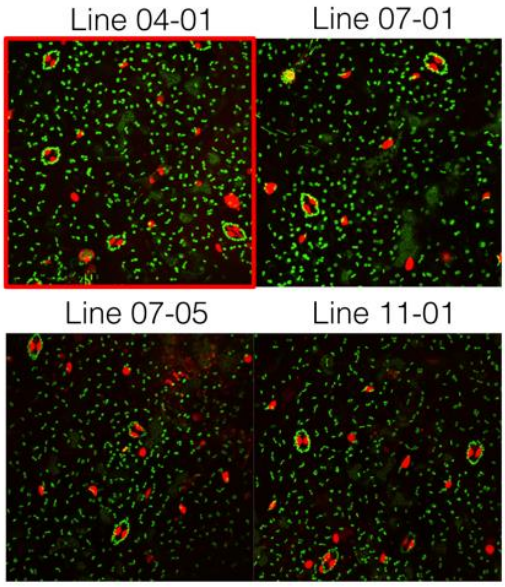

Supplementary figure 2: *N. Benthamiana* (Nb) wild type (WT) background pn lines selection based on the fluorescence protein brightness. Selected lines #04-01, #07-01, #07-05, and #11-01. The red square shows the selected line used for further experiments

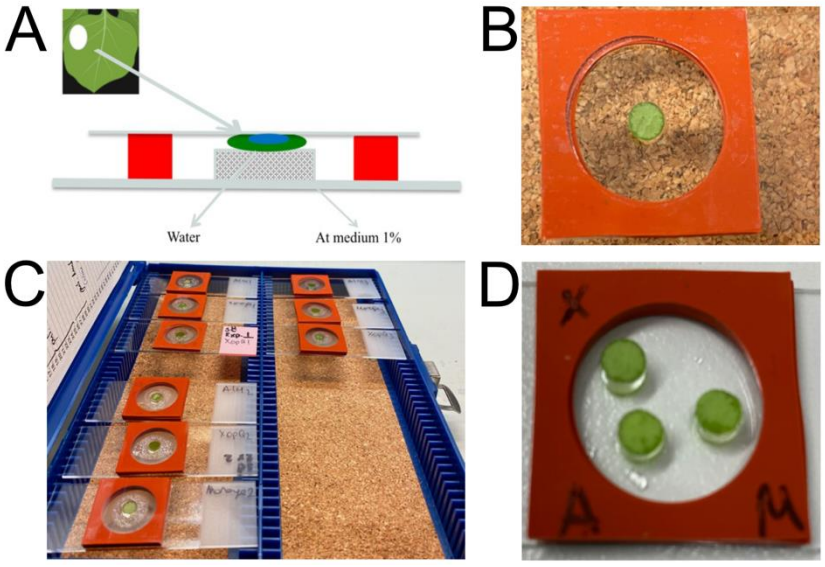

Supplementary figure 3: A Schematic demonstration of the created chamber for the long-term experiment. Red squares show the plastic chamber in the middle of the chamber AT medium. The green color indicates the plant specimen, and on top of the water, a drop is shown and covered with cover slide **B** Created Microscope slide of the plastid chamber (red) and plant specimen green. **C** Snap shots experiment for XopQ and controls. **D** Long-term imaging, 3 specimens are used at the same time. X: XopQ M:mORANGE control and A: AIM infiltration buffer

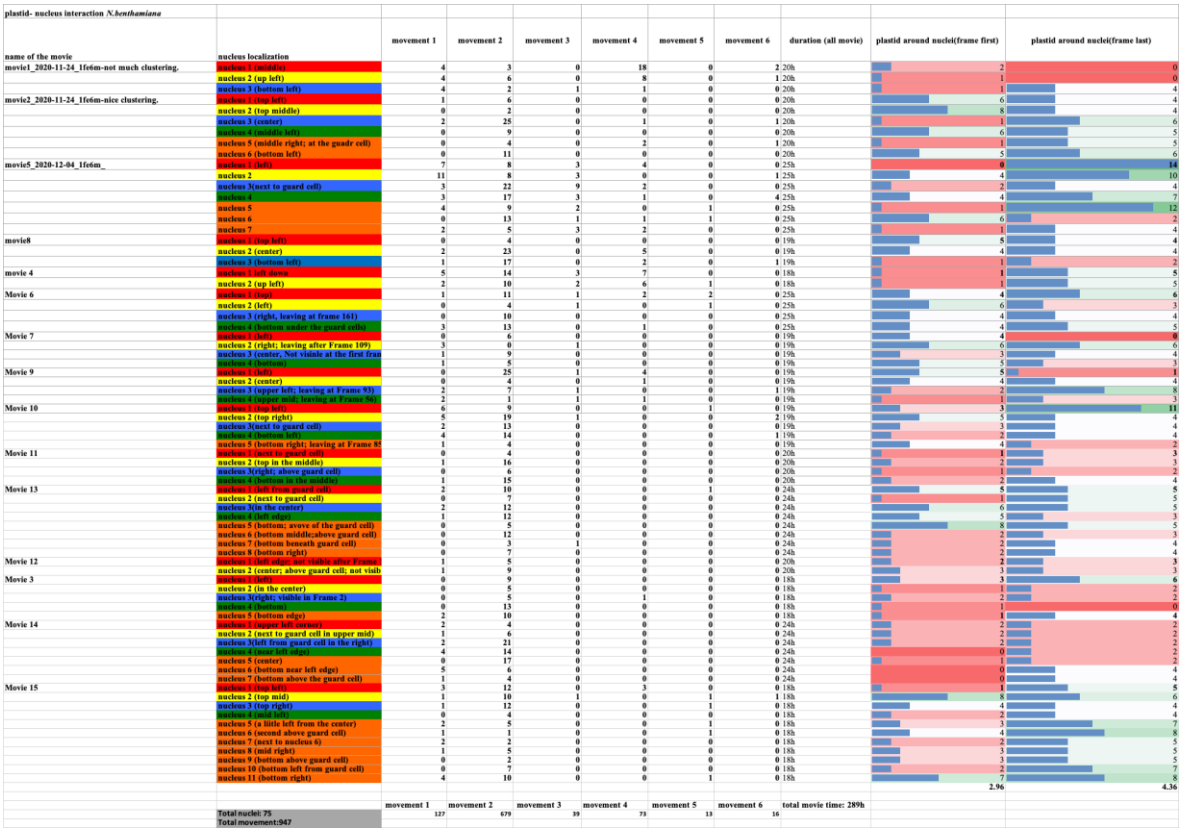

plastid- nucleus interaction *N.benthamiana*										
name of the movie	nucleus localization	movement 1	movement 2	movement 3	movement 4	movement 5	movement 6	duration (all movie)	plastid around nuclei(frame first)	plastid around nuclei(frame last)
movie1_2020-11-24_1f60m-not much clustering.	nucleus 1 (middle)	4	3	0	18	0	2	20h	2	0
	nucleus 2 (up left)	4	6	0	8	0	1	20h	1	0
	nucleus 3 (bottom left)	4	2	1	1	0	0	20h	1	4
movie2_2020-11-24_1f60m-nice clustering.	nucleus 1 (top left)	1	6	0	0	0	0	20h	6	4
	nucleus 2 (top middle)	0	2	0	0	0	0	20h	8	4
	nucleus 3 (center)	2	25	0	1	0	1	20h	1	6
	nucleus 4 (middle left)	0	9	0	0	0	0	20h	6	5
	nucleus 5 (middle right; at the guadr cell)	0	4	0	2	0	1	20h	1	5
	nucleus 6 (bottom left)	0	11	0	0	0	0	20h	5	6
movie5_2020-12-04_1f60m_	nucleus 1 (left)	7	8	3	4	0	0	25h	0	14
	nucleus 2	11	8	3	0	0	1	25h	4	10
	nucleus 3(next to guard cell)	3	22	9	2	0	0	25h	2	4
	nucleus 4	3	17	3	1	0	4	25h	4	7
	nucleus 5	4	9	2	0	1	0	25h	1	12
	nucleus 6	0	13	1	1	1	0	25h	6	2
	nucleus 7	2	5	3	2	0	0	25h	1	4
movie8	nucleus 1 (top left)	0	4	0	0	0	0	19h	5	4
	nucleus 2 (center)	2	23	0	5	0	0	19h	4	4
	nucleus 3 (bottom left)	1	17	0	2	0	1	19h	1	2
movie 4	nucleus 1 left down	5	14	3	7	0	0	18h	1	5
	nucleus 2 (up left)	2	10	2	6	1	0	18h	1	5
Movie 6	nucleus 1 (top)	1	11	1	2	2	0	25h	4	6
	nucleus 2 (left)	0	4	1	0	1	0	25h	6	3
	nucleus 3 (right, leaving at frame 161)	0	10	0	0	0	0	25h	4	4
	nucleus 4 (bottom under the guard cells)	3	13	0	1	0	0	25h	4	5
Movie 7	nucleus 1 (left)	0	6	0	0	0	0	19h	4	0
	nucleus 2 (right; leaving after Frame 109)	3	0	1	0	0	0	19h	6	6
	nucleus 3 (center; Not clearly at The first fan	1	9	0	0	0	0	19h	3	4
	nucleus 4 (bottom)	1	5	0	0	0	0	19h	5	3
Movie 9	nucleus 1 (left)	0	25	1	4	0	0	19h	5	1
	nucleus 2 (center)	0	4	0	1	0	0	19h	4	4
	nucleus 3 (upper left; leaving at Frame 93)	2	7	1	0	0	1	19h	2	8
	nucleus 4 (upper mid; leaving at Frame 56)	2	1	1	1	0	0	19h	1	3
Movie 10	nucleus 1 (top left)	6	9	0	0	1	0	19h	3	11
	nucleus 2 (top right)	5	19	1	0	0	2	19h	5	4
	nucleus 3(next to guard cell)	2	13	0	0	0	0	19h	3	4
	nucleus 4 (bottom left)	4	14	0	0	0	1	19h	2	4
	nucleus 5 (bottom right; leaving at Frame 8	1	4	0	0	0	0	19h	4	2
Movie 11	nucleus1 (next to guard cell)	0	4	0	0	0	0	20h	1	3
	nucleus 2 (top in the middle)	1	16	0	0	0	0	20h	2	3
	nucleus 3(right; above guard cell)	0	6	0	0	0	0	20h	1	2
	nucleus 4 (bottom in the middle)	1	15	0	0	0	0	20h	2	4
Movie 13	nucleus 1 (left from guard cell)	2	10	0	0	1	0	24h	5	5
	nucleus 2 (next to guard cell)	0	7	0	0	0	0	24h	1	5
	nucleus 3(in the center)	2	12	0	0	0	0	24h	6	5
	nucleus 4 (left edge)	1	12	0	0	0	0	24h	5	3
	nucleus 5 (bottom; avove of the guard cell)	0	5	0	0	0	0	24h	8	5
	nucleus 6 (bottom middle;above guard cell)	0	12	0	0	0	0	24h	2	3
	nucleus 7 (bottom beneath guard cell)	0	3	1	0	0	0	24h	2	4
	nucleus 8 (bottom right)	0	7	0	0	0	0	24h	2	4
Movie 12	nucleus 1 (left edge; not visible after Frame	1	5	0	0	0	0	20h	2	3
	nucleus 2 (center; above guard cell; not visib	1	9	0	0	0	0	20h	3	3
Movie 3	nucleus1 (left)	0	9	0	0	0	0	18h	3	6
	nucleus 2 (in the center)	0	5	0	0	0	0	18h	1	2
	nucleus 3(right; visible in Frame 2)	0	5	0	1	0	0	18h	2	2
	nucleus 4 (bottom)	0	13	0	0	0	0	18h	1	0
	nucleus 5 (bottom edge)	2	10	0	0	0	0	18h	1	4
Movie 14	nucleus 1 (upper left edge)	2	4	0	0	0	0	24h	2	2
	nucleus 2 (next to guard cell in upper mid)	1	6	0	0	0	0	24h	2	2
	nucleus 3(left from guard cell in the right)	2	21	0	0	0	0	24h	2	2
	nucleus 4 (near left edge)	4	14	0	0	0	0	24h	0	2
	nucleus 5 (center)	0	17	0	0	0	0	24h	1	2
	nucleus 6 (bottom near left edge)	5	6	0	0	0	0	24h	0	4
	nucleus 7 (bottom above the guard cell)	1	4	0	0	0	0	24h	0	4
Movie 15	nucleus 1 (top left)	3	12	0	3	0	0	18h	1	5
	nucleus 2 (top mid)	1	10	1	0	1	1	18h	3	6
	nucleus 3 (top right)	1	12	0	0	1	0	18h	4	4
	nucleus 4 (mid left)	0	4	0	0	0	0	18h	2	4
	nucleus 5 (a litle left from the center)	2	5	0	0	1	0	18h	3	7
	nucleus 6 (second above guard cell)	1	1	0	0	1	0	18h	4	8
	nucleus 7 (next to nucleus 6)	2	2	0	0	0	0	18h	2	5
	nucleus 8 (mid right)	1	5	0	0	0	0	18h	3	5
	nucleus 9 (bottom above guard cell)	0	2	0	0	0	0	18h	3	5
	nucleus 10 (bottom left from guard cell)	0	7	0	0	0	0	18h	2	7
	nucleus 11 (bottom right)	4	10	0	0	1	0	18h	7	8
									2.96	4.36
		movement 1	movement 2	movement 3	movement 4	movement 5	movement 6	total movie time: 289h		
	Total nuclei: 75	127	679	19	73	13	16			
	Total movement:947									

Supplementary table 2: Overview of movement type counts of the plastid-nucleus-interaction analysis in long term movies of *N. benthamiana* pn lines. First column: ID of time series; second column: ID of individual nuclei in each time series; third column to eighth column: count of interaction type 1 to 6; ninth column total duration of imaging for this time series in h; tenth and eleventh column: number of plastids attached to the nuclei at the beginning and the end of the time series.

	Time	Nucleus all frame	Drift
Movie1	**20h**	**3**	-
Movie2	**20h**	**6**	-
Movie3	**18h**	**5**	+
Movie4	**18h**	**2**	+
Movie5	**25h**	**7**	-
Movie6	**25h**	**4**	+
Movie7	**19h**	**4**	+
Movie8	**19h**	**3**	-
Movie9	**19h**	**4**	+
Movie10	**19h**	**5**	+
Movie11	**20h**	**4**	+
Movie12	**20h**	**2**	+
Movie13	**24h**	**8**	-
Movie14	**24h**	**7**	-
Movie15	**18h**	**11**	+
Total	**289h**	**75**	

Supplementary table 3: Overview of all recorded long-term movies. In total, 15 movies were captured in *N.benthamiana's* lower epidermis cell. Based on movies, we could detect 75 nuclei to observe the plastid accumulation around the nucleus.

Mann-Whitney Rank Sum Test

Data source: plastid-accumulation around the nucleus during long-term imaging

Group	N	Missing	Median	25%	75%
the first frame	75	0	2.000	1.000	4.000
last frame	75	0	4.000	3.000	5.000

Mann-Whitney U Statistic= 1836.500

T = 4686.500 n(small)= 75 n(big)= 75 (P = <0.001)

The difference in the median values between the two groups is greater than would be expected by chance; there is a statistically significant difference (P = <0.001)

Supplementary table 7: Statistical test for plastid accumulation during long term imaging in *N. benthamiana*. The results were obtained and copied from Sigmaplot11.

7.2 Establishing AvrRPS4 inducible expression lines (METI) (B)

Position in Level 2	Flank 1*	P+5U	Sp or CDS	cTag	Ter	Flank	Module
1	TGCC	AtNOS	BAR		AtuNos	GCAA	Basta
2	TTAC	AtActin2	XVE		AtuMas	CAGA	XVE
3	GCAA	p35s	Ssu:tp	eGFP	tNOS	ACTA	p35S:ssutp:eGFP
4	ACTA	pUBQ10	NLS:mCardinal	FlagTag	tOCS	TTAC	pUBQ10:NLSmCardinal:FlagTag
5	CAGA	LexA	PsAvrRps4	mKOK*	tAct2	TGTG	LexA:AvrRps4:mKOK
End linker	TGTG					GGGA	pICH41800
Back Bone	TGCC					GGGA	pAGM4673,pAGM4723

Supplementary table 4: Overview of used L0 modules to clone the final METI construct.

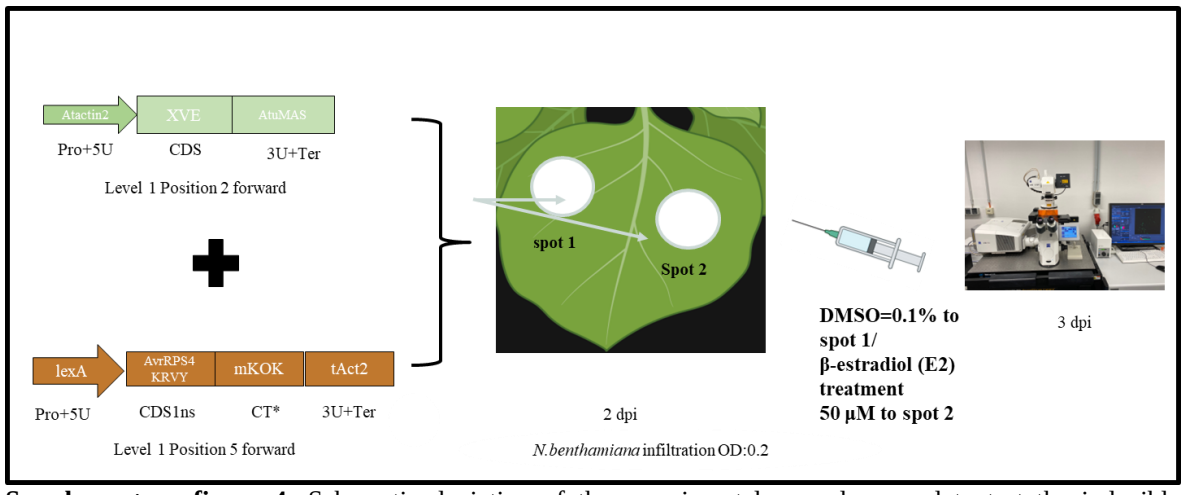

Supplementary figure 4: Schematic depiction of the experimental procedure used to test the inducible expression of AvrRPS4 proteins in the L1 METI modules.

METI selection table	GFP	mCARDINAL	mKOK
LINE 1	1	1	0
LINE 2	1	2	0
LINE 3	1	2	0
LINE 4 gfp not visible	0	1	0
LINE 5	2	3	0
LINE 6	3	3	0
LINE 7 (almost no seeds)	3	3	0
LINE 9	2	3	0
LINE 10	1	1	0
LINE 11 (almost no seeds)	2	2	0
LINE 12 (almost no seeds)	1	1	0
LINE 13	3	3	0
LINE 15 (almost no seeds)	3	3	0
LINE 16	2	2	0
LINE 17 (almost no seeds)	1	1	0
METI E187A mutant	**GFP**	**mCARDINAL**	**mKOK**
line 1 p1	2	1	0
line 2 p5	1	1	0
line 3 p6	2	2	0
line 4 p9	2	1	0
line 5 p 10	2	1	0
line 6 p11	3	2	0
line 7 p12	3	2	0
line 8 p13	3	2	0
line 9 p14	3	2	0
line 10 p15	2	1	0
line 11 p16 (so far best)	3	3	0
METI KRVY mutant	**GFP**	**mCARDINAL**	**mKOK**
line 1 p7	2	2	0
line2 p8	1	1	0
cdsmkok control	**GFP**	**mCARDINAL**	**mKOK**
line 1 p2	1	2	0
line 2 p3	2	1	0
line 3 p4	3	3	0
line 4 p5	3	1	0
line 5 p6	3	3	0

Supplementary table 5: Overview of all selected transgenic METI lines with a scoring on transgene expression (0 = no detectable fluorescence, 1 = detectable but week fluorescence, 2 = well detectable fluorescence suitable for life imaging, 3 = strong expression with strong fluorescence suitable for life imaging).

Wild type/mutant	line number	Reference	Analysis
msl2-1/msl3-1	line 1	Sedef Özyürek	this thesis
msl2-1/msl3-1	line 3	Sedef Özyürek	this thesis
msl2-1/msl3-1	line 4	Sedef Özyürek	this thesis
WT-pn	line 2-1-2	Dr.Martin Schattat	this thesis
WT-pn	line 3-1	Dr.Martin Schattat	this thesis
WT-pn	line 10-1-2	Dr.Martin Schattat	this thesis

Supplementary table 6: Overview of used pn transgenic plants (*msl*).

One Way Analysis of Variance

Normality Test (Shapiro-Wilk) Passed (P = 0.958)

Equal Variance Test: Passed (P = 0.246)

Group Name	N	Missing	Mean	Std Dev	SEM
wt	6	0	317.167	35.958	14.680
msl2/3	18	0	117.556	20.760	4.893

Source of Variation	DF	SS	MS	F	P
Between Groups	1	179300.681	179300.681	286.022	<0.001
Residual	22	13791.278	626.876		
Total	23	193091.958			

The differences in the mean values among the treatment groups are greater than would be expected by chance; there is a statistically significant difference (P = <0.001).

Supplementary table 8: Statistical test for plastid counting in wt pn and *msl2-3* pn lines. The results were obtained and copied from Sigmaplot11.

Mann-Whitney Rank Sum Test

Group	N	Missing	Median	25%	75%
stromule in mutant	23	0	0.000	0.000	1.000
stromule in wt	5	0	6.000	3.000	8.000

Mann-Whitney U Statistic= 12.500

T = 117.500 n(small)= 5 n(big)= 23 (P = 0.002)

The difference in the median values between the two groups is greater than would be expected by chance; there is a statistically significant difference (P = 0.002)

Supplementary table 9: Statistical test for stromule frequency in wt pn and *msl2-3* pn lines. The results were obtained and copied from Sigmaplot11.

7.3 Analysis of nucleus behaviour in transgenic *A. thaliana* plants (C)

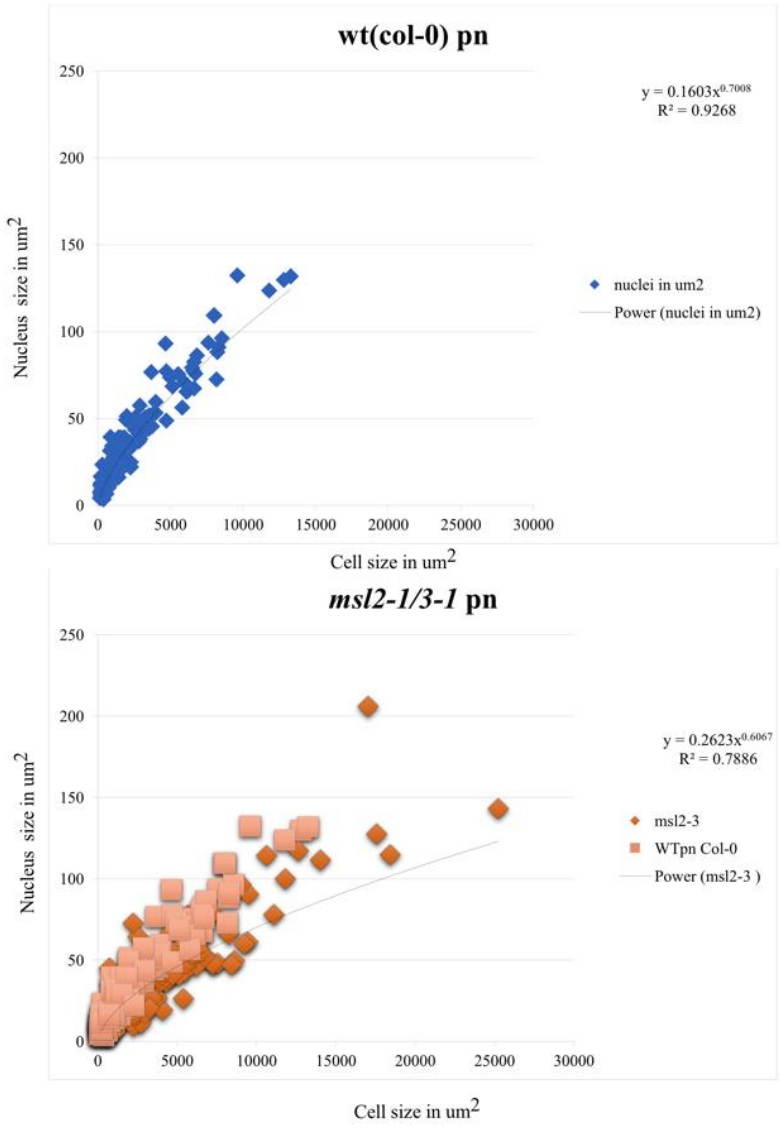

Supplementary figure 5: correlation between nucleus size and cell size in pn transgenic *A. thaliana* Columbia and the msl2_msl3 double mutant. The resulting fitted curved equations have been used to calculate cell size for categorisation of nucleus speed measurements.

Wild type/mutant	line number	Reference	Analysis
kac1-2,kac2-2 pn	line 4	Sedef Özyürek	this thesis
kac1-2,kac2-2 pn	line 5	Sedef Özyürek	this thesis
kac1-2,kac2-2 pn	line 6	Sedef Özyürek	this thesis
chup1-3,kac1-2,kac2-2 pn	line 2	Sedef Özyürek	this thesis
chup1-3,kac1-2,kac2-2 pn	line 3	Sedef Özyürek	this thesis
chup1-3,kac1-2,kac2-2 pn	line 4	Sedef Özyürek	this thesis
WT-pn	line 2-1-2	Dr.Martin Schattat	this thesis
WT-pn	line 3-1	Dr.Martin Schattat	this thesis
WT-pn	line 10-1-2	Dr.Martin Schattat	this thesis

Supplementary table 10: Overview of used pn transgenic plants (*ckk-kk* pn lines).

List of the supplementary figures

List of supplementary tables

VII. Acknowledgments

First, I would like to express my sincere gratitude to my supervisor, Dr. Martin Harmut Schattat, for his invaluable comments, insights, and consistent support throughout my journey toward completing my PhD thesis. His exceptional guidance and prompt responses to my research and writing inquiries have been instrumental in my progress.

I would also like to extend my appreciation to Prof. Dr. Ralf Bernd Klösgen and Prof. Dr. Bettina Hause, who served as the readers of this thesis.

I am immensely grateful to all the members of RTG2498 for their contributions during our seminars and meetings. I want to offer a special thank you to our RTG coordinator, Dr. Julia Grimmer, for her invaluable assistance.

To the members of the "Form and Dynamics of Plant Organelles" group, both past and present, including Dr. Jessica Erickson, Jolina Marx, Jennifer Prautsch, Alexander Guroweitz, and Julian Arndt, I extend my sincere appreciation.

I would like to mention Dr. Jessica Erickson for her guidance and outstanding work/experiments. Her previous research inspired and guided me throughout my doctoral journey. To Jolina, thank you again for the project on interaction during steady-state conditions in Arabidopsis, and best wishes for your PhD. My dear Jenny, your support with my thesis, especially in stromule counting, was invaluable, and I wish you the best in your master's studies. Julian, my special thanks to you also; working with you during the N.benthamina project was a pleasure. I wish you all the best in your academic pursuits.

I would also like to thank the AG Kühn group for their feedback during lab meetings and continuous support, especially Prof. Dr. Kristina Kühn and Dr. Etienne Meyer, along with all group members. Sarlita Dwani and Theresa Schöller are the greatest team members. I am so grateful that I crossed paths with you; without you, my lunch would be so empty, and who could I share gossip or complaints with? Thank you again to each of you, especially Sarlita, for

exchanging ideas during my construct planning, and I wish you all the best for your wonderful career.

A profound thank you goes to my best friend, Simge Parlar. Her support was a constant source of strength during my time in Halle. Whenever I encountered difficulties, she was there for me, making my stay in Halle more enjoyable.

I also wish to express my gratitude to Anja Meents for her constructive feedback and support over the past five years.

Lastly, I must acknowledge the continuous support of my parents, Belma Özyürek. Their encouragement and support throughout my years of study and during the research and writing of this thesis have been invaluable. I would also like to thank my sisters, Fahriye Nur Nazlican and Canan Özyürek, for their continuous support. This achievement would not have been possible without them. I want to express my gratitude to them once more.

"*Ever tried. Ever failed. No matter. Try again. Fail again. Fail better*."
Samuel Beckett

Curriculum Vitae

Sedef Özyürek

Education

Since 07.2019	**Dr. rer. nat. in Botany** Martin Luther University Halle – Wittenberg Research group: Plant Organelle Shape and Dynamics (Dr. Martin H. Schattat) Department of Plant Physiology (Prof. Dr. Ralf Bernd Klösgen) Member of the RTG 2498 **Project 03**: Stromule mediated plastid-nucleus interaction
09.2016 – 02.2019	**Master of Science in Microbiology** Friedrich Schiller University Jena, Germany
09.2007 – 06.2011	**Bachelor of Science in Biology** Gazi University, Ankara, Turkey

Publications

Prautsch J, Erickson JL, **Özyürek S**, Gormanns R, Franke L, Lu Y, Marx J, Niemeyer F, Parker JE, Stuttmann J, Schattat MH. Effector XopQ-induced stromule formation in Nicotiana benthamiana depends on ETI signaling components ADR1 and NRG1. Plant Physiol. 2023 Jan 2;191(1):161-176. doi: 10.1093/plphys/kiac481. PMID: 36259930; PMCID: PMC9806647.

Meents AK, Furch ACU, Almeida-Trapp M, **Özyürek S**, Scholz SS, Kirbis A, Lenser T, Theißen G, Grabe V, Hansson B, Mithöfer A, Oelmüller R. Beneficial and Pathogenic Arabidopsis Root-Interacting Fungi Differently Affect Auxin Levels and Responsive Genes During Early Infection. Front Microbiol. 2019 Mar 12;10:380. doi: 10.3389/fmicb.2019.00380. PMID: 30915043; PMCID: PMC6422953.

Declaration

I hereby declare that I have completed this thesis independently. I also declare that source and auxiliary materials from external works are identified as such and with an indication of the sources marked. With this thesis, I am applying for the first time for the doctoral degree. This thesis has not been submitted for review at any other university.

Halle, 2023

Sedef Özyürek